ULTRACAPACITOR BOOSTED FUEL CELL HYBRID VEHICLE

A Thesis

by

BO CHEN

Submitted to the Office of Graduate Studies of
Texas A&M University
in partial fulfillment of the requirements for the degree of

MASTER OF SCIENCE

August 2009

Major Subject: Electrical Engineering

ULTRACAPACITOR BOOSTED FUEL CELL HYBRID VEHICLE

A Thesis

by

BO CHEN

Submitted to the Office of Graduate Studies of
Texas A&M University
in partial fulfillment of the requirements for the degree of

MASTER OF SCIENCE

Approved by:

Chair of Committee,	Mehrdad Ehsani
Committee Members,	Shankar Bhattacharyya
	Chanan Singh
	Salih Yurttas
Head of Department,	Costas Georghiades

August 2009

Major Subject: Electrical Engineering

ABSTRACT

Ultracapacitor Boosted Fuel Cell Hybrid Vehicle.

(August 2009)

Bo Chen, B.S., Wuhan University

Chair of Advisory Committee: Dr. Mehrdad Ehsani

With the escalating number of vehicles on the road, great concerns are drawn to the large amount of fossil fuels they use and the detrimental environmental impacts from their emissions. A lot of research and development have been conducted to explore the alternative energy sources. The fuel cell has been widely considered as one of the most promising solutions in automobile applications due to its high energy density, zero emissions and sustainable fuels it employs. However, the cost and low power density of the fuel cell are the major obstacles for its commercialization.

This thesis designs a novel converter topology and proposes the control method applied in the Fuel Cell Hybrid Vehicles (FCHVs) to minimize the fuel cell's cost and optimize the system's efficiency. Unlike the previous work, the converters presented in the thesis greatly reduce the costs of hardware and energy losses during switching. They need only three Metal–Oxide–Semiconductor Field-Effect Transistors (MOSFETs) to smoothly accomplish the energy management in the cold start, acceleration, steady state and braking modes.

In the converter design, a boost converter connects the fuel cell to the DC bus because the fuel cell's voltage is usually lower than the rating voltage of the motor. In this way, the fuel cell's size can be reduced. So is the cost. With the same reason, the bidirectional converter connected to the ultracapacitor works at the buck pattern when the power is delivered from the DC bus to the ultracapacitor, and the boost converter is selected when the ultracapacitor provides the peaking power to the load. Therefore, the two switches of the bi-directional converter don't work complementarily but in different modes according to the power flow's direction.

Due to the converters' simple structure, the switches' duty cycles are mathematically analyzed and the forward control method is described. The fuel cell is designed to work in its most efficient range producing the average power, while the ultracapacitor provides the peaking power and recaptures the braking power. The simulation results are presented to verify the feasibility of the converter design and control algorithm.

DEDICATION

To my parents

ACKNOWLEDGEMENTS

I would like to thank my committee chair, Dr. Mehrdad Ehsani, and my committee members, Dr. Shankar Bhattacharyya, Dr. Chanan Singh, Dr. Salih Yurttas, and Dr. Yimin Gao, for their guidance and support throughout the course of this research.

Thanks also go to my friends and colleagues and the department faculty and staff for making my time at Texas A&M University a great experience, especially the fellow students in the Power Electronics & Motor Drives Laboratory.

Finally, thanks to my mother and father for their encouragement and love.

TABLE OF CONTENTS

LIST OF FIGURES

Page

Page

Page

LIST OF TABLES

CHAPTER I

INTRODUCTION

1.1 Introduction

With the highly increased number of vehicles on the road, the issues of their environmental impacts and fuel consumption are becoming more and more severe. The appeal for low emissions and high fuel economy from the cars is urgent and arouses great attention from different realms of the society.

To solve this problem, many alternative drive trains have been proposed, such as pure electric vehicles (EVs), hybrid electric vehicles (HEVs) and fuel cell hybrid vehicles (FCHVs) [1]. The motor is used to either replace or assist the conventional internal combustion engine (ICE) to increase the overall efficiency. The pure electric vehicle is powered by the battery. Its major problem is its short driving range provided by the battery of reasonable size. The hybrid electric vehicle combines the battery and internal combustion engine together as the hybrid energy sources. The driving range and system efficiency rise, while the control strategy becomes more complicated by virtue of two or more sources. Additionally, with the internal combustion engine on board, the hybrid electric vehicle still can't fully realize zero emissions. As for the fuel cell hybrid electric vehicle, the fuel cell is the energy source to provide the average power for the

---

This thesis follows the style and format of *IEEE Transactions on Industry Applications.*

motor resulting from its high energy density and slow response capability. There are several possible power sources to assist the fuel cell for the transient loads, such as the battery, the ultracapacitor, the flywheel and etc. In this thesis, the ultracapacitor is selected. The design of the drive train will be elaborated in Chapter III.

Similar to hybrid electric vehicles, the fuel cell hybrid vehicles have multiple sources, which introduces the complicated control issue. In this thesis, a simple converter topology is designed. A forward control methodology is proposed and implemented on the system to optimize the system's efficiency. The simulation results verifies that the converter topology and the control methods can realize better performance, higher fuel economy, higher system efficiency and much less environmental pollution than the conventional vehicles.

1.2 Review of current transportation issues and its future

With the tremendous energy demands, and the failure of new oil findings to complement on a global scale, it is necessary to explore other alternative energy sources. The statics from the Department of Energy show the major consumers of the petroleum are cars and trucks [1]. During 1970s, the dramatically declined production of oil and gas changed the way automobiles were made. Auto makers manufactured more compact cars to achieve better fuel efficiency. The recent past bill raising fuel efficiency standards to 35 mpg by 2020 forced car manufacturers to build more fuel efficient cars and promoted the alternative energy further.

The air pollution of conventional fossil fuel vehicles has also raised great concern around the world. Report from Robert Q. Riley [2] shows that motor vehicle

emissions account for 30%-50% of hydrocarbon, 80%-90% of carbon monoxide, and 40%-60% of nitrogen oxide emissions. Cars and light trucks are responsible for about 20% of the nation's carbon dioxide, which is a powerful greenhouse gas. Motor vehicle carbon emissions are essentially proportional to the total fuel consumed. If we can increase the fuel economy, the fuel consumption decreases, and the emissions can be efficiently reduced.

The increasing impetus of less contingency on fossil fuels and less pollutions drives the trend towards the sustainable alternative energy sources. A considerable amount of research and commercial development are in progress to explore novel vehicles driven by these alternative sources. Not only can these vehicles relieve the energy pressure on the rapid depletion of petroleum, but they also emit no or few toxic emissions (HC, CO and NO_x), greenhouse gas (CO_2), or other harmful gas. Moreover, the new energy vehicles can provide better performance and higher efficiency than conventional vehicles.

This thesis focuses on the fuel cell hybrid vehicular application. It proposes a novel drive train configuration with the fuel cell as its main source and the ultracapacitor as its auxiliary source as in Figure 1. A specific converter topology is designed to regulate the system voltage and control the current among these two sources and a dynamic load, the motor. Along with the converter, this thesis brings forth a forward control algorithm by changing the duty cycle of the switches in the converter to achieve the optimum system efficiency.

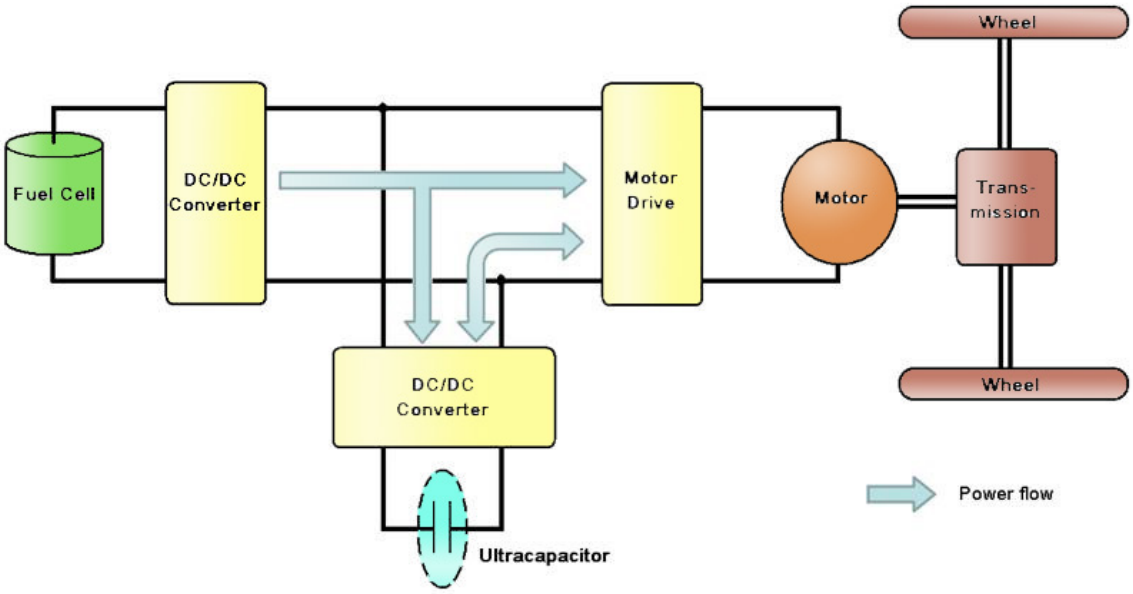

Figure 1 Fuel cell hybrid vehicle structure

Many research and development activities have been conducting in producing alternative fuels, such as biodiesel, electricity, ethanol, hydrogen, methanol, natural gas, and etc. Alternative fuels can store the energy in a stable form and be easily transported from the production area to end users. There are commercialized or demonstrative hybrid vehicles using biodiesel, electricity, ethanol, methanol and natural gas [3]. In the thesis, the hydrogen is used as the vehicle's fuel as an example.

In the fuel cell hybrid vehicle application, the fuel cell is the main energy source and has being widely considered as a potential alternative for internal combustion engine (ICE) to drive vehicles. It converts the chemical energy from certain fuels, such as hydrogen and methanol, directly to electricity.

1.3 Review of fuel cell technology and suitability for transportation application

The fuel cell, like the battery, is an electrochemical device, which converts the

chemical energy in the reactants directly to the electrical energy as shown in Figure 2. It gives higher potential efficiency than the conventional internal combustion engine. As expressed in Figure 2, both the fuel cell and the internal combustion engine get the same potential energy from the identical fuel and oxidizers. As far as the internal combustion engine is concerned, the reactants combust first to generate heat. Then the heat is converted into useful work and waste heat via mechanical process. On the contrary, the fuel cell converts the chemical energy released from the fuel and oxidizer directly into electrical energy, avoiding the energy loss in the middle process. With current technology, the fuel cell's efficiency is able to reach 65%, while the efficiency of the internal combustion engine is about 10 – 30% [4].

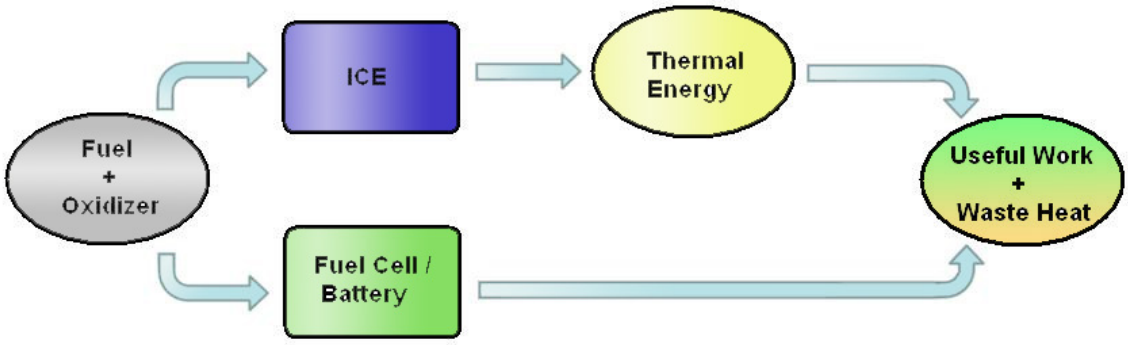

Figure 2 ICE and fuel cell / battery general working process

As for the comparison between the fuel cell and the battery, they are both electrochemical devices converting chemical energy of the reactants directly into electrical energy as mentioned above. The major difference between them lies in that the reactants in the battery are basically being consumed and will be drained at some point when the battery is operating, while the fuel (such as hydrogen, methanol, natural gas or

petroleum) and oxidizer (pure oxygen or air) can be constantly filled in the fuel cell tank during the fuel cell's operation. Therefore, the fuel cell can be seen as a rechargeable battery with constant performance. Although the secondary battery is also rechargeable, it involves the reversal of the electrochemical reactions and takes much longer time than refilling the fuel and oxygen into the fuel cell tank.

1.3.1 Operation principle of fuel cell

There are several types of fuel cells, which will be briefly introduced later. Generally, all the fuel cells consist of an electrolyte sandwiched between two electrodes. The fuel and oxidizer flow into the electrodes and react with the facilitation of specific catalyst there. At the anode electrode, the fuel is oxidized and produces electrons. The particular features of the electrolyte prohibit the electrons to pass through and only allow the ions to permeate. So electrons generated by the fuel flow to the external circuit, while the ions migrate through the electrolyte and recombine with the oxidizer and the returned electrons to complete the circuit.

Since the Proton Exchange Membrane Fuel Cell (PEMFC) is considered the most viable candidate for the automotive applications and under the most advanced R&D among all the fuel cells, we take it as an example to further discuss the working principles of the fuel cell. Assuming hydrogen is the fuel, the hydrogen gas would pass over one electrode, called the anode, and with the help of a catalyst, separates into electrons and hydrogen protons as shown in Figure 3 and expressed in Equation (1.1) ,

$$2H_2 \rightarrow 4H^+ + 4e^- \qquad (1.1)$$

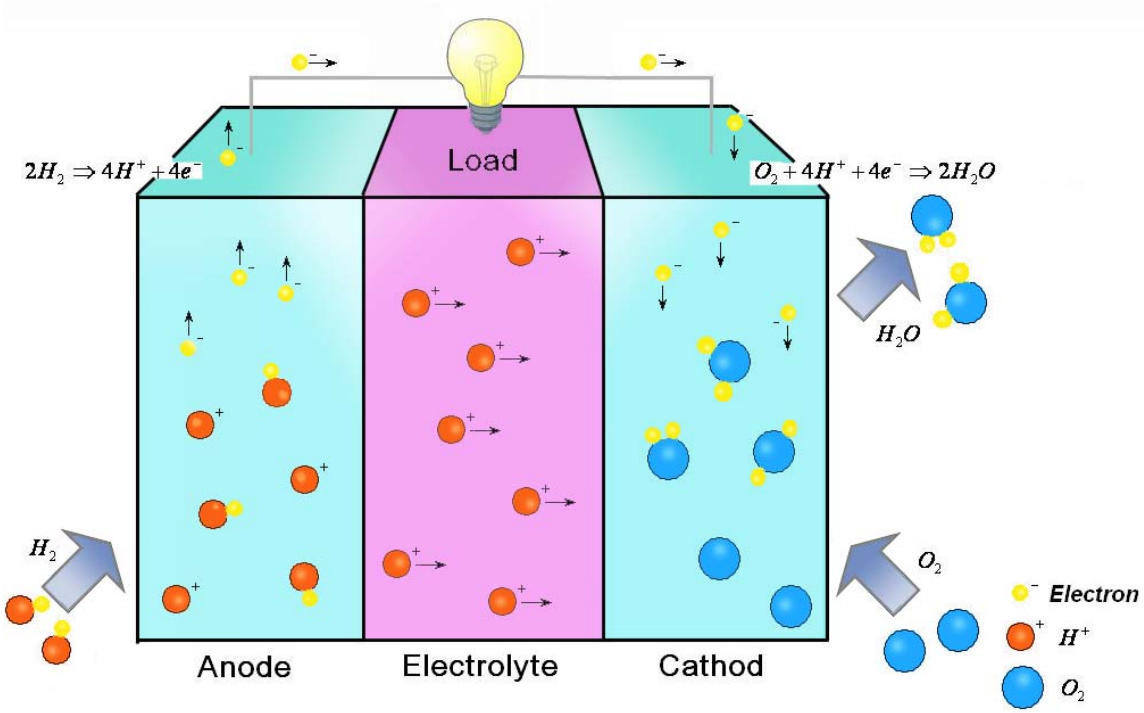

Figure 3 Fuel cell reaction

The protons flow to the other electrode, called a cathode, through the electrolyte while the electrons pass through the external circuit, thus creating electricity. The hydrogen protons and electrons combine with oxygen flow at the cathode, and produce water as Equation (1.2).

$$O_2 + 4H^+ + 4e^- \Rightarrow 2H_2O \tag{1.2}$$

The overall reaction at the fuel cell is

$$2H_2 + O_2 \Rightarrow 2H_2O + \Delta g_f \tag{1.3}$$

where Δg_f is the change in Gibbs free energy, which is the difference between the Gibbs free energy of the products and that of the reactants,

$$\Delta g_f = (g_f)_{H_2O} - (g_f)_{H_2} - (g_f)_{O_2} \tag{1.4}$$

It is this Δg_f amount of energy transferred to electric energy per cell if ignoring the losses. It varies with temperature and pressure. The lower the temperature, the more energy the fuel cell can generate, and even more if the water product is in the liquid form [3]. However, the low temperature also leads to a large voltage drop. 80^oC is the optimal temperature at which the maximum efficiency is achieved. At standard condition (25°C and 1 atm.), the theoretical open circuit voltage of an H-O fuel cell is expressed by

$$V = \frac{\Delta G^0}{nF} V = \frac{\Delta G^0}{nF} \tag{1.5}$$

where ΔG^0 is the Gibble energy change, n is the electron number transferred in the reaction and F is Faraday constant. As a matter of fact, the voltage produced from one cell is usually between 0 and 1 volt depending on the fuel cell operating conditions and the size of the load connected to the fuel cell. To get higher voltage, multiple cells are stacked in series. The total stack voltage is the number of cells multiplied by the average cell voltage. Typical voltage characteristics of fuel cells are normally given versus cell current density (current per unit cell active area), shown in Figure 4. Thus, the current the fuel cell can produce equals the current density times the fuel cell's active area. The current density of the fuel cell varies from 0 to 1.2 A per square-centimeter. Increasing the active area can enlarge the current producing capability of the fuel cell.

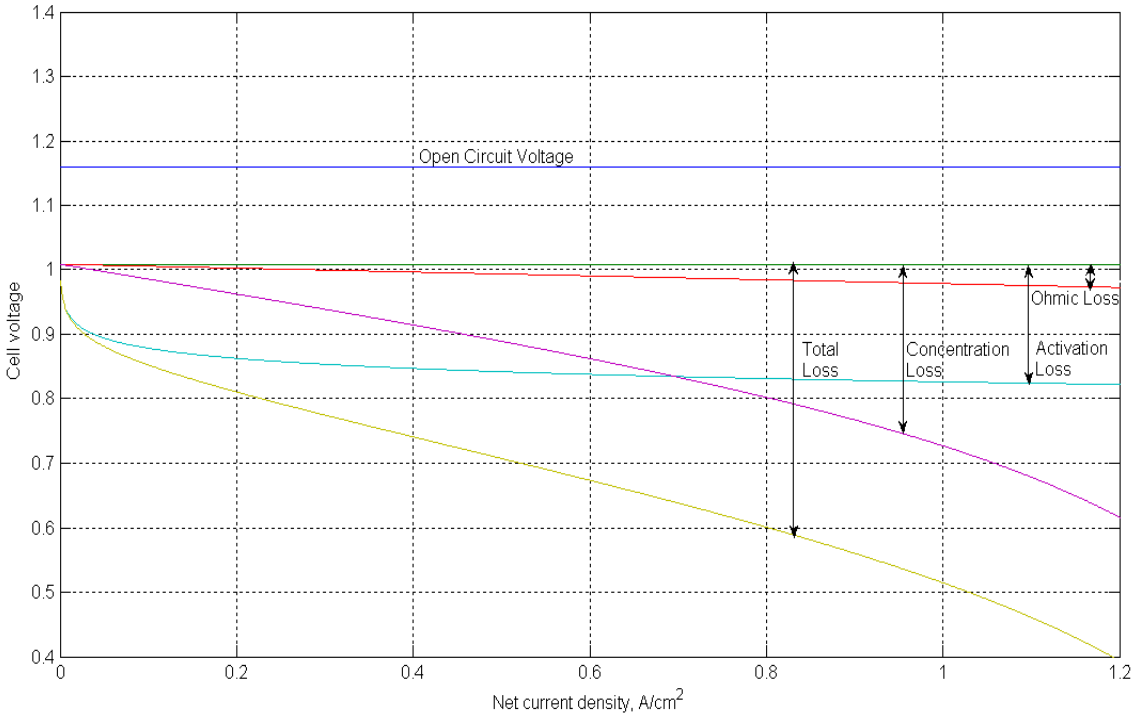

Figure 4 Fuel cell voltage characteristics

Figure 4 shows the fuel cell voltage drops from about 1V at no load to 0.4V at full load. The differences between actual voltage and the ideal voltage of the fuel cell represent the loss in the cell. The fuel cell losses are attributed to three categories: the activation loss, the ohmic loss and the concentration loss as shown in Figure 4. The activation loss or activation overvoltage arises from the demands to move electrons and to break and form chemical bonds in the anode and cathode. The ohmic loss arises from the resistance of the polymer membrane to the transfer of protons and the resistance of the electrode and the collector plate to the transfer of electrons. Concentration loss or concentration overvoltage results from the drop in concentration of the reactants as they are consumed in the reaction. Concentration loss is the reason for rapid voltage drop at high current density.

The fuel cell stack is the major function part of the fuel cell. The fuel cell also consists of other indispensible auxiliary components. The fuel cell system can be categorized into four subsystems, namely reactant flow subsystem, heat and temperature subsystem, water management subsystem and power management subsystem [5]. Figure 5 shows the fuel cell system's block diagram. As in Figure 5, the hydrogen and air flow loops form the reactant flow subsystems. When the driver presses the acceleration pedal and sends the torque command, the corresponding amount of fuel flows are consumed from the tank. The heat and temperature subsystem is responsible for dissipating the heat generated during the operation process and maintaining the desired temperature for the fuel cell's normal performance. It spreads in the reactants cooler and the stack's cooling system. The water management is required to ensure the reactants get enough water to react efficiently and the byproduct recycled properly. The power management subsystem controls the power drawn from the fuel cell. According to specific control strategy, the fuel flowing into the stack and the current generated is controlled to meet the objective of satisfactory vehicle performance, optimal efficiency and etc.

With these different subsystems, the fuel cell system's efficiency is limited during the light load because the auxiliary components still operate and consume energy even if the output power is low. On the other hand, when the load is heavy, the output voltage of the fuel cell is low as shown in Figure 3, resulting in low efficiency. Thus, the fuel cell system's efficiency is represented as Figure 6.

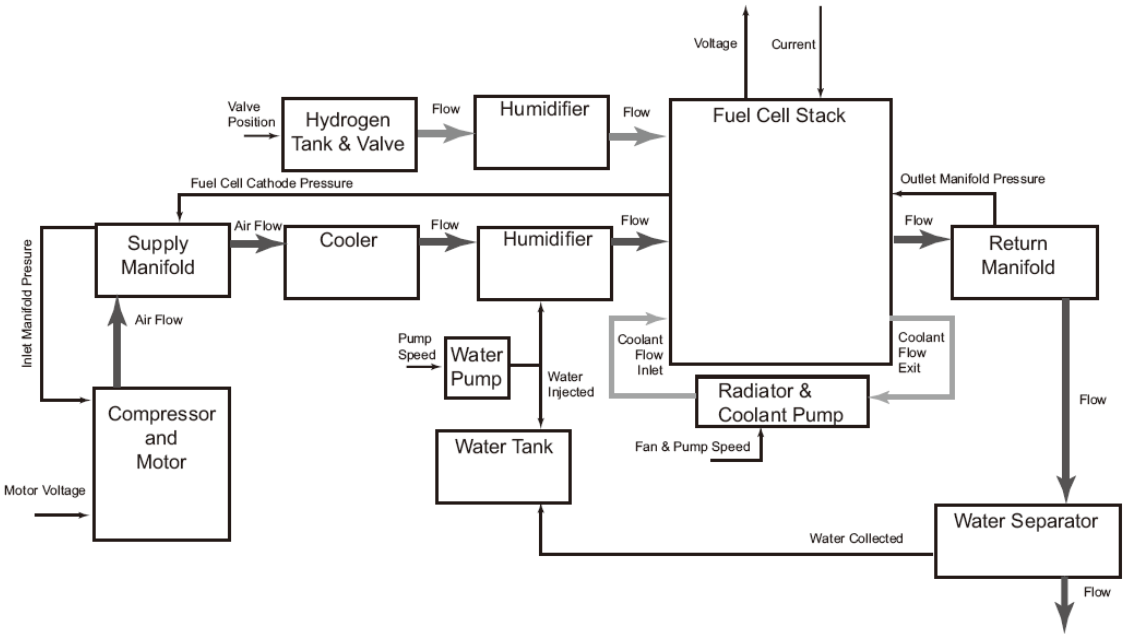

Figure 5 Fuel cell system block diagram [5]

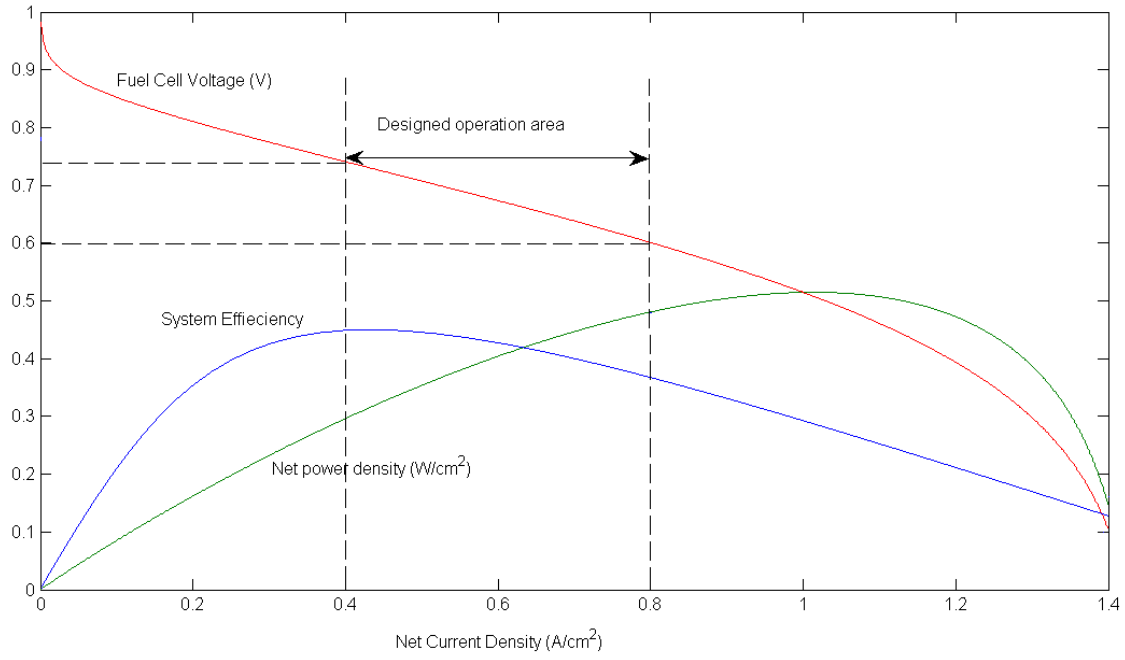

Figure 6 Fuel cell characteristics

The data is collected from the fuel cell model built by University of Michigan [5]. And its prototype is the fuel cell used by Ford P2000.

1.3.2 Different types of fuel cells

There are many types of fuel cells under research and development as shown in Table 1. The fuel cells reaching the application level at present are: Proton Exchange Membrane Fuel Cells (PEMFC), Alkaline Fuel Cells (AFC), Phosphoric Acid Fuel Cells (PAFC), Molten Carbonate Fuel Cells (MCFC), Solid Oxide Fuel Cells (SOFC) and Direct Methanol Fuel Cells (DMFC). Different types of fuel cells are mainly distinguished by the types of their electrolytes as represented in Figure 2. Among them, the Proton Exchange Membrane Fuel Cell technology is covered more extensively than the other leading fuel cell technologies with more R&D efforts exerted.

Proton exchange membrane fuel cells

The working principles of PEMFCs, the Pronton Exchange Membrane Fuel Cells, are stated in the previous section. The PEMFCs use solid polymer membranes as the electrolyte. That's why the PEMFC can also stand for Polymer Electrolyte Membrane Fuel Cell. Polymer electrolyte membrane is desirable because it allows protons (hydrogen ions) to pass through but not electrons or gas, which otherwise would lead to short circuit and gas crossover respectively. PEMFC has about 55% efficiency at 90°C , which is around the automotive operating temperature. The relatively low working temperature range is another advantage to be applied in the vehicle.

Table 1 Operating data of various fuel cell systems [3, 4]

Fuel Cell Type	Temperature(°C)	Advantages	Disadvantages	Applications
PEMFC	60 - 100	Low temperature operation, high efficiency, high H_2 energy density, relatively fast cold start-up	Expensive catalyst, CO poison, heat and water management, durability	Portable, vehicles, and stationary power
AFC	60 - 230	High efficiency, low oxidization losses	Intolerance of CO_2	Space applications with pure O_2 available
PAFC	160 - 220	Relatively higher CO tolerance, thermal management, durable	Low energy density, expensive catalyst, slow start-up	Premium stationary power
MCFC	500 - 800	CO tolerant, fuel flexible, high-quality waste heat, inexpensive catalyst	Electrolyte dissolves cathode catalyst, slow start-up, electrolyte maintenance	Stationary power
SOFC	1000 - 1200	CO tolerant, fuel flexible, high-quality waste heat, inexpensive catalyst	Slow start-up, inactivity of electrode below 600 °C, durability, proper cell-sealing	Industrial co-generation, utility applications
DMFC	50 - 85	Simple structure, high energy density	Methanol crossover, poor catalyst activity	Portable, emergency power generators, and vehicles

Although temperatures in internal combustion engines of vehicles do reach above 1000°C, these temperatures are restricted by the gases themselves and most parts of the engine are kept cool (around 100°C) by the cooling system. Additionally, PEMFC is fueled with pure hydrogen and oxygen or air as oxidant, which can provide a relatively high energy density compared with other fuel cells. The PEMFC's electrolyte is solid membrane, whose manipulation and maintenance are much easier than using liquid electrolyte.

Alkaline fuel cells

AFCs use liquid potassium hydroxide (KOH) as the electrolyte, which is alkaline, while the electrolyte of PEM fuel cells is acidic. In the AFCs, water is produced at the anode, and consumed at the cathode as follows.

At the anode: $2H_2 + 4OH^- \rightarrow 4H_2O + 4e^-$ (1.6)

At the cathode: $O_2 + 4e^- + 2H_2O \rightarrow 4OH^-$ (1.7)

There are several advantages of AFCs. First, AFCs are capable of operating over a wide range of temperatures and pressures from 60 to 230°C and 2.2 to 45 atm. Second, AFCs can achieve very high efficiencies (60% demonstrated for space applications [6]) because of the fast kinetics allowed by the hydroxide electrolyte. The oxygen reduction ($O_2 \rightarrow OH^-$) is much easier than that in acidic fuel cells. It also allows AFCs to use silver or nickel as catalysts instead of platinum, which greatly reduces the costs. Third, the AFC kinetics is further improved by the eventual circulation of the liquid electrolyte. When the electrolyte is circulated, the fuel cell is said to be a "mobile electrolyte fuel cell." The advantages of such an architecture are: an easy thermal management because

the electrolyte is used as coolant; more homogeneous electrolyte concentration, which solves problems of concentration around the cathode; the possibility of using the electrolyte for water management, replacing the electrolyte if it has been polluted by the carbon dioxide and removing the electrolyte from the fuel cell when it is turned off, which has the potential to greatly lengthen the lifetime of the stack.

The use of a circulated electrolyte, however, poses some problems. The greatest problem is the increased risk of leakage. The potassium hydroxide is highly corrosive and has a natural tendency to leak even through the tightest seals. The construction of the circulation pump, the heat exchanger and the eventual evaporator is very complicated. Another problem is the risk of internal electrolytic short-circuit between two cells if the electrolyte is circulated too violently or if the cells are not sufficiently isolated.

The major frailty of AFCs is the poisoning by carbon dioxide. The alkaline electrolyte has a great affinity for carbon dioxide and together they form carbonate ions (CO_3^{-2}). These ions do not participate in the fuel cell reaction and will diminish its normal performance. There is also a risk that the carbonate will precipitate and obstruct the electrodes. To avoid this problem, AFCs require pure oxygen or a carbon dioxide scrubber to remove as much carbon dioxide as possible. By the reason of the high costs to generate and store the pure oxygen, few companies are engaged in manufacturing AFCs.

Phosphoric acid fuel cells

PAFCs rely on an acidic electrolyte, like PEM fuel cells, to conduct hydrogen

ions and operates at around 160 – 220 °C. The anode and cathode reactions are the same as PEM fuel cell reactions. Phosphoric acid (H_3PO_4) is a viscous liquid contained by capillarity in the fuel cell in a porous silicon carbide matrix. The high working temperature allows 1 – 2 % CO in the fuel stream. The liquid electrolyte can conduct the ions and avoid using water, which makes the water management simpler.

PAFC is the first fuel cell technology to in the market. Many hospitals, hotels, and military bases make use of a PAFC to cover part or total of their electricity and heat needs. Few of its applications are in the automotive field, probably because of the high working temperature.

The phosphoric acid electrolyte temperature must be kept above 42°C, making the startup difficult and restraining the continuous operation of PAFCs.

Another problem arising from the high operating temperature (above 150°C) is the energy consumption associated with warming up the stack. Every time the fuel cell is started, certain energy must be spent to heat it up to the operating temperature and every time the fuel cell is turned off, the heat is wasted. The loss is significant for short travel time, which is a common occurrence for urban drivers. Also the heavy, chunky system, limited vapor pressure of the liquid electrolyte, and the slow start-up are the technical restraints of the PAFC.

Molten carbonate fuel cells

MCFCs are high-temperature fuel cells (500 to 800°C). They rely on a molten carbonate salt to conduct ions, usually lithium–potassium carbonate or lithium–sodium carbonate. The ions conducted are carbonate ions (CO_3^{-2}). The ion conduction

mechanism is that of a molten salt like in PAFC or highly concentrated alkaline fuel cells.

The major difference from other fuel cells is the necessity to provide carbon dioxide at the cathode. It is not necessary to have an external source since it can be recycled from the anode. MCFCs use hydrocarbons instead of the pure hydrogen. The high-temperature fuel cells can almost directly process hydrocarbon fuels because the high temperature allows decomposing them to hydrogen on the electrodes. This would be a tremendous advantage for automotive applications because of the present availability of hydrocarbon fuels. In addition, the high temperatures enhance the kinetics to the point that cheap catalysts may be used.

On the other hand, MCFCs has many problems due to the nature of their electrolytes and the operating temperatures they require. The carbonate is an alkali, and is extremely corrosive especially at high temperatures. Not only is this unsafe, there is also the problem of corrosion on the electrodes. So the carbon dioxide injection is necessary for the safety and stability purpose. With 500 to 800°C high operating temperature, the evaporation of the reactants and the energy losses are deteriorated. These problems, as well as the long start-up time, are likely to confine molten carbonate fuel cells to stationary or steady power applications.

Solid oxide fuel cells

SOFCs are the high-temperature fuel cell systems with solid electrolyte. They conduct ions in a ceramic membrane at high temperature (1000 to 1200°C).

The great advantage of SOFCs is this static electrolyte. There is no moving part, except perhaps in the ancillaries. The very high operating temperature allows the use of hydrocarbon fuels as in MCFCs and also the inexpensive raw materials as catalysts. SOFCs are not prone to carbon monoxide and they process it about as efficiently as hydrogen.

Additionally, SOFCs have low activation losses due to their high operating temperature. The losses are dominated by the ohmic component.

Like MCFCs, the disadvantages of SOFCs are mostly associated with their high operating temperature. Supplementary problems arise because the ceramic electrolyte and electrodes are extremely brittle. This is a major frailty for vehicular applications where vibrations are a common occurrence. Thermal cycling further stresses the ceramics and is a major concern for planar fuel cells. Besides, the high operating temperature and the extremely slow start-up are the challenges the SOFC faces.

Direct methanol fuel cells

DMFC is actually a subcategory of PEMFC with methanol as the fuel instead of hydrogen. DMFC is generally visioned as the most viable alternative to the Li-ion batteries for the following reasons. First, methanol is a liquid fuel that can be stored, distributed, and marketed easily for vehicle applications by reason that the current infrastructure of fuel supply can be used without too much further investment. Second, methanol is the simplest organic fuel, which can be most economically and efficiently produced on a large scale from relatively abundant fossil fuel, namely coal and natural gas. It can be produced from agriculture products, such as sugar cane.

The overall reaction happened in DMFC is as follows.

$$CH_3OH + \frac{2}{3}O_2 \rightarrow CO_2 + 2H_2O \quad (1.8)$$

The DMFC is relatively immature among the aforementioned fuel cells. At present, it generally operates at 50 to 85°C. This low operating temperature potentially prevents the DMFC to reach the same power level as the direct hydrogen fuel cells. Additionally, the high permeation of methanol through the membrane, resulting in the methanol crossover, and the poor catalyst activity are the issues affecting the performance of DMFC. Typically a platinum-ruthenium catalyst is utilized on the anode and a platinum catalyst is used on the cathode [7].

Referring to the above analysis and comparisons as in Table 1, the PEM Fuel Cell is the most suitable type of fuel cells for the automobile.

1.4 Review of fuel cell application in transportation

Fuel cell hybrid vehicle (FCHV) is believed to be the best way to solve the problems that we will face in the near future, such as shortage of energy, pollution caused by exhausted gas, etc. Although it is still far away from commercial operation, billions of dollars have been invested in this area to exploit it, not only by government but also by large automobile groups.

Daimler-Chrysler

Since 1990, DaimlerChrysler engineers and researchers have been working on the automotive application of the fuel cell technology. The first fuel cell vehicle, the NECAR 1 was introduced in 1994. More than 20 other research vehicles and prototypes have been presented since. The performance and reliability have been steadily enhanced

while the size and weight of the drive system have been reduced. The Mercedes-Benz B-Class F-Cell is another significant milestone along the road to market maturity for the fuel cell. Fuel cell vehicles are part of DaimlerChrysler's advanced propulsion technology umbrella, which includes efficient gasoline engines, advanced diesels and hybrid power train systems.

General Motors

In 2008, GM's HydroGen4 fuel-cell vehicles hit the road in Berlin as part of the company's extensive global zero-emission test program. Having completed over 400,000 miles of testing in the U.S. (where its known as the Chevrolet Equinox Fuel Cell), the tests in Germany are the first European outing for the hydrogen EV which is capable of 0-62mph in around 12 seconds, has a top speed of 100mph and a range of around 200 miles. GM deploys more than 100 vehicles of this type in its Project Driveway testing program in the U.S., Japan, Korea, China, and Germany.

Toyota

Toyota Motor Corporation (TMC) started development of fuel cell hybrid vehicles in 1992. TMC developed the fuel cell stack and major components of the fuel cell hybrid system completely in house, and began limited marketing of the TOYOTA FCHV (Fuel Cell Hybrid Vehicle) in December 2002.

Honda

There has been continuous progress in the fuel cell vehicle development. One of the fuel cell vehicles that has been commercially available is the Honda FCX. In 2002, Honda's FCX was certified by the U.S. Environmental Protection Agency (EPA) and the

California Air Resources Board (CARB), making it the first and only fuel cell car in history to be approved for commercial use. CARB and the EPA have also certified the FCX as a Zero-Emission Vehicle (ZEV), Tier-2 Bin 1.

The 2005 and 2006 Honda FCX is powered by Honda designed and manufactured fuel cell stacks. With an EPA city/highway rating of 62/51 miles per kilogram (mpkg), it can achieve an EPA-rated driving range of 210 miles. In terms of energy efficiency, one mile per kilogram (mpkg) of hydrogen is almost equivalent to one mile per gallon (mpg) of gasoline.

1.5 Previous work

With the fuel cell being the most viable replacement for the ICE in the vehicle, a lot of research and development have been carried out centered on fuel cell vehicles [7 – 15]. There are several different drive train designs for the fuel cell vehicle.

[7 - 9] implement only the fuel cell to drive the vehicle, which give the system simple structure and control strategy. Nevertheless, this configuration requires a very large size fuel cell, since the fuel cell needs to provide all the power the load asks for and it can't recapture the braking energy. Therefore, this architecture can't essentially improve the fuel economy but increases the vehicle's costs as shown in Chapter II. [10 - 14] combine the fuel cell with either battery or ultracapacitor or both, and proposed different kinds of converter topology to manage the energy flow of the system. [10] propose a very simple structure as shown in Figure 7(a), but the load can't draw the power from the two sources simultaneously and the battery or the ultracapacitor can't recapture the braking energy from the motor. The vehicle's performance is sacrificed.

[11, 12] use transformer and full bridge converters to regulate the voltage changes between the high voltage end and low voltage end as shown in Figure 7(b). However, the electrical isolation is not necessary for the fuel cell hybrid vehicle. The introduction of the transformer also brings in the phase shift issue and adds the complexity of the power management. With the utilization of full-bridge converter, the current ripple is reduced and the system's performance becomes smoother. But more than 12 switches increases the costs, weight and volume of the system. Additionally, since the fuel cell can't be charged, the bi-directional converter is redundant for the fuel cell's end in [13, 14].

As for the control strategy, a lot of control methods have been studied to apply in the fuel cell hybrid vehicle system [16 – 20], such as the fuzzy logic control, predictive control and so on. [16, 17] can't provide the accurate control intrinsically because the system can't be analyzed mathematically itself. [18, 19] have very complicated algorithm and can't be implemented fast enough to generate satisfactory performance. In [20], its control method accumulates error and the former error would impact the following results.

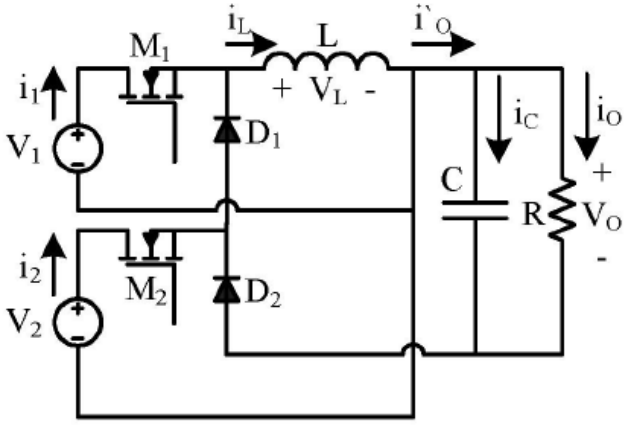

(a) Integrated buckboost-buckboost converter [10]

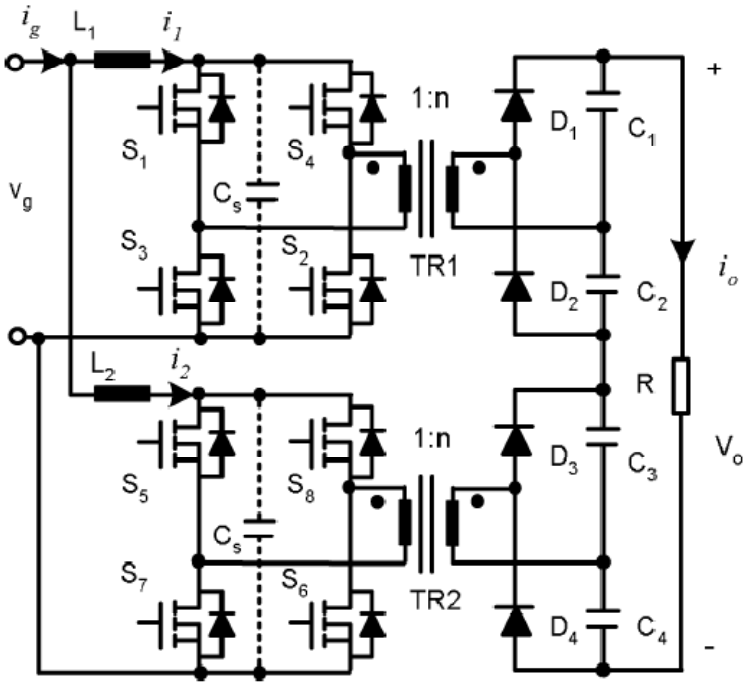

(b) Schematic diagram of interleaved current-fed full-bridge converter [12]

Figure 7 Previous converter topologies applied in fuel cell hybrid vehicles

1.6 Research objectives

The fuel cell's system efficiency has reached 65 %, while the ICE's efficiency is 10 – 30 % [21]. Besides, fuel cell is environmentally friendly, with zero emission for the hydrogen PEMFC. Also, fuel cell's low noise operation can provide more comfortable driving experience than the ICE in conventional vehicles. The main obstacle for the fuel cell's large-scale production is its high cost. How to make fuel cell vehicle affordable and desirable is the main goal for this project.

A converter topology is introduced in the thesis to apply in fuel cell hybrid vehicles among two sources and a dynamic load. The sources here are the fuel cell as the main energy source and the ultracapacitor as the auxiliary power source. The dynamic load is the DC motor. The reasons using ultracapacitor are

- Fuel cell system has low power density. When fuel cell is used alone to power a vehicle and meet the vehicle performance, the fuel cell is mandated to be built very large in order to provide the demanded power.
- Fuel cell is a unidirectional power unit and can not operate in reverse direction.
- At very load and very high load, the fuel efficiency is low.

To solve these problems, a hybrid system is used. The control strategy and methods are proposed in order to achieve the minimum converter hardware and the optimum system efficiency. The architecture of the hybrid system and the vehicle drive train operation principles are presented in Chapter II. In Chapter III, the configuration of the converter in the hybrid system is selected and designed; the characteristics of various

sources' are addressed; and all the possible converter topologies are analyzed. The control strategy is proposed and the vehicle propulsion system is designed in Chapter IV. Chapter V describes the detailed control methods and its implementation. Simulation and experiment results are given and used to verify the expected operation characteristics in Chapter VI. Chapter VII draws the conclusion and presents the possible directions for future research.

CHAPTER II

GENERAL ANALYSIS OF VEHICLE POWER TRAIN

During the past 100 years, the automobiles have gone through a tremendous and rapid development. They are built more comfortable, more versatile, with better performance, higher efficiency and no increased costs. All of these changes lead to an increase in the number of cars on the road. With the unprecedented popularity of vehicles, their environmental impact and fuel economy become significant issues more and more people are concerned about. The pollution and energy consumption are two of the vehicle performance criteria [22], which will be explained later.

2.1 Architecture of the vehicle drive train

Some of the vehicle performances have been predetermined by the intrinsic properties of the architecture of the vehicle drive train. In the conventional vehicle, all the torque required by the load is exclusively from the internal combustion engine to propel the vehicle. For hybrid electric vehicles, they are generally categorized into two types, namely series hybrid and parallel hybrid as shown in Figure 8. The series hybrid propulsion system is driven exclusively from the motor. For the parallel hybrid drive train, the torque supplied from the internal combustion engine is mechanically coupled with torque from the motor. In both architectures, the ICE represents the main energy source, so it can also be replaced by the fuel cell. Similarly, the battery represents the auxiliary energy storage, for example ultracapacitor, flywheel or their combinations.

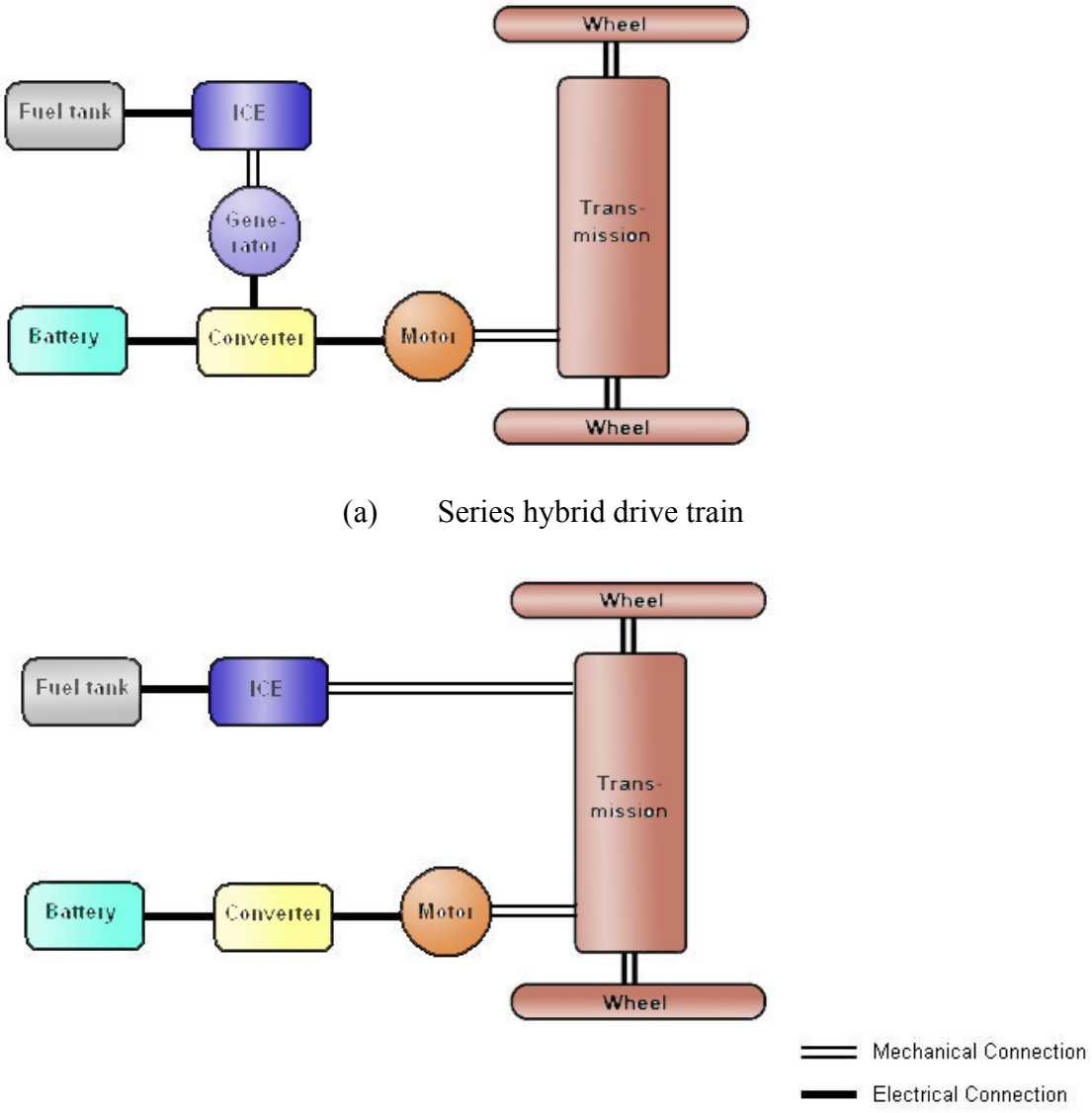

(a) Series hybrid drive train

(b) Parallel hybrid drive train

Figure 8 Classification of hybrid drive train

For the fuel cell hybrid vehicle, the fuel cell serves as the main energy source and the auxiliary sources as the energy buffer. Both of these sources supply power to the electric motor, which propels the vehicle. Based on the above analysis, fuel cell hybrid vehicle falls into the series hybrid vehicle's category.

2.2 Fuel cell based hybrid vehicles

The drive train of the fuel cell based vehicle is as Figure 9. As mentioned in Chapter I, the fuel cell stack needs to be integrated with at least four auxiliary components [5]: hydrogen supply system to the anode, air supply system to the cathode, de-ionized water serving as coolant in the stack cooling channel, and de-ionized water supply to the humidifier to humidify the hydrogen and the air flows.

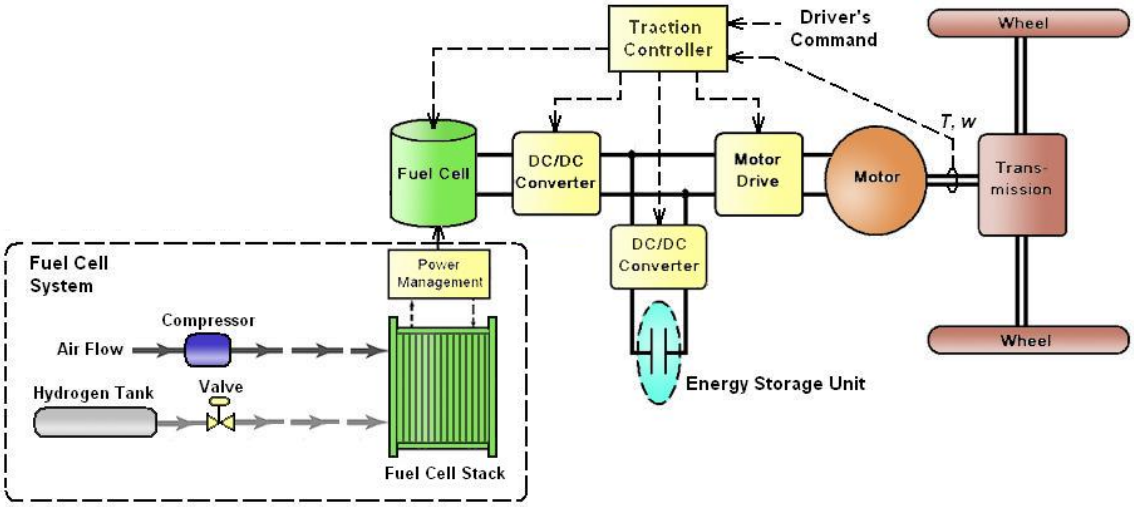

Figure 9 Fuel cell based hybrid vehicle

On the cathode side, the air flow first needs to be pressurized to a desired pressure level by the compressor. After leaving the compressor, the air flow is at a high temperature. Hence, the coolant is needed to reduce the air's temperature before it enters the stack. The humidifier is to add the humidity into the air to avoid the dehydration of the membrane. As the air leaves the stack, it carries the vapor produced in the fuel cell. The water separator is used here to recycle the water from the air. On the anode side, the hydrogen is released from the fuel tank. A valve is used to control its flow rate. Then the

hydrogen and air react in the stack generating electricity, water and heat. Because the temperature of the stack must maintain below 100 $^{\circ}C$ for the membrane to be humidified properly, the excessive heat is removed by the de-ionized water coolant. A power conditioner is usually needed at the output side of the stack because the fuel cell's typical characteristics are not suitable for the power converters or traction motors. There are a lot of research carried out about the power management integrated in the fuel cell system, such as the predictive control method [18, 19], fuzzy logic control [20, 21], feedback linearization method [23] and etc. The thesis won't go into details about the control over the fuel cell system. The conditioned power is then supplied to the DC bus and drive the vehicle.

Due to the fuel cell's relatively slow response which will be further explained in Chapter III, it's necessary to hybridize the fuel cell with the energy storage unit providing the peaking power during transients. The converters are responsible to balance the power flow among different sources and the motor. With motor working at various conditions, the request for different current will send to the fuel cell system. Then the corresponding amount of hydrogen will flow into the fuel cell stack according to the conditioning of the power management subsystem. Based on Equation (1.1), the amount of hydrogen is proportional to the fuel cell's output current. The more current the fuel cell is required to produce, the faster the hydrogen is flowing into the fuel cell stack. With the fuel cell providing the average power, the ultracapacitor serves as the local energy cache to quickly get charged and discharged. With the diversifying sources, their

different characteristics can be fully employed and the control strategy can be more flexible with more control freedoms.

2.3 Vehicle performance

The reason HEV/FCHV offers better performance than the conventional vehicle is that the ideal performance characteristics of the vehicle power train are quite similar to the electric motor's. But they don't match the characteristics of the internal combustion engine that well.

To achieve the optimum efficiency, the output power of the vehicular power plant is maintained the rating power over the entire speed range as shown in Figure 10. It requires the torque to vary with speed hyperbolically based on $P = T\omega$. During the low speed, the torque is restrained by its upper limit in consideration of the friction between the tire and the ground. So the torque keeps its maximum value during the low speed range, to meet the needs of acceleration, hill climbing and etc.

Figure 11 illustrates the power and torque characteristics of the internal combustion engine versus its speed, which is quite different from Figure 10. The torque is increasing smoothly from the idle speed, reaches its maximum at a certain speed and then starts to decrease. With higher speed, the torque drops more severely, which leads to the power reaches its highest point and then falls with the torque. It's obvious that the engine can't keep working at its rating power. And it is modified by utilizing multiple gears to contact the curve of the vehicle’s ideal as Figure 12.

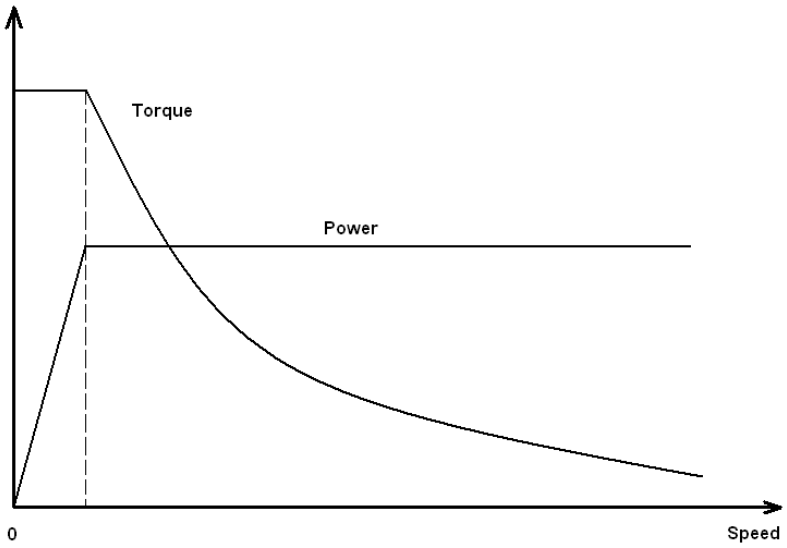

Figure 10 Ideal performance characteristics of the vehicle

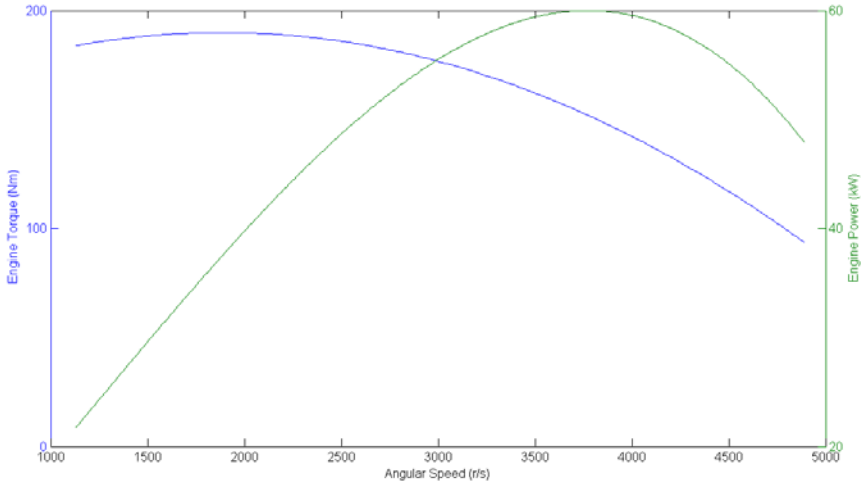

Figure 11 Performance characteristics of the engine

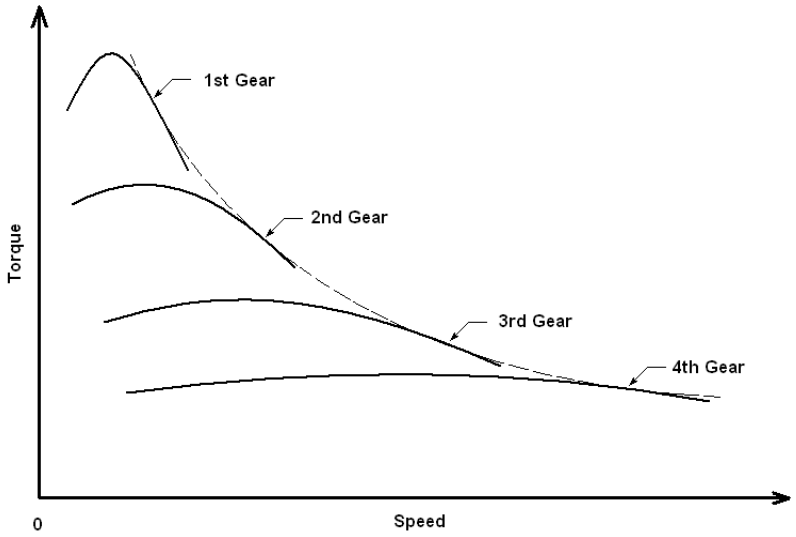

Figure 12 Multigear transmission system

On the other hand, the motor has remarkably similar characteristics with those of the vehicle power train depicted in Figure 13. The characteristics are obtained by employing the rated armature voltage and field flux control when the motor generates the full torque. In such control, the base speed, the normal armature voltage full field speed [3], is designed as 104 rad/s. From standstill to the base speed, the armature voltage control is employed, and the field is maintained constant at the rated value. When the speed reaches the base speed, the armature voltage can't be increased because it's increased to the rated voltage and can't go beyond that. Thus, the field weakening is utilized and enables the motor to reach the speed above the base speed. According to the above comparison, it's clear to see that the motor can provide the automobiles almost ideal performance, while the engine needs several gears to get close to the ideal performance.

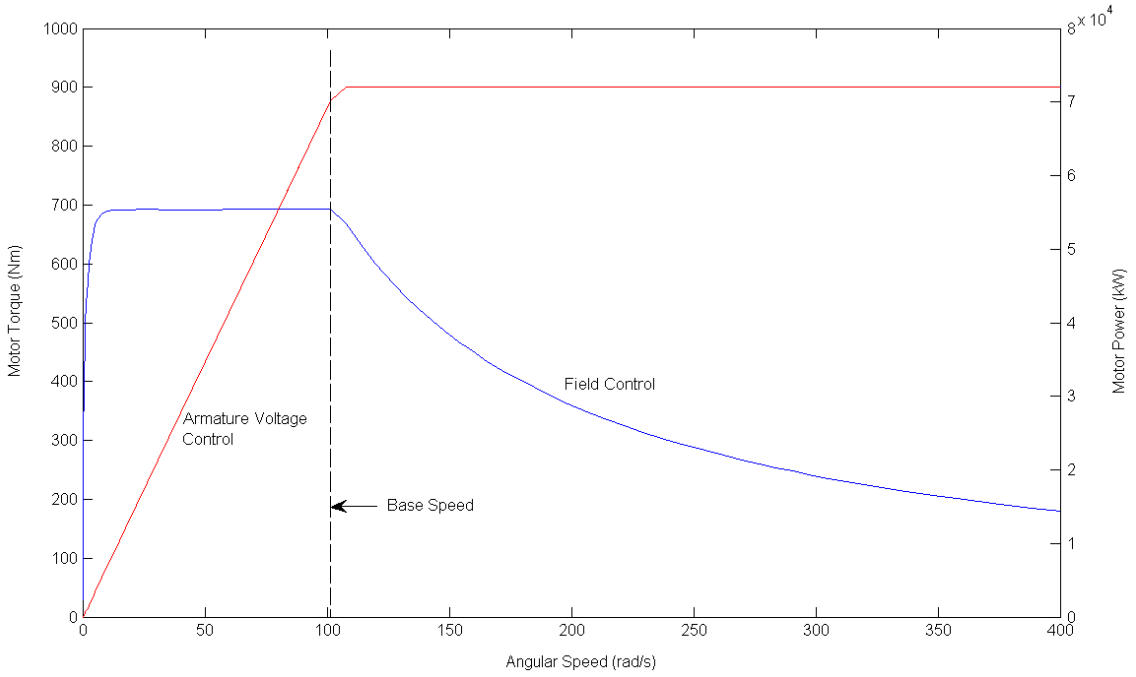

Figure 13 Performance characteristics of the motor

With the motor on board, its working condition is determined by the driver's torque command. Figure 13 shows the motor's performance when the driver hits the acceleration pedal of the car to its highest boundary, and the motor works at its rated power and generates certain speed. The driver's torque command can be quantified by q, the ratio of the angular degree of the acceleration or braking pedal pressed by the driver to the angle when the pedal is pressed to its limit,

$$q = \frac{Pedal's \quad Operational \quad Angle}{Pedal's \quad Max \quad Angle} \tag{2.1}$$

With different strength the driver applies to the pedal, the q varies from -1 to 1. The negative q indicates the force exerted on the braking pedal. Figure 14 and Figure 15 present the motor's performance with different force the driver steps on the pedal.

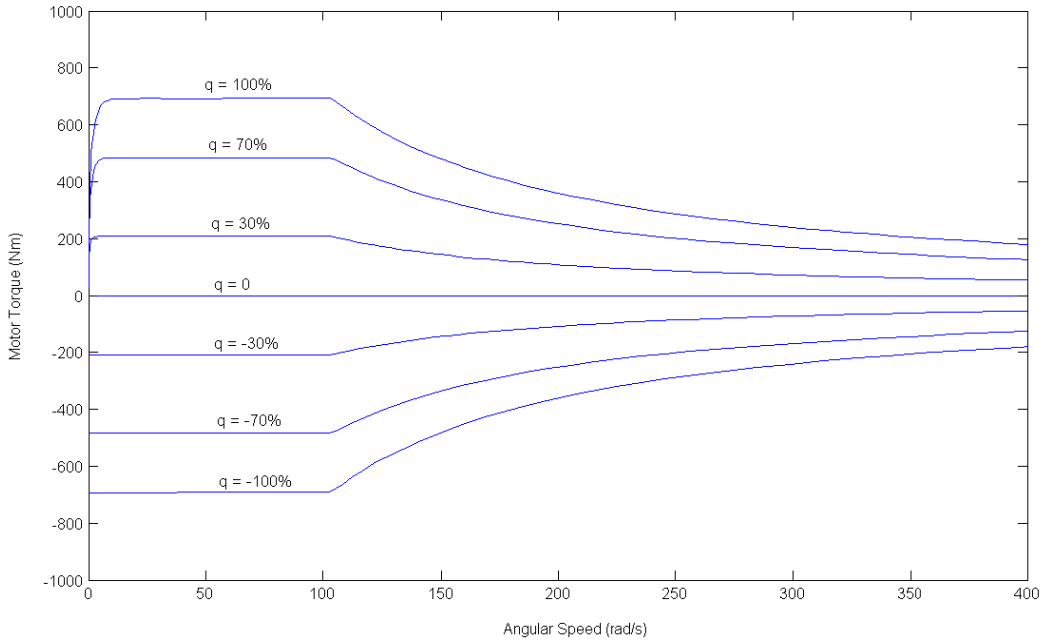

Figure 14 Torque generated by motor with different q

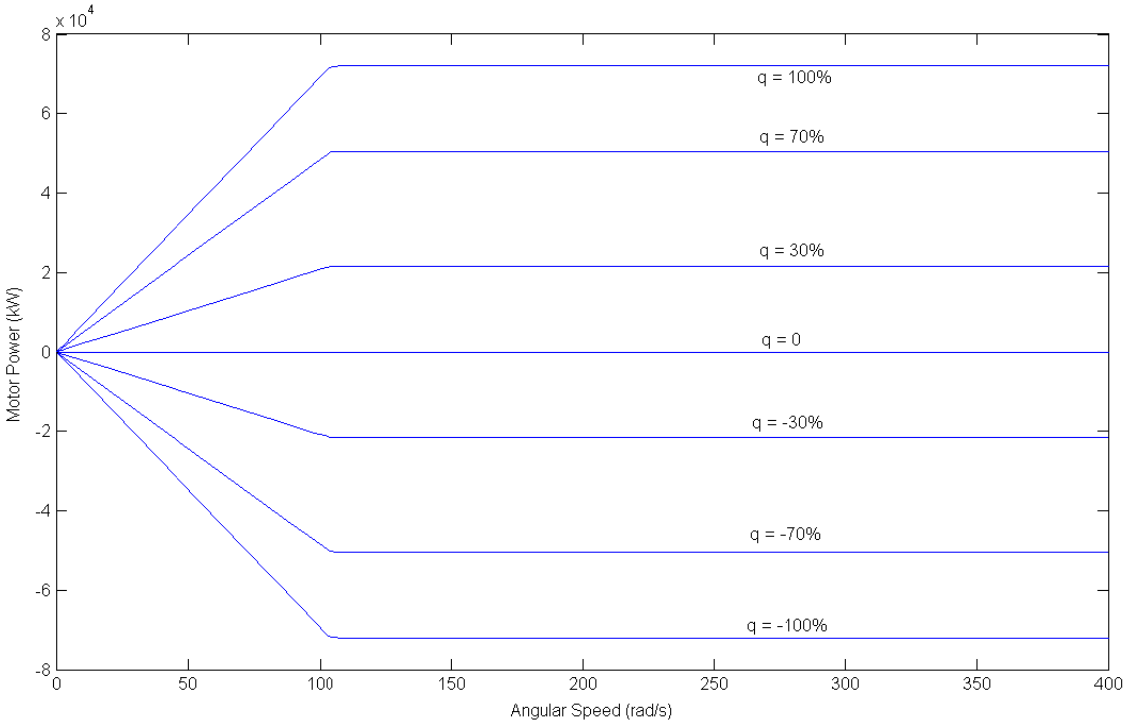

Figure 15 Power generated by motor with different q

Figure 14 and Figure 15 show that the torque and power generated by the motor decreases with the q, which means the motor generates less torque and consumes less power if the driver presses the acceleration pedal with less force. When q is negative, which means the driver steps on the braking pedal, the torque in Figure 14 and the power in Figure 15 are both negative, indicating that the torque is reversed and the motor works as a generator sending the power out. This control is accomplished by the motor drives integrated with the motor.

There are several criteria for the vehicle performance as follows [24].

2.3.1 Maximum speed

The maximum speed of the vehicle determines the rating power of the motor and the smallest gear ratio with a specific maximum speed of the motor. In the fuel cell hybrid vehicle, the maximum speed determines the rating power of the fuel cell and the ultracapacitor, which are the main factors of the drive train system costs.

Figure 16 illustrates the external forces acting on the vehicle. Based on Newton's second law, the traction of the vehicle F_t should always be larger than the total resistance acting on the vehicle so that the vehicle can move. When the traction equals the resistance, the maximum speed is reached. The resistance consists of the rolling resistance of the front tires F_{rf} and rear tires F_{rr}, the aerodynamic drag F_ω and the grading resistance F_g if there is a gradient α.

$$\begin{aligned} F_t &= F_{rf} + F_{rr} + F_\omega + F_g \\ &= Mgf\cos\alpha + \frac{1}{2}\rho_a C_D A_f V^2 + Mg\sin\alpha \end{aligned} \tag{2.2}$$

Where M is the total mass of the vehicle, V is the vehicle speed, f is the rolling resistance coefficient, ρ_a is the air density, C_D is the aerodynamic drag coefficient that characterizes the shape of the vehicle and A_f is the vehicle frontal area.

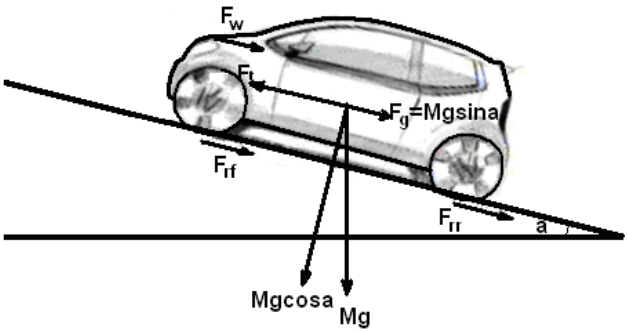

Figure 16 Force diagram of the automobile

From Figure 17, the maximum speed of the vehicle can be decided at different gradients, which is the intersection of the traction and the resistance.

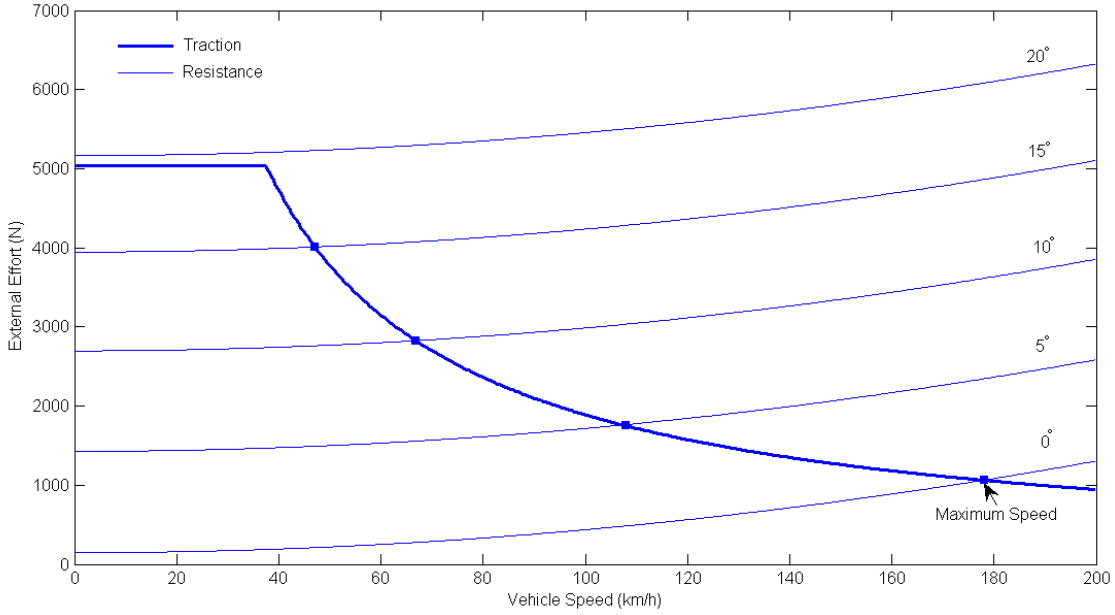

Figure 17 Traction and resistance of fuel cell hybrid vehicle

In this thesis, the maximum speed of the fuel cell hybrid vehicle is designed as 150 km/h. It can satisfy most customers' requirements and won't make the fuel cell rating power too large.

2.3.2 Gradeability

Gradeability is the steepness of a incline the vehicle can climb at a given speed. From Figure 13 and Figure 16 in the maximum speed analysis, one can see that the gradient is the predominant factor affecting the speed and the highest gearbox is required when encountering highest gradient. There are different rules to set the maximum road gradient in different area. But usually the highway gradient is less than 7%. The fuel cell hybrid vehicle is designed to climb at least 7% with full load.

2.3.3 Acceleration

The acceleration determines the maximum motor torque and the gear ratio. And it's often described by the acceleration time and distance covered from the zero speed to a certain high speed on the flat ground. According to Newton's second law, Equation (2.2) and $F_t = T_p i_0 i_g \eta_t / r_d$ [3], the acceleration of the vehicle is

$$a = \frac{dV}{dt} = \frac{F_t - F_r - F_\omega}{M\delta} = \frac{\left(T_p i_0 i_g \eta_t / r_d\right) - Mgf\cos\alpha - \frac{1}{2}\rho_a C_D A_f V^2}{M\delta} \tag{2.3}$$

Where T_p is the torque output from the power plant, i_0 is the gear ratio of the final drive, i_g is the gear ratio of the transmission, η_t is the efficiency of the driveline from the power plant to the driven wheels, r_d is the radius of the tire, and δ is the mass

factor, considering the equivalent mass increase due to the angular moments of the rotating components. For simplicity, δ =1.

Figure 19 shows the acceleration of multiple gear engine and electric motor. One can see that the motor's operation is much smoother than the engine's, because engine needs to switch gears to realize the full range acceleration.

2.3.4 Driving range

Driving range is an important factor affecting vehicles' versatility. With wider driving range, cars can be responsible for more than just commute, but also long distance road trip as customers' wish. Conventional automobiles can basically satisfy the driving range requirements because the specific energy of the fossil fuel is relatively high and the fossil fuel is very easy to refuel with the mature infrastructure. On the contrary, the driving range is one serious restrain upon electric vehicles because the battery's energy density is lower than the petroleum and it takes longer time to charge the battery, let alone lack of infrastructures to charge the battery by the road like gas stations. Hybrid electric vehicles make some improvements in driving range with the driving range extender, internal combustion engine. Still, charging the battery is an issue. As for fuel cell hybrid vehicle, since fuel cell is also highly energy-densified, similar to the petroleum's, and it's easy to refuel only if the gas station serves the alternative fuel, fuel cell hybrid vehicle's driving range is very competitive.

2.3.5 Noise

Noise of the automobile mostly comes from its power plant, tires and air resistance. Automobile manufacturers are inclined to lessen the vehicle mass to reduce

the resistance at the tires and design the vehicle in the shape to reduce the air resistance according to the aerodynamics. The power plant for conventional vehicle is mainly the internal combustion engine, and the fuel cell and motor for fuel cell hybrid vehicles. Fuel cell and motor are very quiet, while the internal combustion engine makes more noise, especially when the speed is low.

2.3.6 Pollution

As mentioned in Chapter I, the conventional vehicles burn fossil fuels, whose reservation is far less than the demands, and generate toxic CO, NO_x, and etc. Fuel cell hybrid vehicles use available hydrogen and oxygen as their alternative fuels, with competitive energy density as fossil fuels, and their only byproduct is water. So in terms of energy sustainability and pollution, the fuel cell hybrid vehicle is a better choice.

2.3.7 Handling/comfort

For the fuel cell hybrid vehicles, the heavy engine is replaced by several small components, such as the fuel cell and the motor, the vehicle is easier to control with less inertia. As previously mentioned, the fuel cell hybrid drive train is one type of series hybrid, which allows flexible positioning for optimum weight distribution. Unlike engines, motors can provide rating torque from zero speed and the rating power after reaching the base speed. So it avoids using multiple gears and can accelerate faster and smoother than engines. With zero emission and low noise, the driving experience is further enhanced.

2.3.8 Energy consumption

Energy consumption is the integration of the output power at the transmission

terminals. The energy consumption per unit distance is generally used to evaluate the vehicle energy consumption. For the EVs, HEVs and FCHVs, the energy consumption is measured by l/100 km (for liquid fuels) or kg/100 km (for gas fuels). However, for conventional vehicles, the commonly used unit for the energy consumption is a physical unit of fuel volume per unit distance, such as miles per gallon (mpg).

The energy consumption per distance of the FCHVs is much lower than that of the ICE vehicles. It's not only because the FCHVs have more than one energy source, i.e. the fuel cell in combination with the ultracapacitor in this thesis's case, but also because FCHVs can recover the braking energy from the motor, which saves great amount of energy and increases the system's efficiency.

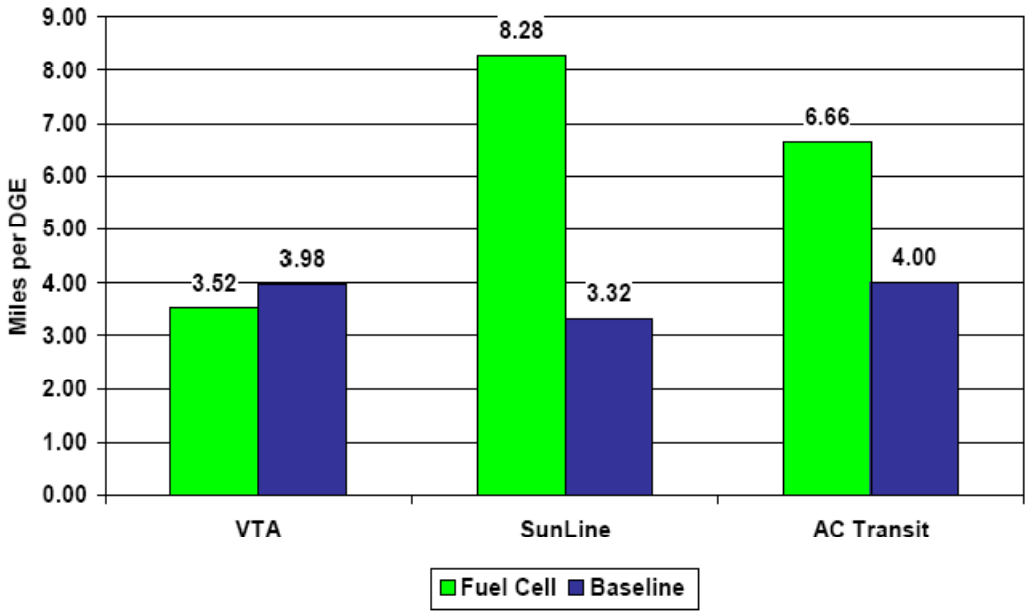

Figure18 Diesel gallon equivalent fuel economies for fuel cell and baseline buses

According to the technical report from the National Renewable Energy Laboratory [25] as in Figure 18, the fuel cell buses' fuel economy is much higher than the diesel baseline buses at the SunLine and AC Transit site. As for the VTA site, the fuel cell bus' fuel economy is lower because the fuel cell bus here isn't hybrid and can't benefit from the regenerative braking energy.

2.3.9 Vehicle mass

The vehicle mass has great influence on most of the criteria mentioned previously. Smaller vehicle mass leads to stronger gradeability, faster acceleration, wider driving range, less noise and lower energy consumption. Thus, the compact vehicle is desirable. It can be obtained by keeping the rating power of the fuel cell and the ultracapacitor small. Also, the motor with high power/mass ratio is selected.

2.3.10 Cost

The main problem of the fuel cell is its high cost and inability to supply enough power within short period, which will be explained in detail in Chapter III. And it's a major hurdle to commercialize the FCHVs. This thesis proposes the approach to assist the fuel cell to provide the peak power and reduce its rating power to lower the costs and achieve better performance.

2.4 Driving cycle description

The vehicle performances are evaluated based on the driving cycles. A driving cycle is a series of vehicle speed versus time. It varies with different locations and time period.

The most common driving cycles are the European NEDC and the American FTP-75. The FTP-75 (Federal Test Procedure) driving cycles are established in 1975 based on the road and vehicle conditions then as shown in Figure 20. With over 30 years development, the FTP-75 is not considered the most suitable driving cycle to conduct the emission test, energy consumption, and etc. due to its low speed and aggressive. LA92 (shown in Figure 19), the driving cycle based on the Los Angeles driving situations in 1992, is used more in vehicle performance analysis to address the FTP-75's shortcomings.

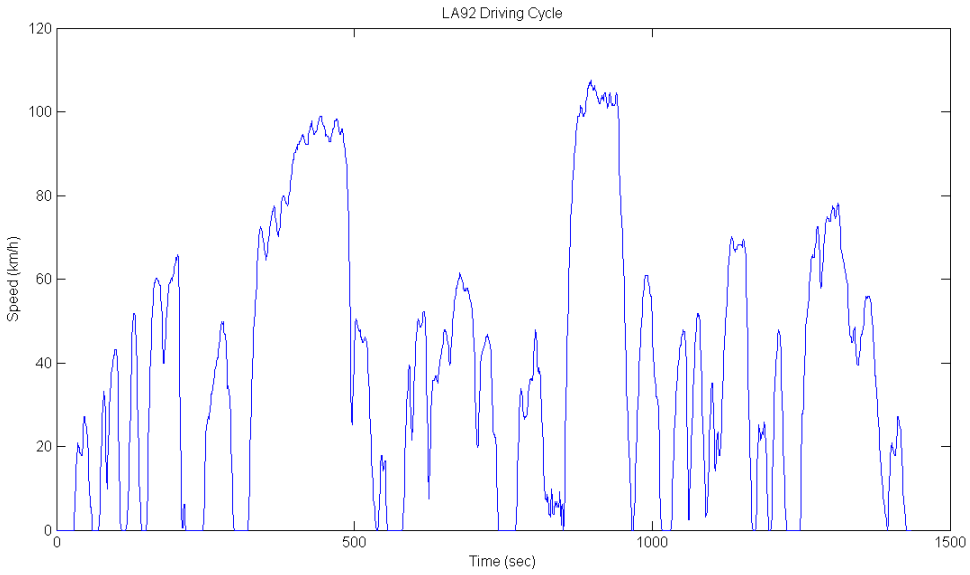

Figure 19 LA92 driving cycle

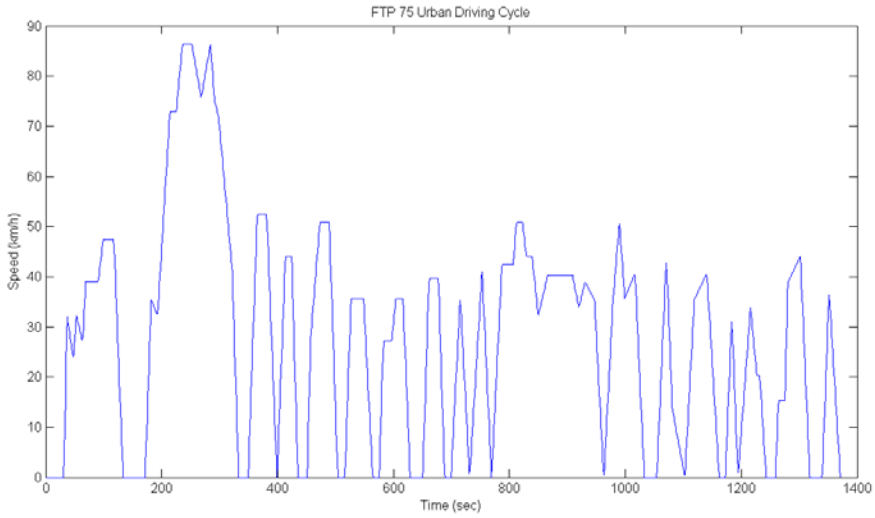

(a) FTP 75 urban driving cycle

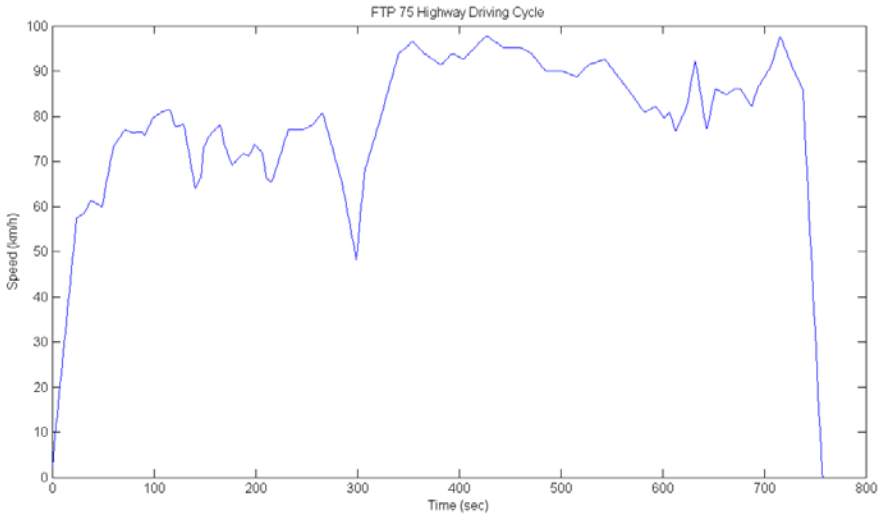

(b) FTP 75 highway driving cycle

Figure 20 FTP 75 driving cycles

CHAPTER III

CONFIGURATION OF THE ULTRACAPACITOR BOOSTED HYBRID ELECTRIC VEHICLE

3.1 Why hybridization

The fuel cell has been considered one of the most promising alternative energy sources to power the vehicle because of its high energy density, excellent performance, and zero emissions if using hydrogen fuel. A lot of fuel cell research and development are carried out. The main obstacle of the fuel cell vehicle commercialization is the high cost of the fuel cell. It can be reduced by hybridizing the fuel cell with the auxiliary sources, so that the size and volume of the fuel cell can be brought down as well as its costs. Additionally, the fuel cell can only operate efficiently within a specific range as Figure 6 described. In order to maintain fuel cell's high efficiency and optimize the whole system's efficiency, the fuel cell is expected to work in the high efficiency range. Beyond that, auxiliary sources are needed to balance the power flow. Therefore, hybridization of the fuel cell would improve the vehicle's efficiency, performance and reduces costs.

There are several hybrid configurations of the drive train as shown in Figure 21. The fuel cell can be combined with the battery, the ultracapacitor or both. The thesis concludes that the drive train design comprising with the fuel cell and ultracapacitor is the most economic and effective way. The reasons are analyzed as follows.

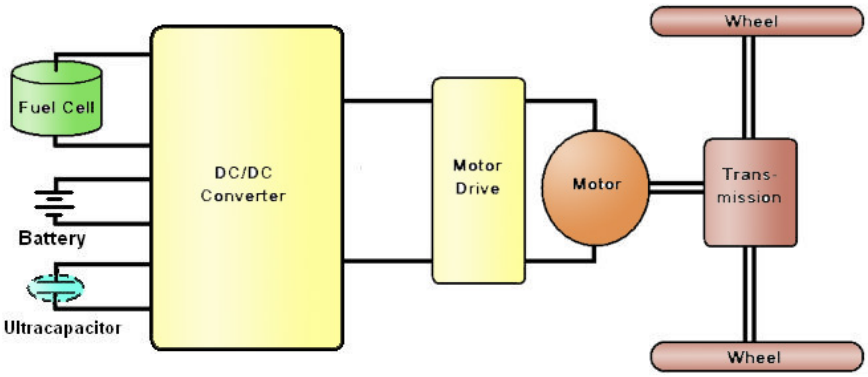

(a) Fuel Cell, battery and ultracapacitor power the drive train

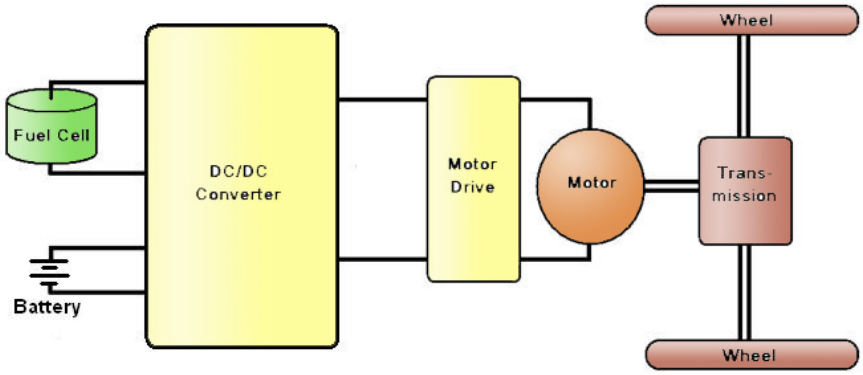

(b) Fuel cell and the battery power the drive train

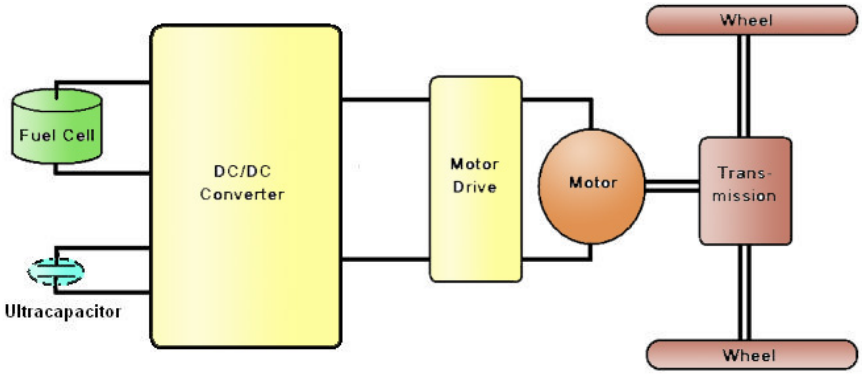

(c) Fuel cell and ultracapacitor power the drive train

Figure 21 Drive train structures of fuel cell hybrid vehicle

3.1.1 For fuel cell

The Ragone chart shows characteristics of the fuel cell, ultracapacitor and electrochemical battery compared with gasoline engine as in Figure 22. From it, we can see that the fuel cell's energy density is very high, comparable with the engine's. That means the fuel cell can provide the similar driving range as the engine does. The battery's energy density is much lower than the fuel cell and the engine. It also becomes the main roadblock of the pure electric vehicle because it leads to a short driving range and can't meet the customers' needs. The energy density of the ultracapacitor is extremely low. It barely can provide any sustained energy. Consequently, the ultracapacitor is not a great choice to serve as the main energy source for the drive train. Certain research has been conducted with ultracapacitor as the main source [26]. But the car can't drive long as a result of the ultracapacitor's fast charging and discharging nature. By comparing the different sources, it's concluded that the fuel cell is the most suitable replacement for the internal combustion engine.

Besides the fuel cell's high energy density, the fuel cell has intrinsically higher efficiency than the internal combustion engine. Because, in the fuel cell, the chemical energy is directly transferred into electric energy. For the internal combustion engine, the reactants need to burn up first and then produce the power mechanically. There is always some extra power loss in the thermal reactions. The fuel cell has reached 50 – 60% efficiency, while the internal combustion engine only has 10 – 30 % efficiency. From the efficiency's perspective, the battery shares the common with the fuel cell. The battery is also an electrochemical source with potentially higher efficiency than the internal

combustion engine. The ultracapacitor has the highest efficiency among all of them due to its electrostatic property.

Another advantage of the fuel cell is that it's fed by the fuel externally as the engine. It enables the fuel cell to refuel conveniently, based on the current gas filling infrastructures. As for the battery, its reaction consumes the chemicals inside the battery. It will be depleted at some point and need to be replaced. From this point of view, the fuel cell can be considered with longer life time than the battery. The ultracapacitor also has long life time because it can charge and discharge quickly by sending and receiving electrons without any consumptions.

Another advantage the fuel cell, the battery and the ultracapacitor over the engine is that they are environmentally friendly. They are independent of petroleum and don't have any emissions. Therefore, they have more sustainable and promising futures.

From the above analysis, the fuel cell is selected as the main source of the drive train in the thesis because of the following factors.

- High efficiency with direct chemical energy transferred into electricity
- High specific energy compared to engine and other power sources
- Zero emission with water as its only byproduct
- Liquid fuel can be charged with current infrastructure

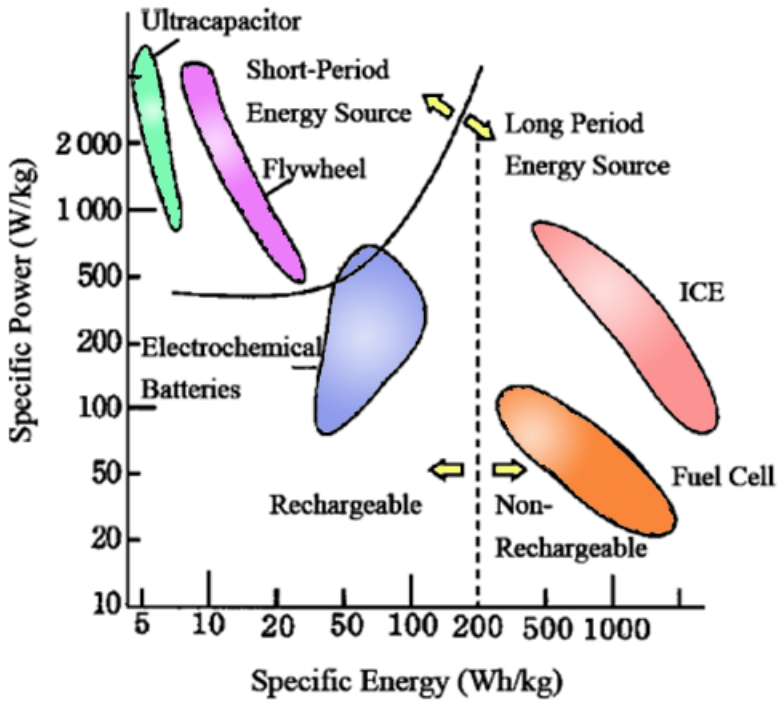

Figure 22 Characteristics of various sources

Whereas, there are some drawbacks of the fuel cell. As shown in Figure 22, the power density of the fuel cell is very low. When there is a transient high power requirement, such as an acceleration or cold start, the fuel cell can't provide that large amount of power. But the ultracapacior is shown with extremely high power density. So the ultracapacitor is capable of supplying pulse energy within a short time. While the battery has higher power density than the fuel cell but lower than the capacitor, the battery can provide high power, just not as high as the ultracapacitor with the same size.

Figure 22 also shows that the fuel cell is not rechargeable. It can only send out power. But the ultracapacitor and the battery are rechargeable. With them on board, the kinetic energy won't be wasted but can be transferred into electric energy and recaptured

by the ultracapacitor or battery. That will save the energy and improve the system's efficiency, especially in urban area.

Although the fuel cell is potentially more efficient than the internal combustion engine, this high efficiency can't stay throughout its entire operation range as shown in Figure 6. When the net current density is low or extremely high, the fuel cell system's efficiency is low. With low net current density, the low efficiency is generated because all the other accessories, like the compressor and pump, still need to work even the output power is low. The efficiency is low at high current density is due to the low voltage the fuel cell can generate and low output power. So the fuel cell can only reach the high efficiency within a specific range. In order to improve the whole system's efficiency, the fuel cell is expected to work in its high efficiency range as shown in Figure 6. For the low efficiency range, other auxiliary sources are needed to assist the fuel cell to meet the loads' requirement.

Another disadvantage of the fuel cell is that it lacks dynamic operation capability due to the time it'll take in its chemistry reaction. If the fuel cell current is mandated to change a large amount within a short period, the stack voltage will drop dramatically because the chemical action can't take place fast enough to track the current. It's called the fuel starvation as shown in Figure 23. The fuel starvation is undesirable because it causes the flow oscillation and impacts the equipment's lifetime. The sources with quick response would smooth fuel cell's performance and avoid the fuel starvation.

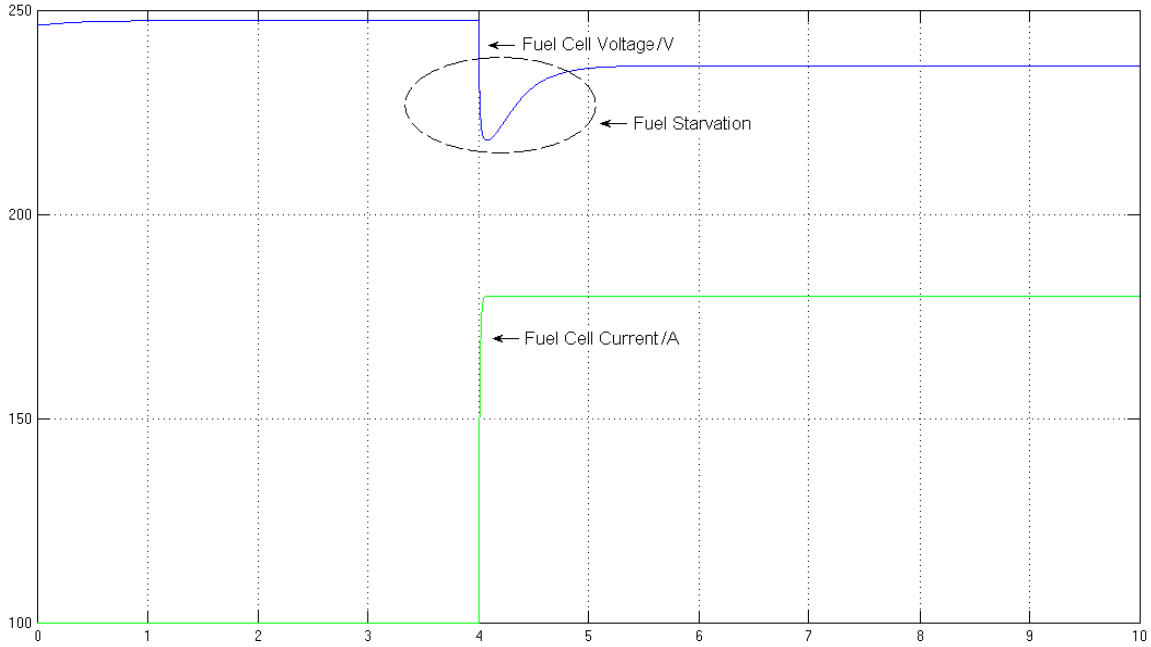

Figure 23 Fuel starvation

The last but not the least, the fuel cell is expensive. It's the major cost in the fuel cell vehicle. If the fuel cell's size and volume can be brought down, it would save a huge amount of costs for the fuel cell and the vehicle system.

Therefore, the disadvantages of the fuel cell and the needs for hybridization are:

- Low power density compared to engine and other power sources
- No bidirectional energy flow
- Low efficiency at very light load
- Slow start dependent on temperature
- Relatively high costs compared with engine and ultracapacitor

3.1.2 For ultracapacitor

Based on the above analysis, the ultracapacitor is more suitable to hybridize with the fuel cell than the battery, although both of them can provide peaking power and absorb the regenerative braking energy. The reasons are as follows.

Firstly, the ultracapacitor has higher power density than the battery. The major role of the auxiliary source is to supply the peaking power the fuel cell can't provide. With higher power density, the ultracapacitor can provide more peaking power than the battery, so that it can further decrease the fuel cell's rating power and its cost.

Additionally, the ultracapacitor can be quickly charged and discharged with its static electricity characteristic. It enables the ultracapacitor to instantly respond to the loads' varying. The battery can't achieve that because of the electrochemical reaction happening inside. The electrochemistry reaction always takes some time to take place and the speed of the reaction time also depends on the surrounding temperature.

Furthermore, the ultracapacitor has much longer life than the battery owe to its electrostatic property. The ultracapacitor charges and discharges by storing or releasing electrons on the surface of the ultracapacitor's layers. For the battery, the electrochemical reactions are always undergoing internally when it sends out or absorbs energy. The material consumption and structure degradation are much more severe for the battery than for the ultracapacitor.

Therefore, in this thesis, the ultracapacitor is integrated into the fuel cell vehicle system to drive the vehicle. The hybrid architecture gives several advantages.

- Improves the fuel cell's operating efficiency

- Overcomes the fuel cell's transient deficiency
- Captures the motor's regenerative braking energy
- Reduces the fuel cell's size and improves the system's efficiency
- Enhances the vehicle's performances

3.2 Converter configuration

The load power varies randomly in actual operation corresponding to frequent acceleration, deceleration, and climbing up and down grades, as shown in Figure 4. The load power can be decomposed into steady (average) power, which has a constant value, and dynamic power, which has a zero average as Figure 24 [3].

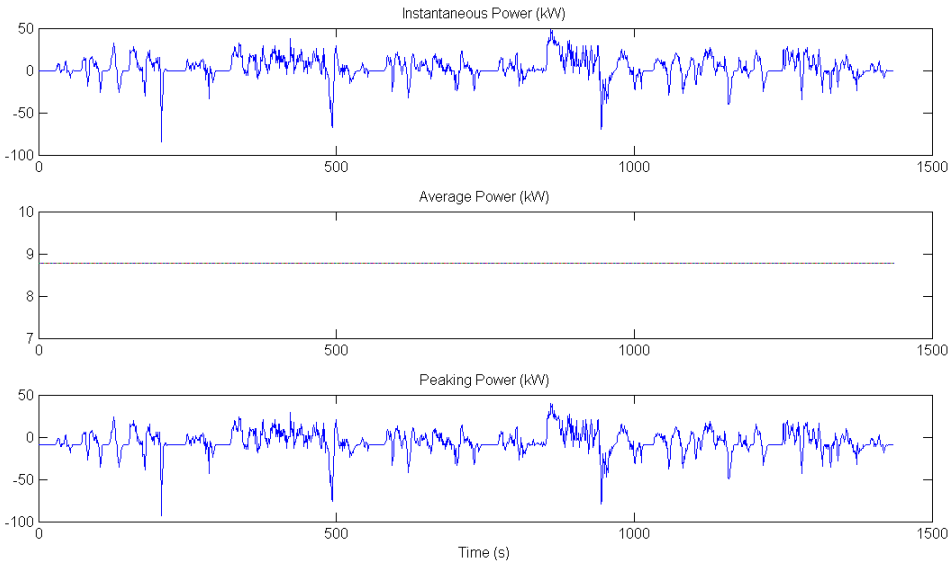

Figure 24 Decomposition of load power into average power and dynamic power

In order to achieve high overall efficiency, it's essential to operate each power train in its optimal efficiency region. So we can assign the fuel cell favoring steady state operation to supply average power, and the ultracapacitor with quicker response to

develop dynamic power. Since average power is much less than peak power, the power rating and cost of the fuel cell, are correspondingly reduced.

Therefore, there are four modes for the fuel cell and ultracapacitor to operate.

Mode 1: Fuel cell delivers power to the load. When the power the load needs is within the average power's range, fuel cell can supply this amount of power without any assistance and keep high efficiency.

Mode 2: Fuel cell charges the ultracapacitor and supplies the load. When the load demands less power than the average, fuel cell will still supplies the average power to maintain high efficiency. Part of the fuel cell's power goes to the load to meet its needs, and the rest of the power charges the ultracapacitor to help them keep their voltage level for future use.

Mode 3: The load draws the power from both the fuel cell and the ultracapacitor simutaneously. When the vehicle is accelerating or cold-starting, it expects a large amount of power in a very short time. On this occasion, fuel cell's average power can't meet the load needs. Ultracapacitor releases its power to the load simultaneously.

Mode 4: Ultracapacitor recapture the braking energy from the load. When the vehicle is braking, the motor's kinetic energy is transferred to the electrical energy. At this time, the motor acts as the generator and ultracapacitor are able to absorb the regenerative braking energy to increase the system's efficiency. Since fuel cell can't absorb the energy, it shuts down to save energy.

3.2.1 Passively connected fuel cell and ultracapacitor

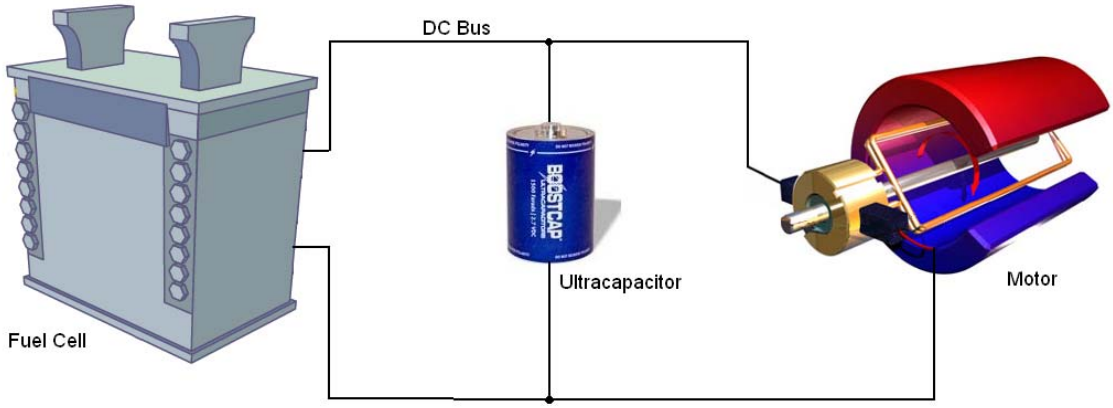

Figure 25 Passive hybrid configuration

Passive hybrid is the simplest hybrid configuration shown in Figure 25. The fuel cell and the ultracapacitor are connected directly to the load. The fuel cell provides the steady state power to the motor. Ultracapacitor can discharge to provide the auxiliary power when acceleration or cold-start. They can also get charged when the motor is regenerative braking or the fuel cell provides more power than the load needs. Additionally, the ultracapacitor can function as the current filter of the fuel cell. Basically, the passive hybrid configuration can realize the 4 modes of operations.

Although it achieves the minimum components' goal, passive hybrid configuration imposes severe restrictions upon the fuel cell, ultracapacitor and the load. This configuration equates the nominal voltage of the fuel cell to that of the ultracapacitor. And the power distribution among the three key components is determined by their impedance. Thus, not only the fuel cell and the ultracapacitor are mandated to be large enough, but also the power flow in this system is completely

passive. The latter issue will bring in a lot of problems, such as intensive current and voltage stresses on the components from the highly dynamic oscillation, fuel starvation of the fuel cell with transients forced upon it, power depletion or overflow of the ultracapactor , unregulated power rushing into the motor and so on. Without any control freedom in the system, the power management can't be achieved, and the devices in the system can't be fully made use of.

3.2.2 Ultracapacitor connected through a converter

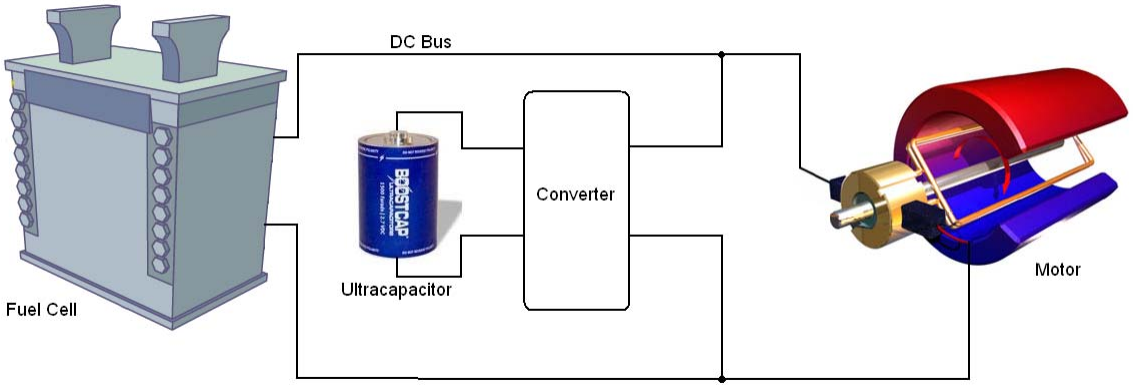

Figure 26 Ultracapacitor is connected to the DC bus through a converter

In Figure 26's configuration, the ultracapacitor connects to the DC bus through a converter, while the fuel cell connects to the DC bus directly. Based on the four modes operation above, the bidirectional converter is indispensible for the interface between the ultracapacitor and the DC bus. Additionally, in order to reduce the ultracapacitor volume and size, their rating voltage is designed to be lower than the motor's rating voltage. By utilizing a boost converter, the ultracapacitor can boost its voltage to the motor's voltage

level when they're discharging. Similarly, a buck converter is used when the ultracapacitor are charged from the load.

However, the direct connection of the fuel cell to the DC bus equates the fuel cell's voltage to the voltage of the DC bus, which is relatively high. In order to accomplish this, the fuel cell's size and volume have to be large enough to observe the voltage restriction. Considering the high cost and weight of the fuel cell, it's not worth to eliminate the converter at the fuel cell's end. Moreover, the fuel cell is easily affected by the highly dynamic operation of both the ultracapacitor and the motor without the converter's protection.

3.2.3 FC connected through a converter

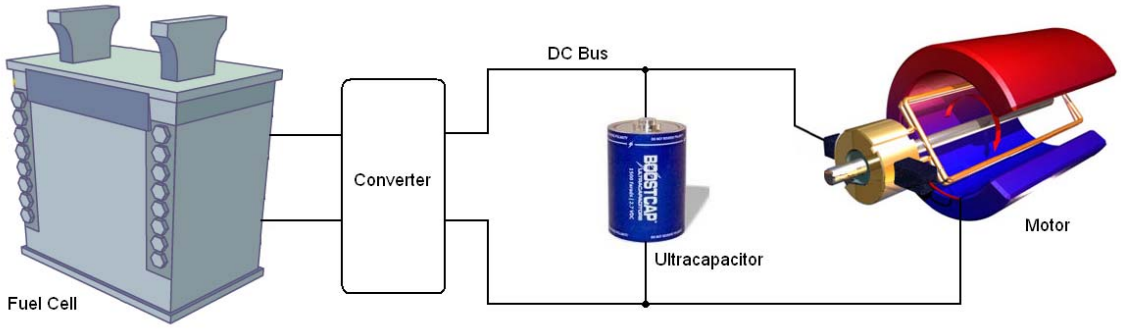

Figure 27 Fuel cell is connected to the DC bus through a converter

Figure 27 depicts the configuration of the fuel cell connected to the DC bus through a converter and the UC connected the DC bus directly. The converter is unidirectional for the fuel cell only sends the power and not absorbs any. In this case, the fuel cell's voltage and current can be controlled with this converter. So the fuel cell's voltage can be made smaller than the load to reduce the weight and costs. It's

compensated by employing a boost converter between the fuel cell and the DC bus. But with the direct connection of the UC to the DC bus, UC's voltage has to equal the load's voltage. Besides, the current division between the UC and the load is uncontrollable, which is predetermined by their impedance. Hence, this configuration has several limitations in achieving the best performance of the system.

3.2.4 Both fuel cell and ultracapacitor connected through converters

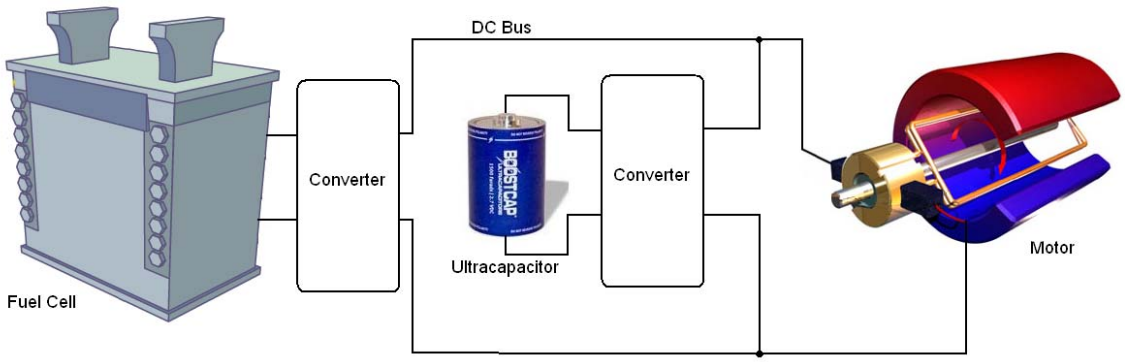

Figure 28 FC and UCs are connected to the DC bus through converters

On the basis of the previous analysis, it's necessary to connect converters to both the fuel cell and the ultrcapacitors to fully utilize the capacity of them and reach the optimum efficiency of the system.

The fuel cell is responsible for generating the average power to the load, so a unidirectional converter is selected. Its nominal voltage of the fuel cell is usually lower than that of the motor, i.e. the voltage on the DC bus. So it's more inclined to employ the boost converter to connect the fuel cell to the load. Besides, lower voltage fuel cell has fewer cells in the fuel cell stack, resulting in a smaller fuel cell and lower costs.

The ultracapacitor is the energy storage unit. When the load asks for average power, only the fuel cell works. If the power required from the load is larger than the average power, both of the fuel cell and the ultracapacitor provide power to meet the needs. Otherwise, if the power demanded by the load is smaller than the average power, fuel cell's power not only goes to the load but also charges the ultracapacitor. When motor is breaking, the ultracapacitor absorb the regenerative energy to improve the system's efficiency. According to the ultracapacitor's function, a bidirectional converter is needed. It allows ultracapacitor to charge and discharge in different scenarios. Like the fuel cell, the rating voltage of the ultracapacitor is generally lower than the motor's voltage. Or it's expected to be lower so that the volume and size of the ultracapacitor can be made smaller and the costs are reduced. So when the power is transferred from the high-voltage DC bus to the low-voltage ultracapacitor, a buck converter is demanded. When the power is delivered from the ultracapacitor to the DC bus, the voltage is step-up, and a boost converter is needed.

To satisfy all the specifications above, this thesis proposes the following converter topology with only three switches as Figure 29. The operation voltage of the DC bus is designed to be 400V, which will be derived in Chapter IV. With this voltage level, no electrical isolation is needed. Hence, the fuel cell and ultracapacitor are connected to the DC bus through converters without transformers. With higher frequency, the current ripple of the fuel cell and the ultracapacitor is reduced to extend the devices' lifetime, but the power loss of the switching goes higher. Hence, the frequency is tradeoff as 20 kHz for all the three switches. Corresponding to this

frequency, power MOSFETs are selected for their high current switching capability and low ON resistance. Therefore, the power losses are further reduced at the switches. The inductor in the ultracapacitor's converter L_{UC} is designed to be much smaller than the inductor of the fuel cell's converter L_{FC}, so that the ultracapacitor can perform more dynamically and meet the transient power needs. On the other hand, the inductance L_{FC} is designed to reduce the current ripple of the fuel cell in order to provide better performance and prolong fuel cell's life time.

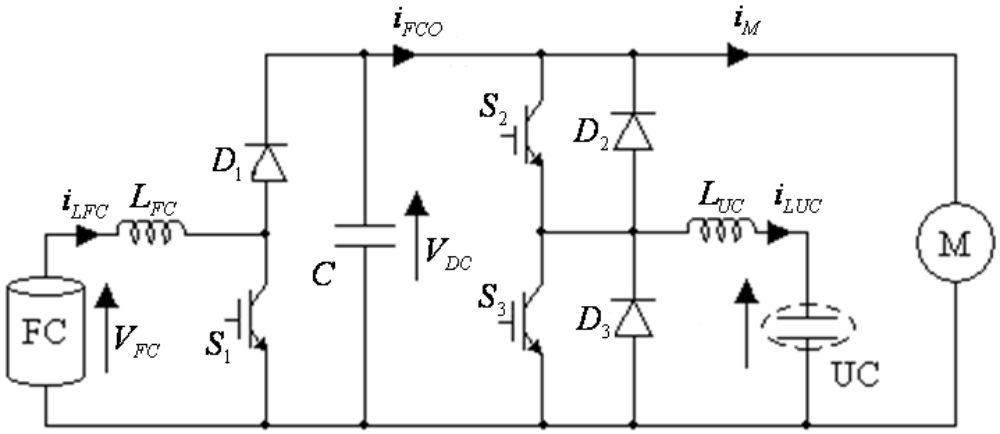

Figure 29 Proposed converter topology

CHAPTER IV

VEHICLE DRIVE TRAIN DESIGN METHODOLOGY

4.1 Motor parameter design

The vehicle parameters are determined based on a mid-size passenger vehicle as shown in Table 2.

Table 2 Vehicle design specifications

Structure Parameters	
Vehicle mass (M)	1500 kg
Rolling resistance coefficient (f)	0.01
Aerodynamic drag coefficient (C_D)	0.3
Vehicle frontal area (A_f)	2 m^2
Tire radius (r)	0.2794 m
Transmission efficiency (η_t)	0.95
Motor efficiency (η_m)	0.9
Fuel cell efficiency (η_{fc})	0.55
Performance Parameters	
Vehicle maximum speed ($v_{\max}$)	150 km/h
Maximum gradeability	30% at low speed and 5% at 100 km/h
Acceleration time from 0 to 100 km/h (t_a)	10 s

Based on the above specifications, we can select the DC motor with maximum angular speed $\omega_{\max} = 4000$ rpm and X factor of 4. So the base speed $v_b = \frac{v_{\max}}{4} = 37.5$ km/h.

It is difficult to directly design the motor power from the acceleration performance specified. It is necessary to make a good estimate based on specified acceleration requirements, and then make a final design through accurate simulation. As an initial estimate, one can make the assumption that the steady-state load (rolling resistance and aerodynamic drag) is handled by the fuel cell and the dynamic load (inertial load in acceleration) is handled by the ultracapacitor. With this assumption, acceleration is directly related to the torque output of a motor by

$$P_t = \frac{\delta M}{2t_a}\left(V_f^2 + V_b^2\right) + \frac{2}{3}MgfV_f + \frac{1}{5}\rho_a C_D A_f V_f^3 \tag{4.1}$$

where t_a is the expected acceleration time in second, V_b is the vehicle base speed in m/s, V_f is the final speed of the vehicle accelerating in m/s, and δ is the mass factor.

With the given parameters in Table 2 and equation (4.1), the power rating of the motor is

$$\begin{aligned} P_t &= \frac{1.05\times 1500}{2\times 10}\left(\left(\frac{100}{3.6}\right)^2 + \left(\frac{37.5}{3.6}\right)^2\right) + \frac{2}{3}\times 1500\times 9.8\times 0.01\times\frac{100}{3.6} \\ &\quad + \frac{1}{5}\times 1.205\times 0.3\times 2\times\left(\frac{100}{3.6}\right)^3 \\ &= 75.13kW \end{aligned} \tag{4.2}$$

According to the above analysis, the motor drive power rating can be obtained as 75.13 kW for the specified acceleration time of 10 sec from zero to 100 km/h. Figure 30 shows the speed-force and speed-power profiles of the motor.

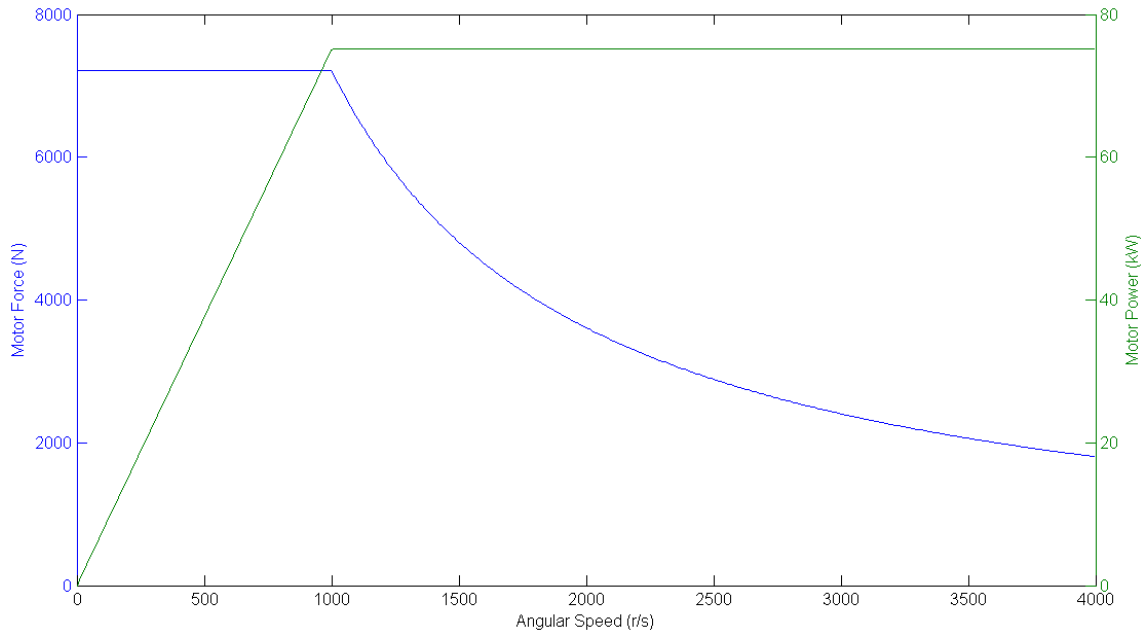

Figure 30 Characteristics of traction motor vs. vehicle speed

The gear ratio is designed such that the vehicle reaches its maximum speed at the motor maximum speed, that is

$$i_g = \frac{\pi n_{m,\max} r}{30 v_{\max}} \tag{4.3}$$

where $n_{m,\max}$ is the maximum motor rpm and $v_{\max}$ is the maximum speed of the vehicle in m/s. With the previous motor selection, $n_{m,\max}$ = 4000 rpm, $v_{\max}$ = 41.7 m/s (150 km/h or 93.75 mph) and r = 0.2794 m (11 in.),

$$i_g = \frac{\pi \times 4000 \times 0.2794}{30 \times 41.7} = 2.81 \tag{4.4}$$

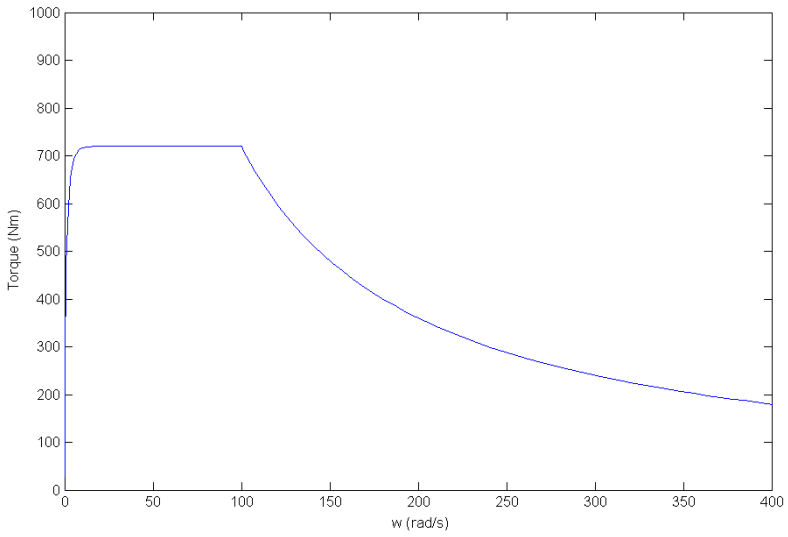

(a) Torque vs. angular speed of the DC motor

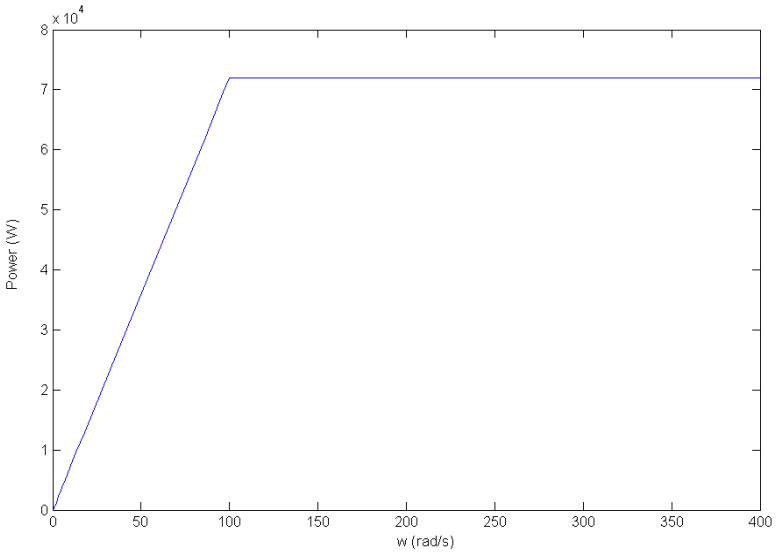

(b) Power vs. angular speed of the DC motor

Figure 31 Operation characteristics of the DC motor

To ensure the motor to work in the most efficient way discussed in Chapter II, the DC motor's rated torque and power versus motor's angular speed is as Figure 31. When the angular speed $\omega <$ 100 rad/s, the preset base speed, the voltage increases linearly to provide the linearly increasing power. The armature voltage changes as Figure 32.

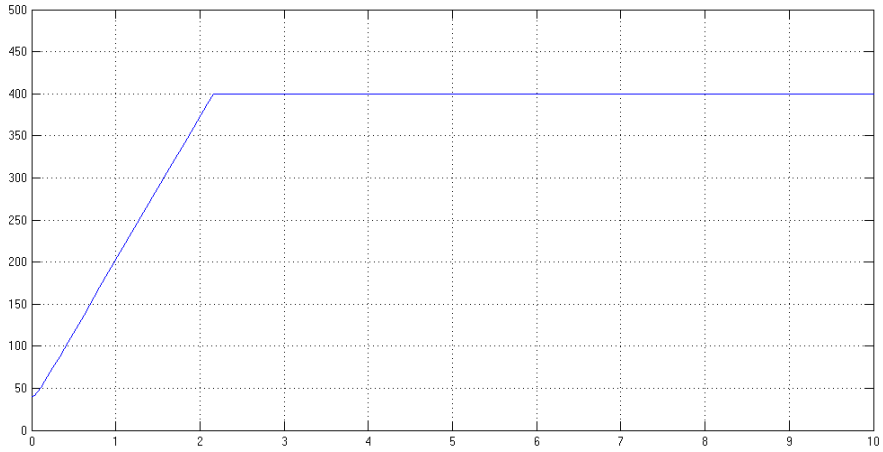

Figure 32 Reference voltage of the FC boost converter

4.2 Design of fuel cell power capacity

The fuel cell should be able to supply sufficient power to support the vehicle operation at normal constant speeds both on a flat and a mild grade road without the help of the ultracapacitor. At the same time, the fuel cell should be able to produce an average power that is larger than the average load power when the vehicle operates with a stop-and-go operating pattern.

The single cell's voltage is usually lower than 1V due to the fundamental electrochemical limitations [27]. To drive the vehicle and serve as the primary source of the vehicle, the individual fuel cells can be connected in series-parallel format to reach

the desired current and voltage values. The fuel cell's current is proportional to the active electrode area, so the fuel cell can be connected in parallel to increase the active electrode area and meet the current requirement. For the voltage demand, the fuel cells can be connected in series to change the stack's output voltage level.

At a constant speed and on a flat road, the power output from the fuel cell can be expressed as

$$P_{fc} = \frac{V}{1000\eta_t\eta_m}\left(Mgf + \frac{1}{2}\rho_a C_D A_f V^2\right)(kW) \tag{4.5}$$

where M is the total mass of the vehicle, V is the vehicle speed, η_t and η_m are the efficiency of the transmission and motor respectively, f is the rolling resistance coefficient, ρ_a is the air density, C_D is the aerodynamic drag coefficient that characterizes the shape of the vehicle and A_f is the vehicle frontal area.

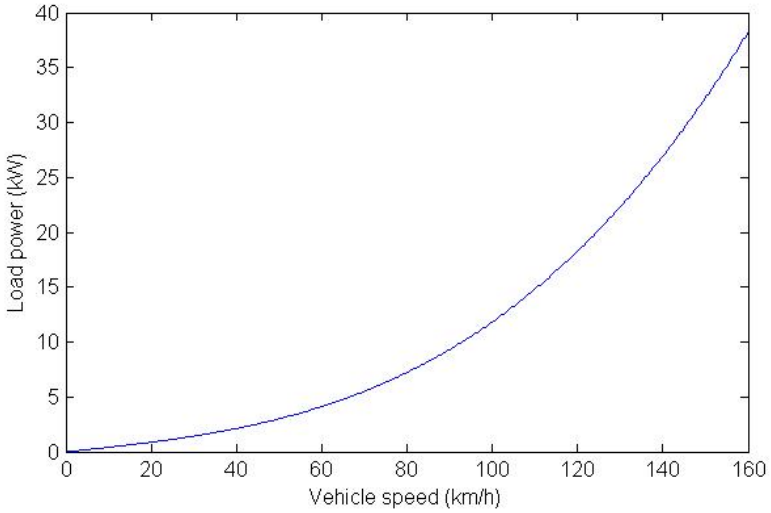

Figure 33 Fuel cell power required at constant speed on a flat road

Figure 33 shows the load power (not including η_t or η_m) versus vehicle speed for the given example conditions. In this example, about 25kW are needed at 130 km/h of constant speed driving.

Considering the inefficiency of the transmission and motor drive, the power output of the fuel cell system is about 20 to 25% more than that shown in Figure 33.

In this design, the fuel cell motor power is expectd to support the vehicle driving at around 150 km/h on a flat road and 100 km/h on a 5% grade road.

At 150km/h on flat road, fuel cell power needed is:

$$\begin{aligned} P_{fc} &= \frac{V}{1000\eta_t\eta_m}\left(Mgf + \frac{1}{2}\rho_a C_D A_f V^2\right) \\ &= \frac{150}{3.6\times 1000\times 0.9\times 0.95}\cdot\left[1500\times 9.8\times 0.01 + \frac{1}{2}\times 1.205\times 0.3\times 2\times\left(\frac{150}{3.6}\right)^2\right] \\ &= 37.75kW \end{aligned} \tag{4.6}$$

At 100km/h on 5% grade road, fuel cell power needed is:

$$\begin{aligned} P_{fc} &= \frac{V}{1000\eta_t\eta_m}\left(Mgf + \frac{1}{2}\rho_a C_D A V^2 + Mgi\right) \\ &= \frac{100}{3.6\times 1000\times 0.9\times 0.95}\times[1500\times 9.8\times 0.01 + \frac{1}{2}\times 1.205\times 0.3\times 2\times\left(\frac{100}{3.6}\right)^2 \\ &\quad + 1500\times 9.8\times 0.05] \\ &= 37.72kW \end{aligned} \tag{4.7}$$

In order to satisfy this specification, the maximum power of the fuel cell is designed as 37.75kW.

When the vehicle is driving in a stop-and-go pattern in urban areas, the power that the fuel cell produces should be equal to or slightly greater than the average load power in order to maintain balanced peaking power source energy storage. The average load power can be expressed as

$$P_{ave} = \frac{1}{T}\int_0^T \left(Mgf + \frac{1}{2}\rho_a C_D A_f V^2 \right) V dt + \frac{1}{T}\int_0^T \delta M V \frac{dV}{dt} dt \,. \tag{4.8}$$

where the vehicle mass factor, δ, is a constant. The first term in equation (4.8) is the average power that is consumed to overcome the tire rolling resistance and aerodynamic drag. The second term is the average power consumed in acceleration and deceleration. When the vehicle has the ability to recover all of the kinetic energy of the vehicle, the average power consumed in acceleration and deceleration is zero. Otherwise, it will be greater than zero.

With equation (4.8), we can get accelerating the vehicle from zero speed to 100 km/h in 10 sec needs

$$\begin{aligned} P_{ave} &= \frac{1}{10}\int_0^{10} \left(1500 \times 9.8 \times 0.01 + \frac{1}{2} \times 1.205 \times 0.3 \times 2 \times \left(\frac{100}{3.6 \times 10} t \right)^2 \right) \cdot \left(\frac{100}{3.6 \times 10} t \right) dt \\ &\quad + \frac{1}{10}\int_0^{10} 1500 \times \frac{100}{3.6 \times 10} dt \\ &= 8.15 kW \end{aligned} \tag{4.9}$$

In the design of a fuel cell system, the power capability should be greater than, or at least not less than, the power that is needed to support the vehicle driving at a constant speed (highway driving) and at average power when driving in urban areas. In actual

design, some typical urban drive cycles may be used to predict the average power of the vehicle. Therefore, the maximum power of fuel cell is designed as 37.5 kW.

Table 3 Parameter of the fuel cell model [5]

Variable	Value
Membrane dry density	$0.002\,kg/cm^3$
Membrane dry equivalent weight	$1.1\,kg/mol$
Membrane thickness	$0.01275\,cm$
Number of cells in fuel cell stack	400
Fuel cell active area	$200\,cm^2$
Compressor diameter	0.2286 m
Compressor and motor inertia	$5\times10^{-5}\,kg\cdot cm^2$
Anode volume	$0.005\,m^3$
Cathode volume	$0.01\,m^3$
Supply manifold volume	$0.02\,m^3$
Return manifold volume	$0.005\,m^3$
Return manifold throttle discharge coefficient	0.0124
Return manifold throttle area	$0.002\,m^2$
Supply manifold outlet orifice constant	$0.3629\times10^{-5}\,kg/(s\cdot Pa)$
Cathode outlet orifice constant	$0.2177\times10^{-5}\,kg/(s\cdot Pa)$

Based on the previous discussion, the fuel cell's efficiency is low when the current density is either low or high as shown in Figure 6. In order to achieve relatively

high efficiency, the operation range of the individual fuel cell is set from 0.4 A/cm^2 to 0.8 A/cm^2 and the corresponding cell voltage is between 0.6 V and 0.74V. Figure 6 is generated from the fuel cell stack model built by the Automotive Research Center at the University of Michigan. And the model's parameters are as Table 3 based on the 75 kW stacks used in the FORD P2000 fuel cell prototype vehicle [5].

Since the current density is designed to be 0.4 – 0.8 A/cm^2, and the cell voltage is 0.6 – 0.74 V/cell, we can get the entire fuel cell system's output current is confined between $(0.4 \times 200) = 80A$ and $(0.8 \times 200) = 160A$, and the corresponding stack voltage is from $(0.6 \times 400) = 240V$ to $(0.74 \times 400) = 296V$.

Because the output current of the fuel cell system is proportional to reacted hydrogen according to

$$2H_2 \rightarrow 4H^+ + 4e,$$

By controlling the flow rate of the hydrogen fuel, the fuel cell system's output current can be effectively controlled. With the given fuel cell current, the corresponding voltage is generated based on the fuel cell's voltage-current characteristics. Thus, the fuel cell's output current and voltage can be actively controlled by controlling the hydrogen fuel's flowing rate into the fuel cell stack.

To maintain fuel cell's relatively high efficiency, the following control strategy is proposed. Among the entire fuel cell hybrid vehicle system, when the current the motor drive need is lower than 48A, the lowest current design value of the fuel cell, the fuel cell generates 48A current. The current and hence the power is shared between the motor and the ultracapacitor. At this time, the fuel cell stack output voltage is 207.2V. If the

current demanded by the motor drive is higher than 96A, the fuel cell will produce 96A current. The rest of the current the motor needs will be supplemented by the ultracapacitor. And the fuel cell output voltage then is 168V. If the motor drive's current falls into the range of 48A and 96A, the fuel cell will feed that exact amount of current the load needs, and the ultracapacitor doesn't work. The output voltage can be estimated according to the fuel cell's voltage-current characteristics. In this case, the fuel cell always works in its high efficiency zone.

4.3 Design of ultracapacitor power capacity

In HEV, the major function of the ultracapacitor is to supply the peaking power to the drive train. In the ultracapacitor power design, acceleration performance and peak load power in typical drive cycles are the major concerns.

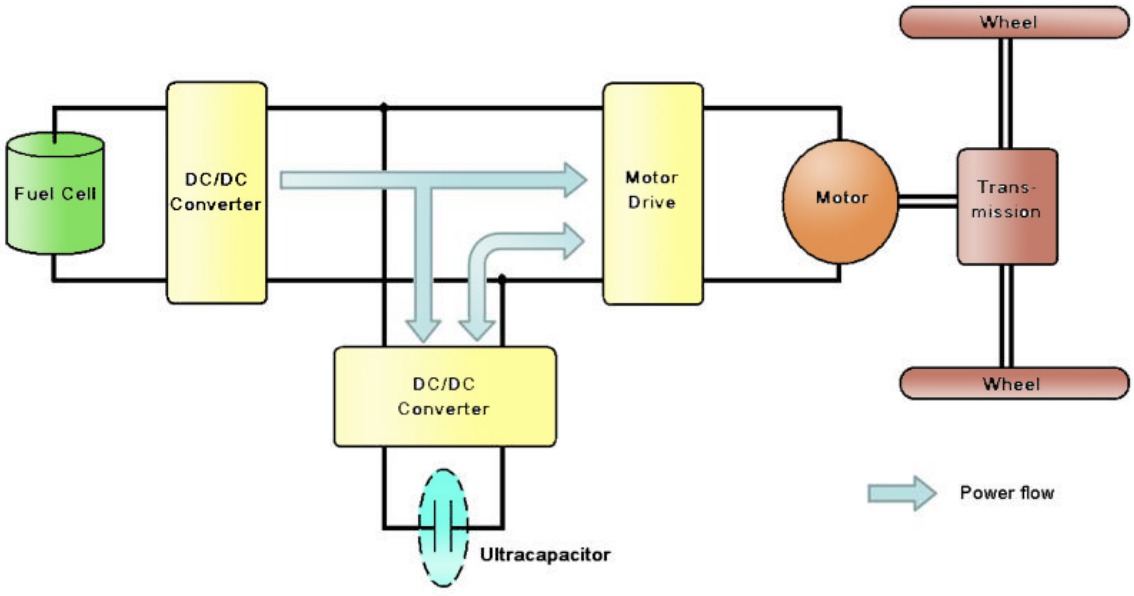

Figure 34 Power flow of fuel cell hybrid vehicle

It should be noted that the ultracapacitor power obtained above is somewhat overestimated. Actually, the fuel cell has some remaining power to help the ultracapacitor, resistance power (rolling resistance, aerodynamic drag, and power losses in transmission), and single-gear transition are plotted along the acceleration time. The sum of the output power of the fuel cell and ultracapacitor should be larger or at least equal to the input power of the traction motor as shown in Figure 34. Therefore, the power capacity of the ultracapacitor is

$$\begin{aligned} P_{UC} &= P_T - P_{FC} \\ &= 75.13 - 37.75 = 37.38kW \end{aligned} \tag{4.10}$$

where P_T and P_{FC} are the traction motor power and the fuel cell power, respectively.

In order to select the ultracapacitor, the following variables need to be determined:

- The maximum voltage, $V_{UC\max}$
- The nominal voltage, V_{UCnom}
- The minimum allowable voltage, $V_{UC\min}$.
- The current requirement, I_{UC}, or the power requirement, P_{UC}
- The time of discharge, t_d
- The time constant

To predict the behavior of the ultracapacitor voltage and current during transient state, physics-based dynamic models are needed to account for the time constant due to the double-layer effects in the ultracapacitor. The reduced order model for the

ultracapacitor is shown in Figure 35 [28]. It consists of a capacitor C_{UC}, a series resistor R_S called the equivalent series resistance (ESR), a parallel resistor R_P and a series stray inductor L. The parallel resistor R_P models the leakage current in the capacitor.

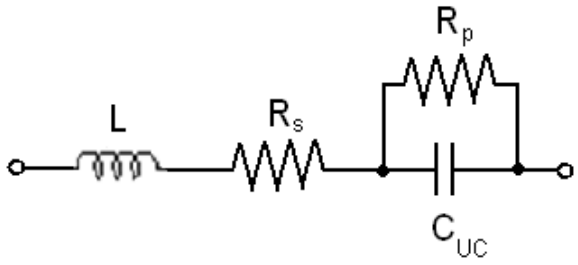

Figure 35 Ultracapacitor model

To estimate the minimum capacitor $C_{UC\min}$, an energy equation can be written without losses (the ESR R_S is neglected) as

$$\frac{1}{2}C_{UC\min}(V_{UCnom}^2 - V_{UC\min}^2) = P_{UC}t_d \tag{4.11}$$

Generally, $V_{UC\min}$ is chosen as $V_{UC\max}/2$, from Equation (4.11), resulting in 75% of the energy being utilized from the full charge (SOC = 100%). When the ultracapacitor's voltage reaches the bottom limit $V_{UC\min}$, the ultracapacitor should stop working and get charged to maintain the state of charge and avoid too much stress on itself.

With

$$P_{UC}(t) = V_{UC}(t) \times i_{UC}(t) = 37.38kW \tag{4.12}$$

$V_{UCnom} = 80V$, $V_{UC\min} = \frac{1}{2} \times V_{UCnom} = 40V$

and the continuous discharge time t_d =10 sec.

Then,

$$C_{UC\min} = \frac{2P_{UC}t_d}{V_{UCnom}^2 - V_{UC\min}^2} = \frac{2\times 37.38\times 10^3 \times 10}{80^2 - (\frac{1}{2}\times 80)^2} = 155.75 \tag{4.13}$$

This ultracapacitor can be realized by BMOD0500-P016 ultracapacitor from Maxwell with five in series times two in parallel. This array gives 200F capacitance with only 0.0075 Ω ESR.

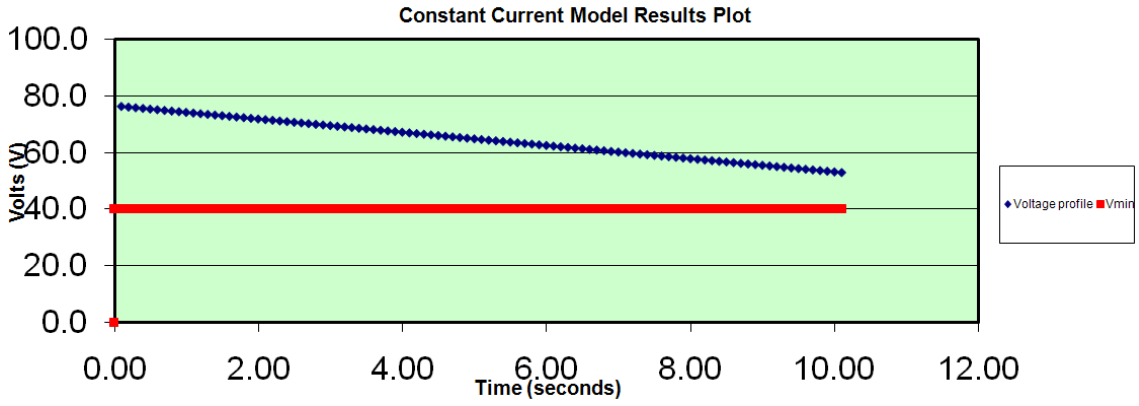

Figure 36 Constant current model results of BMOD0500-P016 [29]

From Equation (4.11) and (4.12), the instantaneous capacitor voltage and current are

$$V_{UC}(t) = V_{UCnom}\sqrt{1-\left[1-\left(\frac{V_{UCnom}}{V_{UC\min}}\right)^2\right]\frac{t}{t_d}} = 80\times\sqrt{1-0.75\frac{t}{t_d}}(V) \tag{4.14}$$

$$i_{UC}(t) = \frac{P_{UC}}{\sqrt{1-\left[1-\left(\frac{V_{UCnom}}{V_{UC\min}}\right)^2\right]\frac{t}{t_d}}} = \frac{37.38\times10^3}{\sqrt{1-0.75\frac{t}{t_d}}}(A) \tag{4.15}$$

When the power ratings of the fuel cell and ultracapacitor are initially designed, a more accurate calculation needs to be performed to evaluate the vehicle performance, mainly maximum speed, gradeability, and acceleration.

CHAPTER V

CONTROL STRATEGY DESIGN

5.1 Control strategy

The driver determines the vehicle's driving speed by changing the force exerted on the accelerating pedal or the braking pedal. As a consequent, the motor will rotate at the expected speed and has a certain amount of power request. As for the fuel cell, it only works in a specific area to guarantee the optimum efficiency. If fuel cell's output power matches the requirement of the motor, the fuel cell will be the only source to supply the loads. If there is a difference between fuel cell's supply and the motor's demand, the ultracapacitor will fill in the gap. It can be categorized into four modes of operation as presented in Figure 37.

1) When fuel cell provides more power than the loads need, the extra power will be used to charge the ultracapacitor. So the power of the fuel cell will flow into both the ultracapacitor and the loads. According to the converters designed in Chapter III, the boost converter at the fuel cell end and the buck converter at the ultracapacitor end will work in this scenario.

2) When fuel cell's output power matches the desired power of the loads, the fuel cell will only supply the power to the loads. At this time, only the boost converter at the fuel cell terminal works.

3) When the power demanded by the loads is beyond the designed range of the fuel cell's output power, ultracapacitor will assist the fuel cell to deliver power to the

loads. The converters in operation are the boost converter at the fuel cell's end and the boost converter at the ultracapacitor's end.

4) When the motor is regenerative breaking and functions as a generator, the ultracapacitor will absorb the energy sent from the motor. The converter at the ultracapacitor end works in the buck mode.

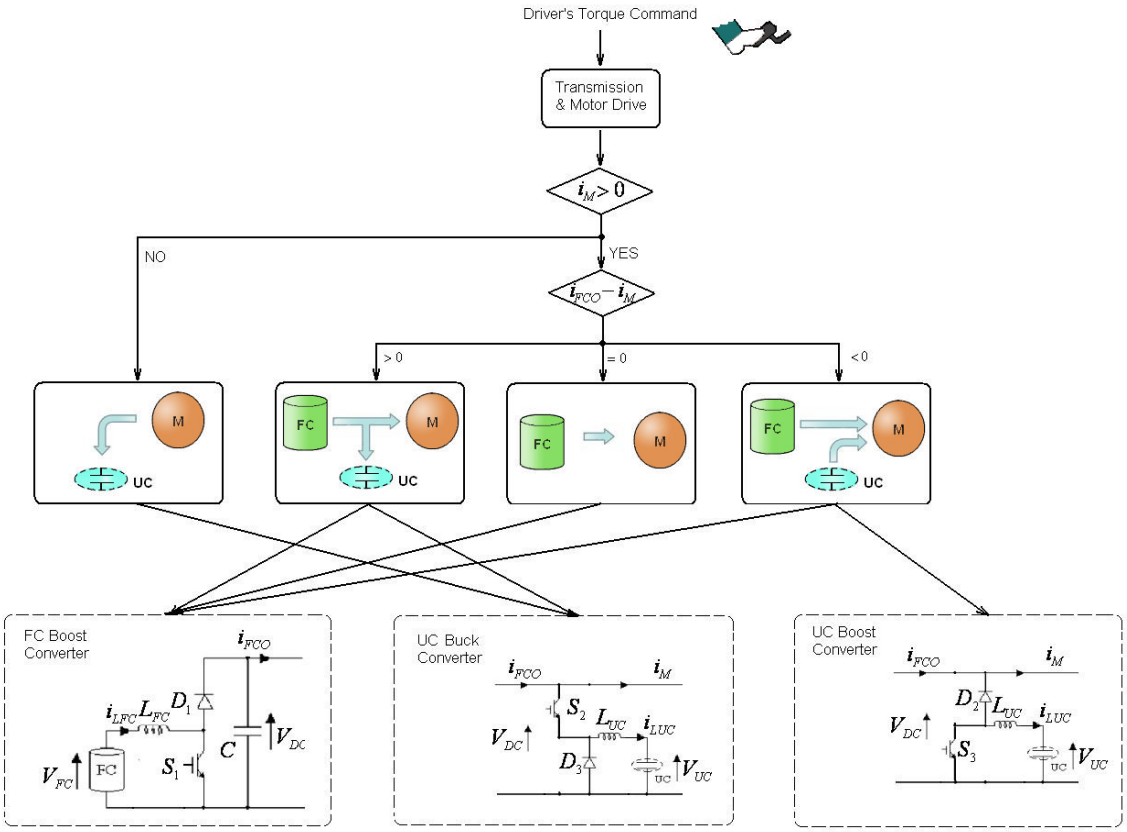

Figure 37 Control strategy flow chart

Therefore, the four modes' selection can be determined by comparing the power at the fuel cell and its converter's output end, the ultracapacitor and its converter's output end and the input side of the motor. With the same DC bus voltage at these points,

their current can be set as the criteria to choose the operation modes as portrayed in Figure 37. The detailed control algorithm will be elaborated in section 5.2.2.

5.2 Converter control algorithm

Based on the previous analysis, it's concluded that the fuel cell provides the average power and the ultracapacitor serves as the energy storage unit to manage the power deficiency or surplus. In order to optimize the system's efficiency, it's designed to match the fuel cell's high efficiency operation range in Figure 6 with the load's average power. On this occasion, a boost converter is utilized to reach the desired DC voltage level without increasing the fuel cell's size. As for the ultracapacitor, the power flow between the ultracapacitor and the load is bidirectional. Therefore, a bidirectional converter is mandated.

To realize the functions and minimize the hardware devices, the following converter topology is proposed as in Figure 38. This converter topology can be divided into two parts, namely one boost converter for the fuel cell as Figure 39 and one bidirectional converter in Figure 40. Both converter here work in the continuous conduction mode (CCM).

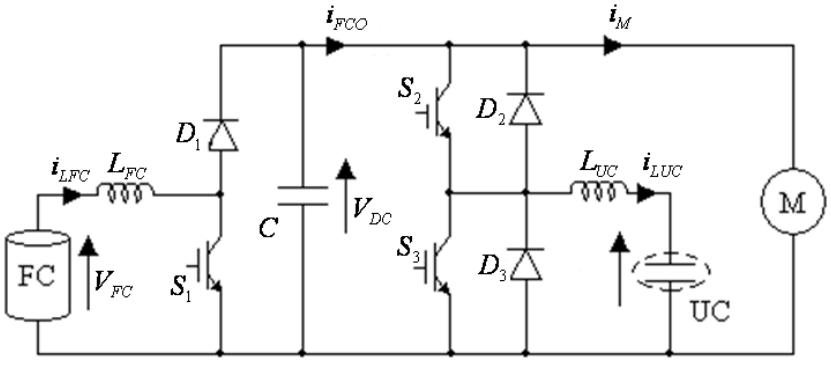

Figure 38 Designed converters in the FCHV application

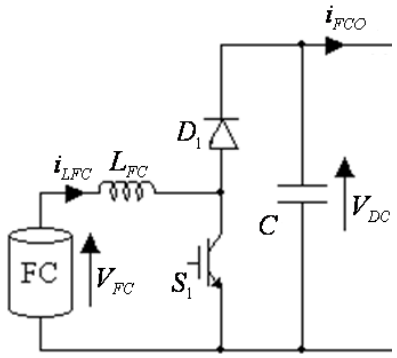

Figure 39 Boost converter for the fuel cell

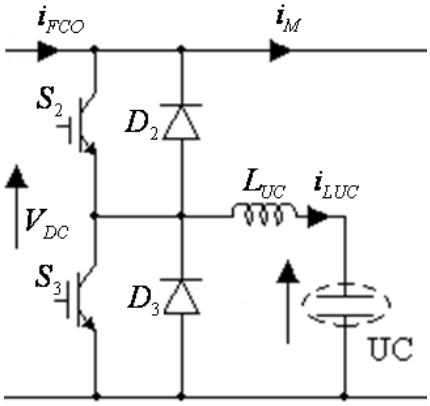

Figure 40 Bidirectional converter for the ultracapacitor

5.2.1 Boost converter at the fuel cell end

The boost converter of the fuel cell is responsible for maintaining the DC bus voltage steady at 400 V. When the switch S_1 is on ($0 < t < d_1 T_1$), the circuit diagram of the converter is depicted as Figure 41. At this time, the voltage across the diode is reverse biased. The fuel cell and the inductor L_{FC} form a closed circuit. The current

through the inductor L_{FC} equals the fuel cell's current and the fuel cell's voltage is added through L_{FC}. Since the diode current is zero, the DC bus's current comes only from the capacitor C of this converter. The capacitor C is discharged through the load. So we can get the following equations.

For $0 < t < d_1 T_1$,

$$V_{FC} = v_{LFC} \tag{5.1}$$

$$L_{FC}\frac{di_{LFC}}{dt} = V_{FC} \tag{5.2}$$

$$i_L(t) = \frac{V_{FC}}{L_{FC}}t + I_{L,\min} \tag{5.3}$$

$$i_L(t = d_1 T_1) = I_{L,\max} \tag{5.4}$$

$$\Delta I_L = I_{L,\max} - I_{L,\min} = \frac{V_{FC}}{L_{FC}} d_1 T_1 \tag{5.5}$$

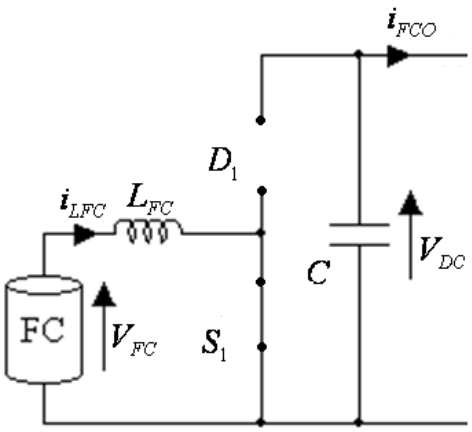

Figure 41 Boost converter of the fuel cell when S_{FC} is on

When the switch S_1 is off ($d_1T_1 < t < T_1$), the circuit diagram of the converter is shown as Figure 42. The diode is forward biased and conducts during this time. The fuel cell's current can only go through the diode to the load. So the current through the switch is zero and the current through the inductor L_{FC}, the diode D_1 and the load is the fuel cell's current. The inductor L_{FC} is depleting its energy to the capacitor C and the load. As the energy is depleting from L_{FC}, the current through L_{FC} is decreasing. The voltage on L_{FC} equals the difference of the voltages between the fuel cell and the load. The state equations during this time interval are as follows.

For $d_1T_1 < t < T_1$,

$$v_{LFC} = V_{FC} - V_{DC} \tag{5.6}$$

$$L_{FC}\frac{di_{LFC}}{dt} = -(V_{DC} - V_{FC}) \tag{5.7}$$

$$i_{LFC}(t) = \frac{-(V_{DC} - V_{FC})}{L_{FC}}(t - d_1T_1) + I_{LFC,\max} \tag{5.8}$$

$$i_{LFC}(t = T_1) = I_{LFC,\min} \tag{5.9}$$

$$\Delta I_{LFC} = I_{LFC,\max} - I_{LFC,\min} = \frac{V_{DC} - V_{FC}}{L_{FC}}(1 - d_1)T_1 \tag{5.10}$$

Since it's in continuous conduction mode, the switch S_1 is turned on and a new cycle starts before the inductor current reaches zero. Additionally, the current change per cycle is negligible by virtue of the slow response of the fuel cell and the high frequency switching of the converter. From Equation (5.1) ~ (5.10), we can get

$$V_{DC} = \frac{V_{FC}}{1 - d_1} \tag{5.11}$$

where $d_1 = \frac{t_{1on}}{T_1}$ is the duty cycle of the fuel cell boost converter, which ranges from 0 to 1.

Figure 43 depicts the variations of the inductor's voltage and current.

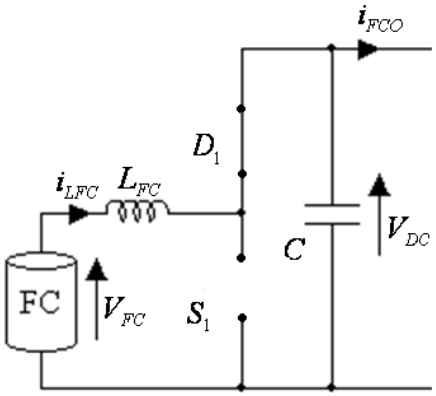

Figure 42 Boost converter of the fuel cell when S_1 is off

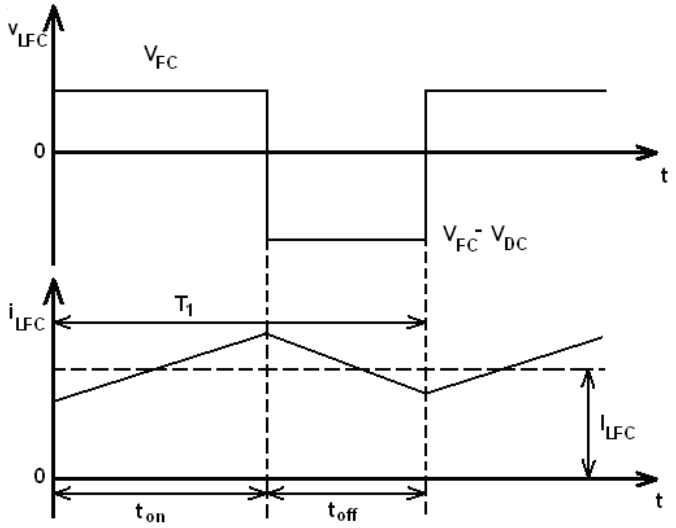

Figure 43 Inductor voltage and current of the FC boost converter

For the reference voltage, it's desired to be constant to maintain the DC bus steadiness. Thus, $V_{DCref} = 400V$ as shown in Figure 44.

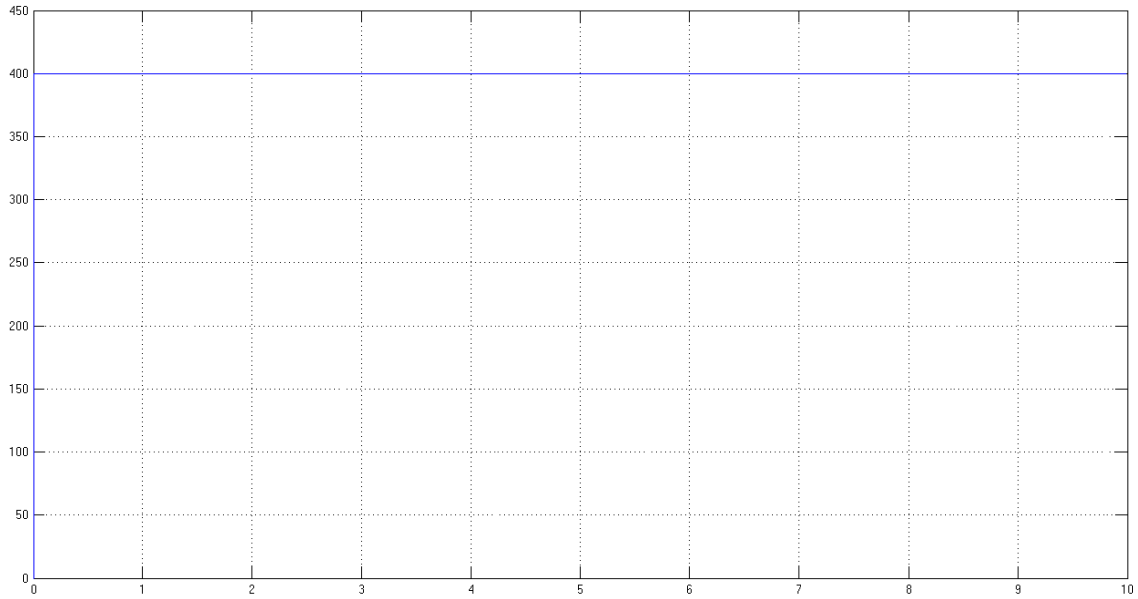

Figure 44 DC bus voltage

5.2.2 Buck converter at the ultracapacitor end

The bidirectional converter is devoted to control the current flow at the interface of the fuel cell, ultracapacitor and the motor and accomplish the power balance. Its topology is designed as Figure 40. S_2 and D_3 form the buck pattern from the DC bus to the ultracapacitor and the boost converter from the ultracapacitor to the DC bus is composed of S_3 and D_2 as Figure 45. These two switches, S_2 and S_3, don't work complementarily. When the power flows into the ultracapacitor from the DC bus, the buck converter operates while the boost converter doesn't work because the DC bus' voltage is designed to be higher than voltage of ultracapacitor. By switching S_2 with

specific duty cycles, the buck converter can step down the DC voltage to the ultracapacitor's voltage level. And keeping S_3 open can stop the boost converter operating. When the power is delivered from the ultracapacitor to the DC bus, the voltage is boosted, the boost converter works and the buck converter doesn't. Similar to the buck converter mode, the operation of the boost converter depends on the S_3 switching according to the calculated duty cycle while the S_2 stays open to cut the buck converter out of this occasion. The detailed control algorithm is as follows.

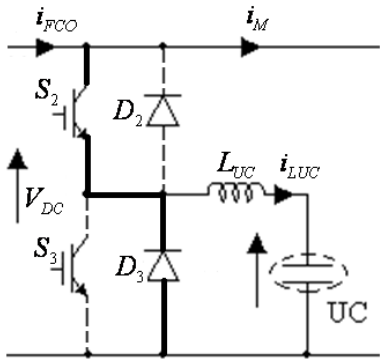

(a) Buck converter from the DC bus to the ultracapacitor

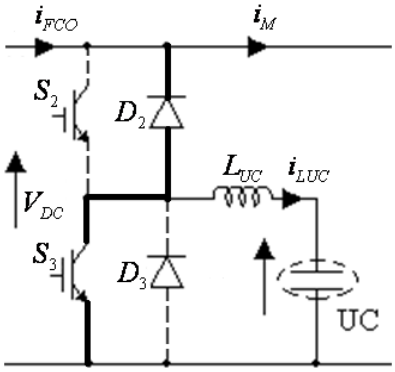

(b) Boost converter from the ultracapacitor to the DC bus

Figure 45 Bidirectional converter connecting the ultracapacitor to the DC bus

The buck module is depicted in Figure 45 (a). It works in the continuous conduction mode (CCM). Once the switch S_2 is on ($0 < t < d_2T_2$), the current flows through the inductor L_{UC} as Figure 46. A negative voltage is imposed on the diode D_3, thus, D_3 is reverse biased. The current through the inductor starts to increase and the ultracapacitor is charged from the DC bus.

For $0 < t < d_2T_2$,

$$V_{DC} = v_{LUC} + V_{UC} \tag{5.12}$$

$$L_{UC}\frac{di_{LUC}}{dt} = V_{DC} - V_{UC} \tag{5.13}$$

$$i_{LUC}(t) = \frac{V_{DC} - V_{UC}}{L_{UC}}t + I_{LUC,\min} \tag{5.14}$$

$$i_{LUC}(t = d_2T_2) = I_{LUC,\max} \tag{5.15}$$

$$\Delta I_{LUC} = I_{LUC,\max} - I_{LUC,\min} = \frac{V_{DC} - V_{UC}}{L_{UC}}d_2T_2 \tag{5.16}$$

When the switch S_2 is off ($d_2T_2 < t < T_2$), the circuit diagram is introduced in Figure 47. The loop is closing via the diode. And the inductor releases the energy stored in it to the ultracapacitor, so the current through the inductor decreases. The voltage across the inductor is negative, and its amplitude is clamped to the ultracapacitor voltage. We can get the following observations.

For $d_2T_2 < t < T_2$,

$$v_{LUC} = -V_{UC} \tag{5.17}$$

$$L_{UC}\frac{di_{LUC}}{dt} = -V_{UC} \tag{5.18}$$

$$i_{LUC}(t) = \frac{-V_{UC}}{L_{UC}}(t - d_2 T_2) + I_{LUC,\max} \tag{5.19}$$

$$i_{LUC}(t = T_2) = I_{LUC,\min} \tag{5.20}$$

$$\Delta I_{LUC} = I_{LUC,\max} - I_{LUC,\min} = \frac{V_{UC}}{L_{UC}}(1 - d_2)T_2 \tag{5.21}$$

So we can get

$$V_{UC} = d_2 V_{DC} \tag{5.22}$$

where $d_2 = \frac{t_{2on}}{T_2}$ is the duty cycle of the fuel cell boost converter, which ranges from 0 to 1.

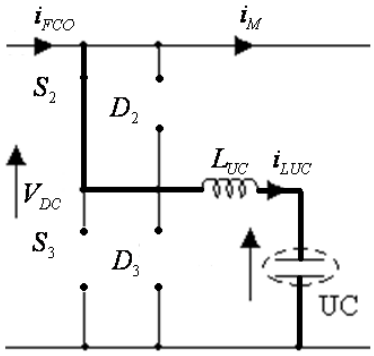

Figure 46 Buck converter from the DC bus to the ultracapacitor when S_2 is on

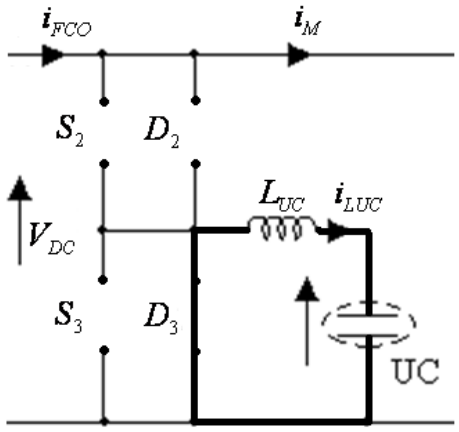

Figure 47 Buck converter from the DC bus to the ultracapacitor when S_2 is off

The waveforms of the inductor L_{UC}'s current and voltage are as Figure 48.

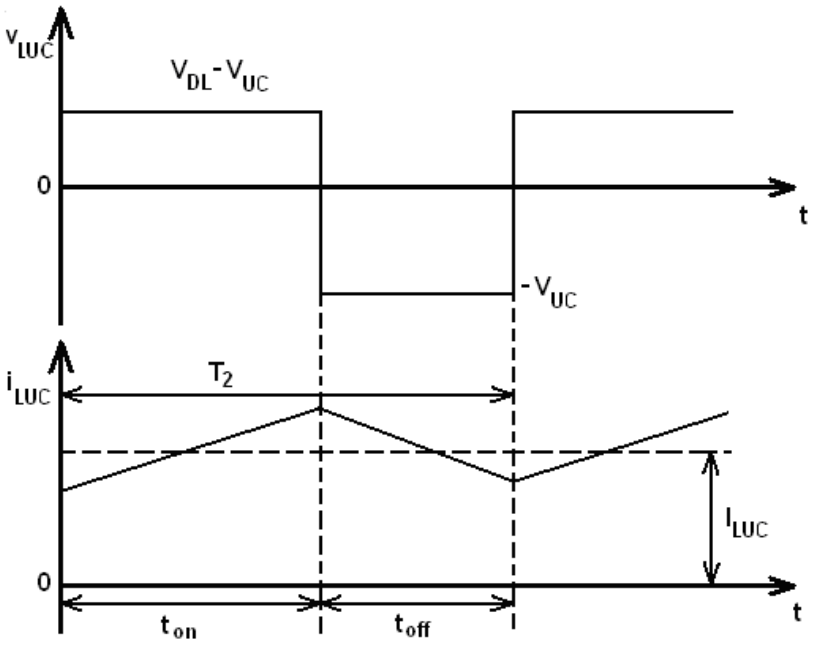

Figure 48 Inductor voltage and current of the UC boost converter

With high frequency of the switch, Equation (5.13) and (5.18) can be written in the following forms.

$$L_{UC}\frac{i_{LUC}[t(n)+d_2(n)\cdot T_2]-i_{LUC}[t(n)]}{d_2(n)\cdot T_2}=V_{DC}[t(n)]-V_{UC}[t(n)] \tag{5.23}$$

$$L_{UC}\frac{i_{LUC}[t(n+1)]-i_{LUC}[t(n)+d_2(n)\cdot T_2]}{[1-d_2(n)]\cdot T_2}=-V_{UC}[t(n)] \tag{5.24}$$

where t(n) and t(n+1) are the beginning time of nth and (n+1) th interval, d_2 (n) is the duty cycle of the nth interval, $i_{LUC}[t(n)]$, $i_{LUC}[t(n+1)]$ are the inductor L_{UC}'s current at the beginning of the nth and the (n+1)th switching cycles as expressed in Figure 49.

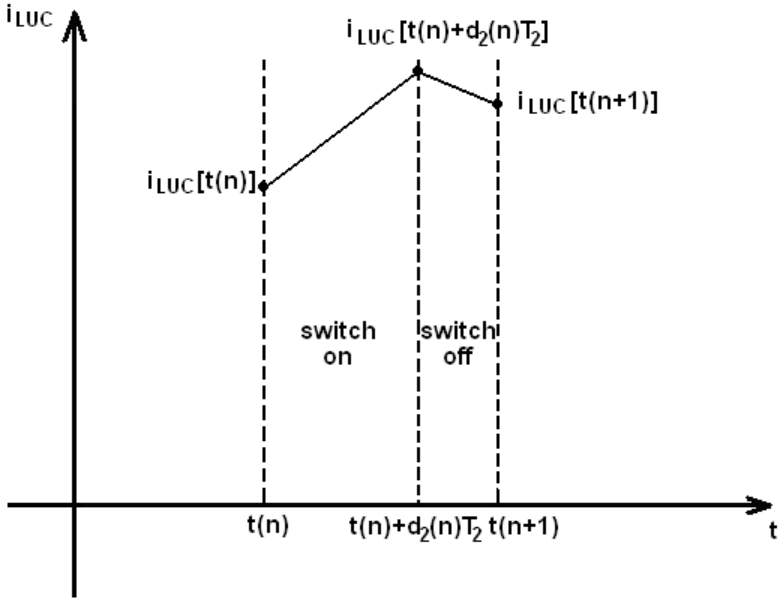

Figure 49 Inductor current i_{LUC} in the nth cycle

From Equation (5.23), we can get the inductor current i_{LUC} at the moment of turning of the switch S_2 as

$$i_{LUC}[t(n)+d_2(n)\cdot T_2] = i_{LUC}[t(n)] + \frac{1}{L_{UC}}\{V_{DC}[t(n)] - V_{UC}[t(n)]\}\cdot d_2(n)\cdot T_2 \quad (5.25)$$

The inductor current i_{LUC} at the beginning of the (n+1)th cycle is derived from Equation (5.24) as

$$i_{LUC}[t(n+1)] = i_{LUC}[t(n)+d_2(n)\cdot T_2] - \frac{1}{L_{UC}}\cdot V_{UC}[t(n)]\cdot[1-d_2(n)]\cdot T_2 \quad (5.26)$$

Substituting Equation (5.25) into Equation (5.26),

$$i_{LUC}[t(n+1)] = i_{LUC}[t(n)] - \frac{1}{L_{UC}}\cdot V_{UC}[t(n)]\cdot T_2 + \frac{1}{L_{UC}}\cdot V_{DC}[t(n)]\cdot d_2(n)\cdot T_2 \quad (5.27)$$

The discrete form of Equation (5.27) is

$$i_{LUC}(n+1) = i_{LUC}(n) - \frac{V_{UC}(n)\cdot T_2}{L_{UC}} + \frac{V_{DC}(n)\cdot d_2(n)\cdot T_2}{L_{UC}} \quad (5.28)$$

From the above equation, we can see that the inductor current i_{LUC} at the beginning of the next cycle is determined by the current at the beginning of the current cycle, the ultracapacitor voltage, the DC bus voltage and the duty cycle of the current cycle.

We can also get the duty cycle d_2 from Equation (5.28),

$$d_2(n) = \frac{L_{UC}}{T_2}\frac{i_{LUC}(n+1) - i_{LUC}(n)}{V_{DC}(n)} + \frac{V_{UC}(n)}{V_{DC}(n)} \quad (5.29)$$

So the duty cycle of the present cycle is determined by the converter parameters, the input voltage V_{DC}, the output voltage V_{UC} and the inductor current i_{LUC}.

To control the power flow between the ultracapacitor and the DC bus, i_{LUC}(n+1) is designed to follow the reference current $i_{LUCref}(n+1)$ as Figure 50 and $V_{DC}(n)$

follows the reference voltage $V_{DCref}(n)$ attributed to the boost converter at the fuel cell end.

The reference current $i_{LUCref}(n+1)$ can be derived as follows based on the Kirchhoff's current law and the conservation of power,

$$i_{LUCref}(n+1) = (i_{FCO} - i_M) \times \frac{V_{DC}(n)}{V_{UC}(n)} \tag{5.30}$$

Substituting $i_{LUCref}(n+1)$ for i_{LUC} (n+1) Equation (5.29),

$$d_2(n) = \frac{L_{UC}}{T_2} \frac{i_{LUCref}(n+1) - i_{LUC}(n)}{V_{DC}(n)} + \frac{V_{UC}(n)}{V_{DC}(n)} \tag{5.31}$$

where i_{LUC} (n) and $V_{DC}(n)$ are the input current and voltage at the beginning of the present cycle.

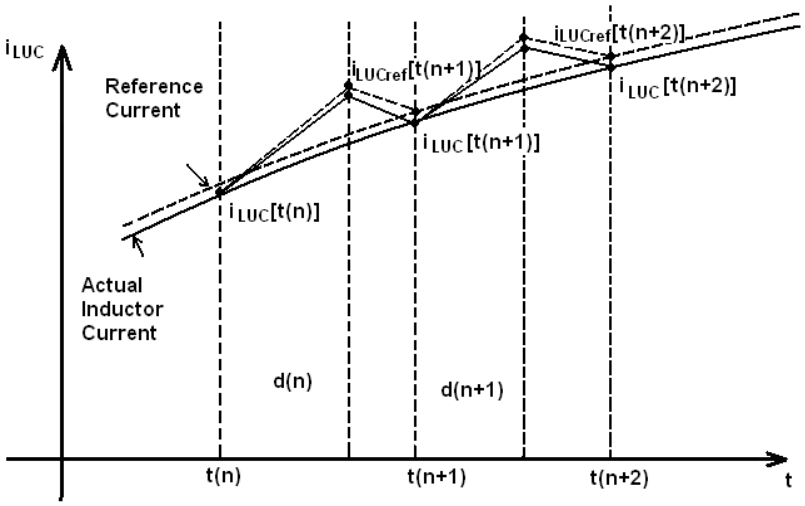

Figure 50 Inductor current tracks the reference current

5.2.3 Boost converter at the ultracapacitor end

The operation principle of the boost converter with S_3 and D_2 is similar to the boost converter of fuel cell with S_1 and D_1. When the switch S_3 is on, the current flows as in Figure 51. And the circuit diagram is as Figure 52 when the switch S_3 is off. The relationship between the DC bus voltage and the ultracapacitor voltage is

$$V_{DC} = \frac{V_{UC}}{1 - d_3} \tag{5.32}$$

where $d_3 = \frac{t_{3on}}{T_3}$ is the duty cycle of S_3, which ranges from 0 to 1.

Different from the traditional bidirectional converter, there are few occasions that S_2 and S_3 are turned on simultaneously. Hence, the conduction losses are greatly reduced as well to improve the conversion efficiency. And no zero voltage switching or zero current switching needs to be taken care of.

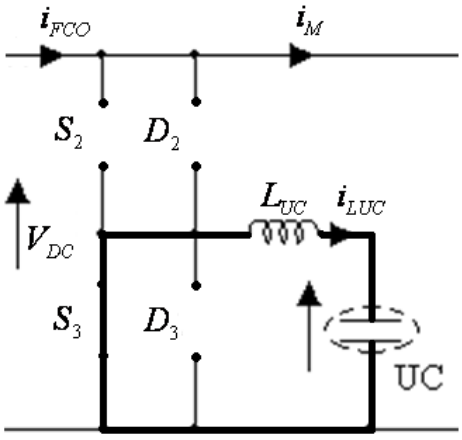

Figure 51 Boost converter from the ultracapacitor to the DC bus when S_3 is on

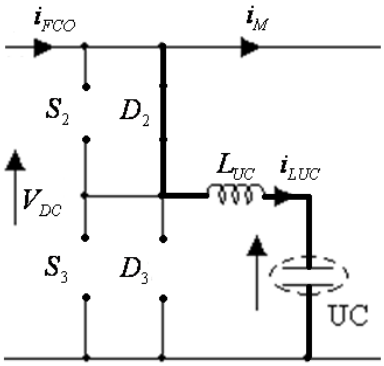

Figure 52 Boost converter from the ultracapacitor to the DC bus when S_3 is off

Similar to the previous buck converter mode, the following equations can be derived.

$$L_{UC}\frac{i_{LUC}[t(n)+d_3(n)\cdot T_3]-i_{LUC}[t(n)]}{d_3(n)\cdot T_3}=-V_{UC}[t(n)] \tag{5.33}$$

$$L_{UC}\frac{i_{LUC}[t(n+1)]-i_{LUC}[t(n)+d_3(n)\cdot T_3]}{[1-d_3(n)]\cdot T_3}=V_{DC}[t(n)]-V_{UC}[t(n)] \tag{5.34}$$

where t(n) and t(n+1) are the beginning time of nth and (n+1) th interval, d_3(n) is the duty cycle of the nth interval, $i_{LUC}[t(n)]$, $i_{LUC}[t(n+1)]$ are the inductor L_{UC}'s current at the beginning of the nth and the (n+1)th switching cycles.

From Equation (5.33), we can get the inductor current i_{LUC} at the moment of turning of the switch S_3 as

$$i_{LUC}[t(n)+d_3(n)\cdot T_3]=i_{LUC}[t(n)]-\frac{1}{L_{UC}}V_{UC}[t(n)]\cdot d_3(n)\cdot T_3 \tag{5.35}$$

The inductor current i_{LUC} at the beginning of the (n+1)th cycle is derived from Equation (5.34) as

$$i_{LUC}[t(n+1)] = i_{LUC}[t(n) + d_3(n)\cdot T_2] + \frac{1}{L_{UC}}\cdot\{V_{DC}[t(n)] - V_{UC}[t(n)]\}\cdot[1-d_3(n)]\cdot T_3 \tag{5.36}$$

Substituting Equation (5.35) into Equation (5.36),

$$i_{LUC}[t(n+1)] = i_{LUC}[t(n)] - \frac{1}{L_{UC}}\cdot V_{UC}[t(n)]\cdot T_3 + \frac{1}{L_{UC}}\cdot V_{DC}[t(n)]\cdot[1-d_3(n)]\cdot T_3 \tag{5.37}$$

The discrete form of Equation (5.37) is

$$i_{LUC}(n+1) = i_{LUC}(n) - \frac{V_{UC}(n)\cdot T_3}{L_{UC}} + \frac{V_{DC}(n)\cdot[1-d_3(n)]\cdot T_3}{L_{UC}} \tag{5.38}$$

From the above equation, we can see that the inductor current i_{LUC} at the beginning of the next cycle is determined by the current at the beginning of the current cycle, the ultracapacitor voltage, the DC bus voltage and the duty cycle of the current cycle.

We can also get the duty cycle d_3 from Equation (5.38),

$$d_3(n) = -\frac{L_{UC}}{T_3}\frac{i_{LUC}(n+1) - i_{LUC}(n)}{V_{DC}(n)} + \frac{V_{DC}(n) - V_{UC}(n)}{V_{DC}(n)} \tag{5.39}$$

So the duty cycle of the present cycle is determined by the converter parameters, the input voltage V_{DC}, the output voltage V_{UC} and the inductor current i_{LUC}.

To control the power flow between the ultracapacitor and the DC bus, i_{LUC}(n+1) is designed to follow the reference current $i_{LUCref}(n+1) = (i_{FCO} - i_M)\times\frac{V_{DC}}{V_{UC}}$. $V_{DC}(n)$ tracks the reference voltage $V_{DCref}(n)$ resulting from the boost converter at the fuel cell end.

Substituting $i_{LUCref}(n+1)$ for i_{LUC}(n+1) in Equation (5.39),

$$d_3(n) = -\frac{L_{UC}}{T_3}\frac{i_{LUCref}(n+1) - i_{LUC}(n)}{V_{DC}(n)} + \frac{V_{DCref}(n) - V_{UC}(n)}{V_{DC}(n)} \tag{5.40}$$

Therefore, the forward control method proposed above can control the current of the FC and the UCs and the voltage of the DC bus, to achieve optimal system efficiency.

CHAPTER VI

SIMULATION

In order to verify the feasibility of the converter topology and the control algorithm, system modeling and simulations are carried out with Simulink as shown in Figure 53. Table 4 shows the electric characteristics of the fuel cell, the ultracapacitor and the motor derived in Chapter IV.

Table 4 Electric characteristics of the key components in the system

Fuel Cell	
Rated Power	37.75 kW
Operating Current Range	80 – 160 A
Operating Voltage Range	240 – 296 V
Ultracapacitor	
Rated Power	37.38 kW
Max Voltage (SOC = 1)	80 V
Min Voltage (SOC = 0.5)	40 V
Motor	
Rated Power	70 kW
Rated Voltage	400 V
Rated Current	175 A

In the simulation, the fuel cell part refers to the model developed by the Automotive Research Center at the University of Michigan [5]. The prototype for this model is FORD P2000 fuel cell. The rating power of the fuel cell is reduced in this vehicle system due to the ultracapacitor's assistance and the advanced control strategy. The fuel cell stack is composed of 400 individual cells with 200 cm^2. The fuel cell's operating performance is depicted in Figure 6. In order to optimize the fuel cell's efficiency, the fuel cell is designed to produce the current from 80A to 160A via controlling the hydrogen flow rate into the fuel cell stack. And the fuel cell stack voltage ranges correspondingly from 168V to 207.2V. The detailed calculation is conducted in Chapter IV.

The simulation is based on Simulink, Matlab and it simulates the vehicle system with the maximum acceleration performance and the four-mode operation.

6.1 Full load operation

With the acceleration pedal being pressed to its limit from zero speed, the vehicle is driven with full torque and achieved the largest acceleration. Figure 54 – 64 are the simulation results for the full load for 10 seconds. Figure 54 shows the motor's angular speed increases from zero to 240 rad/s in 10 seconds. According to Equation (4.3) and $v_{base} = 37.6m/s$ designed in Chapter IV,

$$\omega_{base} = \frac{v_{base} i_g}{r} = \frac{37.6 \times 2.81}{0.28} = 104 rad/s$$

$$v_f = \frac{\omega_f r}{i_g} = \frac{240 \times 0.28}{2.81} = 24 m/s = 86.5 km/h$$

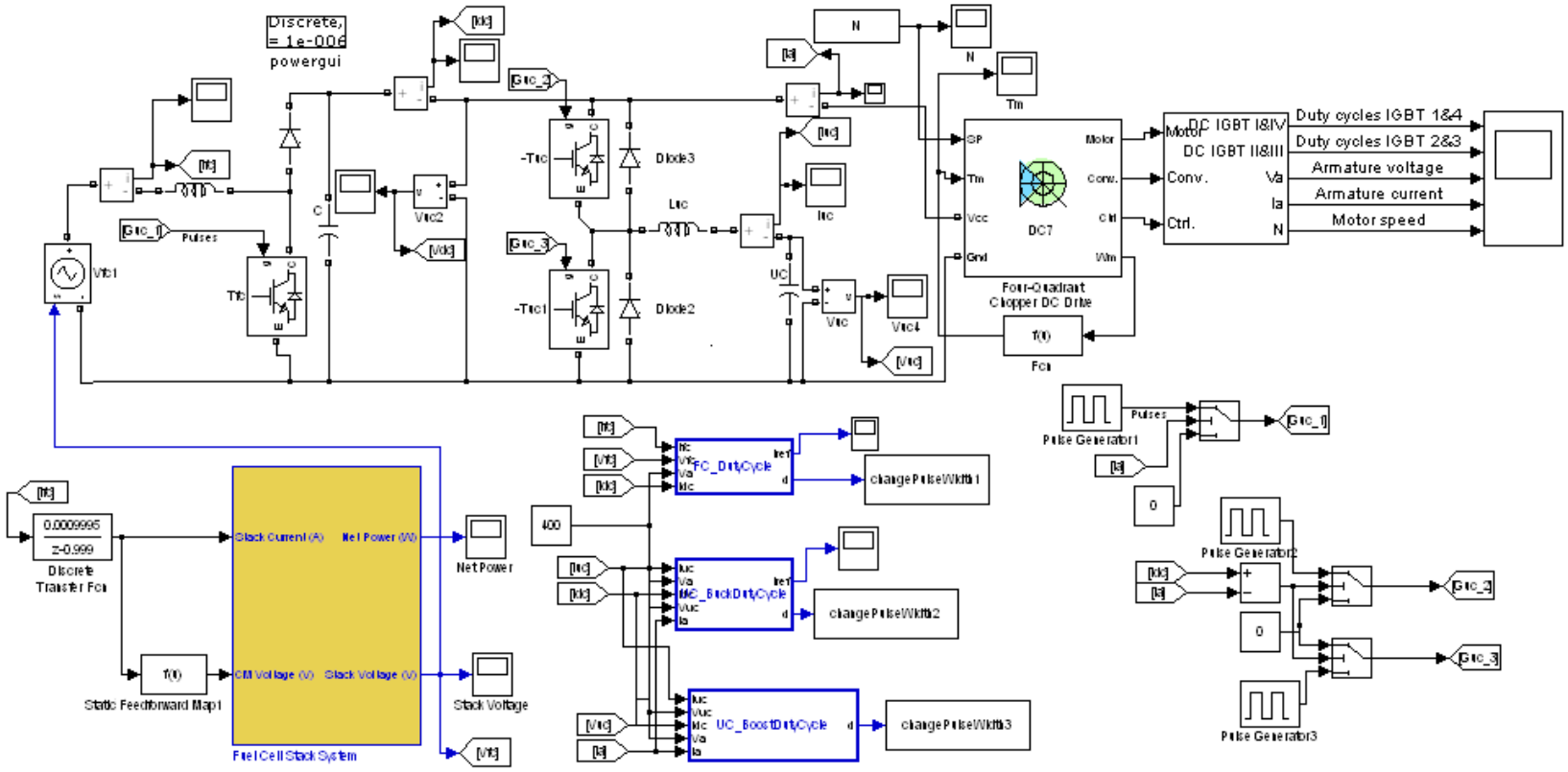

Figure 53 Simulation block of the fuel cell hybrid drive train

Hence, the vehicle reaches 86.5 km/h from standstill within 10 seconds. It confirms the acceleration capability designed in Chapter IV. From Figure 54, the vehicle reaches the base speed $v_{base} = 37.6m/s$ at t = 2.3 sec, when $\omega_{base} = 104rad/s$. Referring to the control approach described in Chapter II, the armature voltage control is employed when the speed is below the base speed $\omega_{base} = 104rad/s$ as shown in Figure 55. And the torque the motor generates is the rated value, 690 Nm, as in Figure 57. When the motor speed reaches the base speed, the armature voltage reaches its rated value, 400 V, and can't increase further. Therefore, the armature voltage keeps the rated value when the speed is above the base speed. In order to increase the speed beyond the base speed, field flux control is utilized and the torque is decreased as shown in Figure 57. Figure 54 shows that the speed increases after reaching the base speed but at a lower rate. The armature current remains the same throughout this process as in Figure 56.

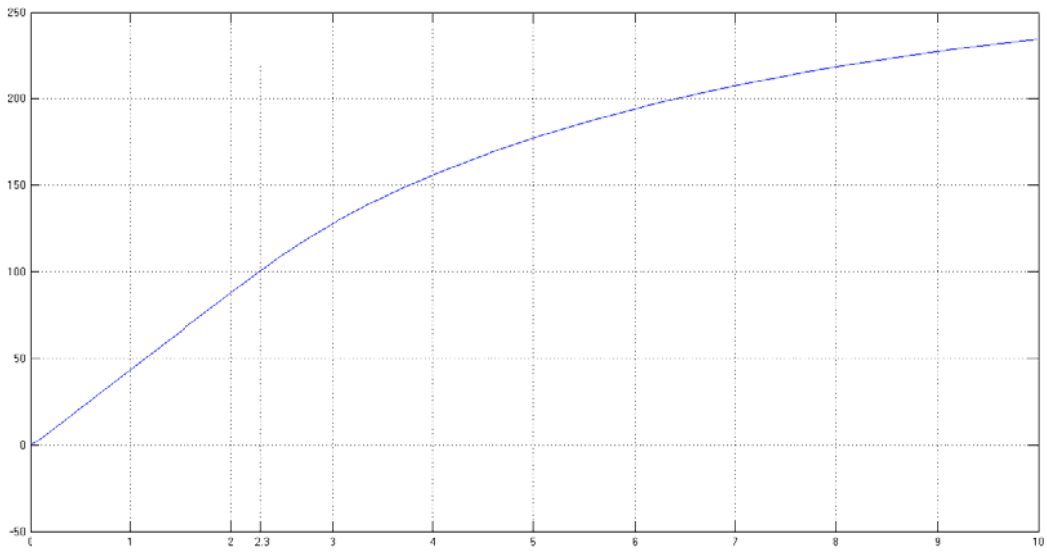

Figure 54 Motor's angular speed with full load

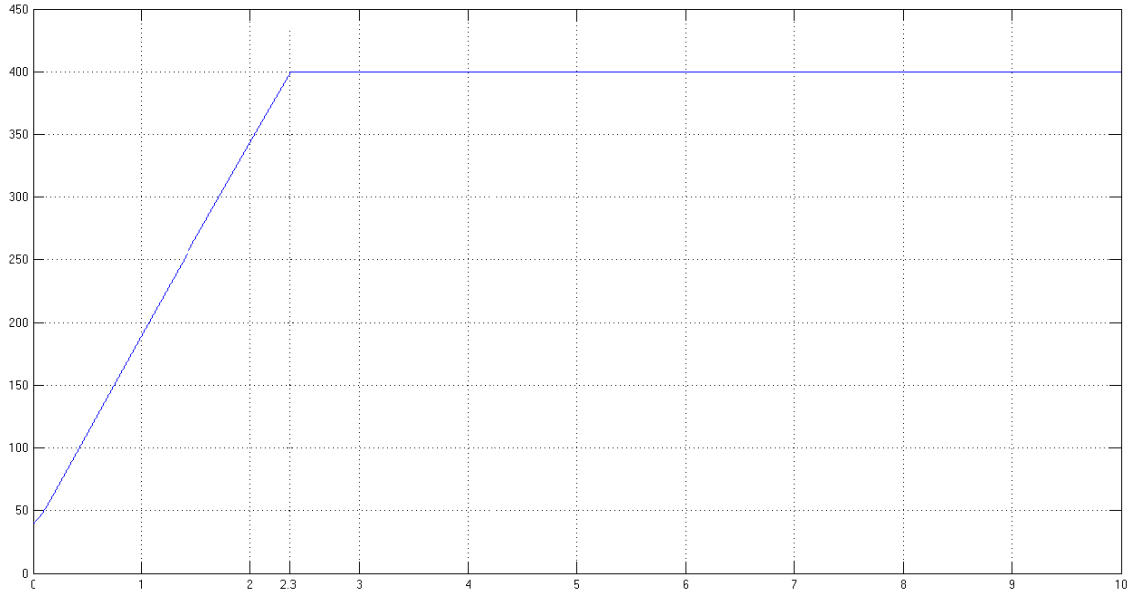

Figure 55 Motor's armature voltage with full load

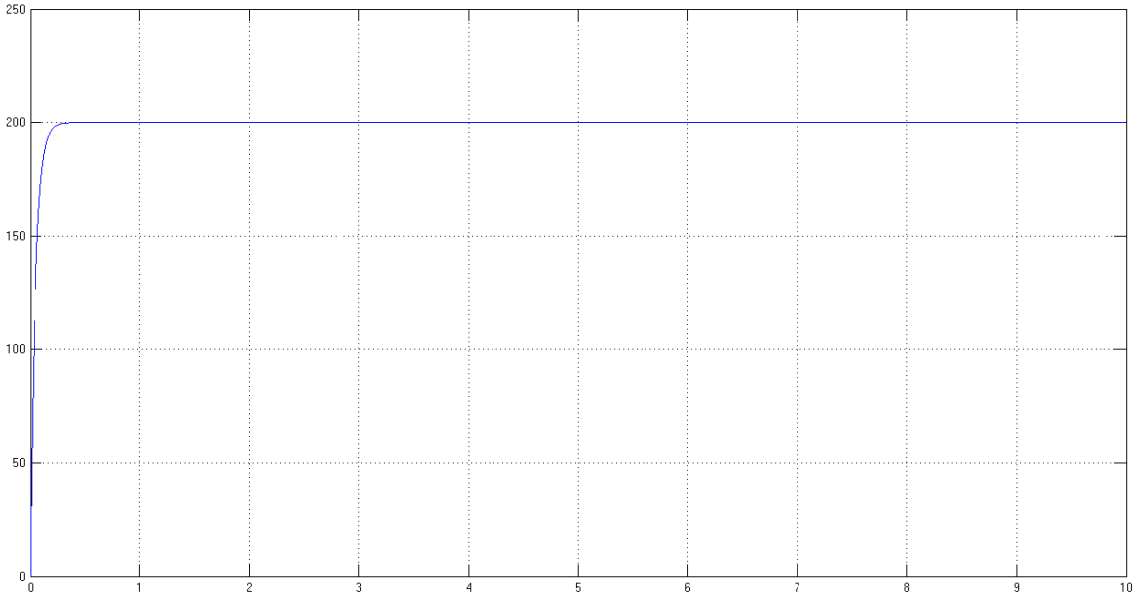

Figure 56 Motor's armature current with full load

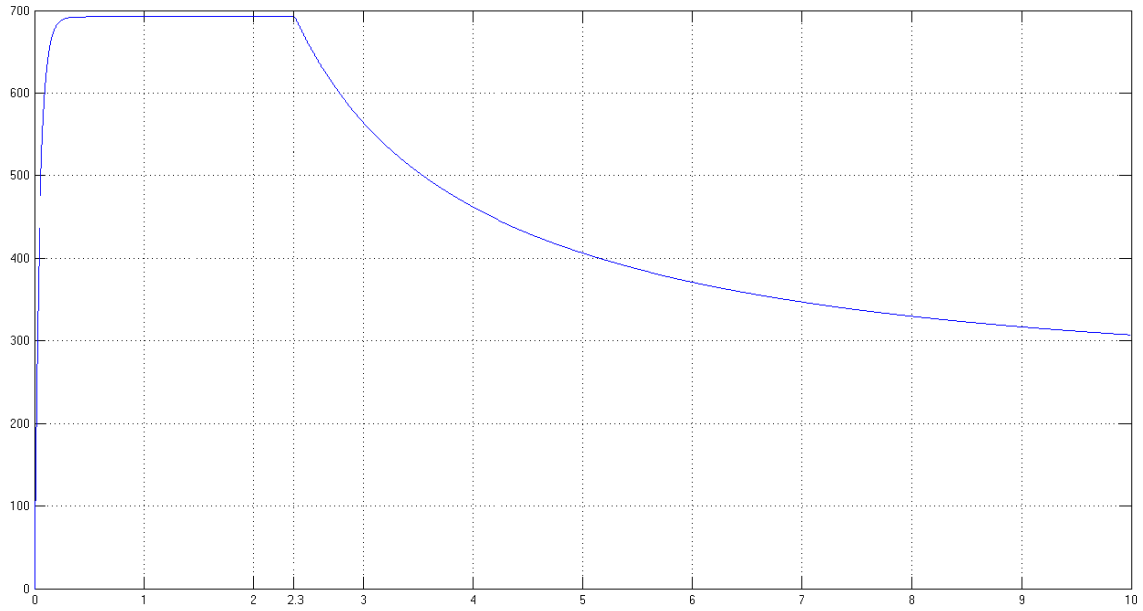

Figure 57 Torque generated by the motor with full load

Figure 58 shows the current variation of the fuel cell and the motor. The blue line represents the output current of the fuel cell; the green line indicates the input current of the motor and the red line is the difference between them. From t = 0 sec to t = 0.43 sec, the fuel cell produces more current than the motor needs. Thus, the fuel cell generates the lowest expected current 80 A set in Chapter IV as in Figure 59. After going through the boost converter, the output current of the fuel cell reduces to 50 A as in Figure 58. During this interval, the fuel cell delivers power to the motor and the ultracapacitor simultaneously. As in Figure 60, the current of the ultracapacitor is positive, indicating the current flows into the ultracapacitor and the ultracapacitor gets charged. In Figure 60, the green line represents the reference current of ultracapacitor, and the blue one is the actual current of the ultracapacitor. The ultracapacitor's reference current is a function of the difference between the fuel cell output current and the motor's input current

discussed in Chapter V. It aims to provide the dynamic peaking power to the load by changing the duty cycle of the converters connected to the ultracapacitor. As shown in Figure 60, the actual current of the ultracapacitor tracks the reference well. Figure 61 also shows a slightly increase in the ultracapacitor's voltage, confirming it's getting charged.

From t = 0.43 sec to t = 0.87 sec, the motor's requirement falls into the working range of the fuel cell as in Figure 58. Therefore, only fuel cell provides the power the motor demands and the ultracapacitor is disconnected from the system as in Figure 60 with zero ultracapacitor current and slightly voltage drop in Figure 61 due to its natural discharge.

After t = 0.87 sec, the fuel cell can't provide the power the motor requires as in Figure 58. The ultracapacitor is the auxiliary source to provide the peaking power to the load as expressed in Figure 60 and Figure 61. The negative current in Figure 60 indicates the current flows out of the ultracapacitor and it's discharging. The voltage drop in Figure 61 also verifies it. At t = 10 sec, the ultracapacitor's voltage is 52.5 V, still above the minimum voltage 40 V designed in Chapter IV. It's concluded that the designed ultracapacitor can provide enough energy as required.

Figure 59 shows the fuel cell's performance in the full load operation scenario. When the current increases, its voltage decreases correspondingly. When the fuel cell produces 80 A at t = 0.43 – 0.87 sec, its voltage is 250 V. And when the current is 160 A after t = 0.87 sec, its voltage is 225 V as designed in Chapter IV.

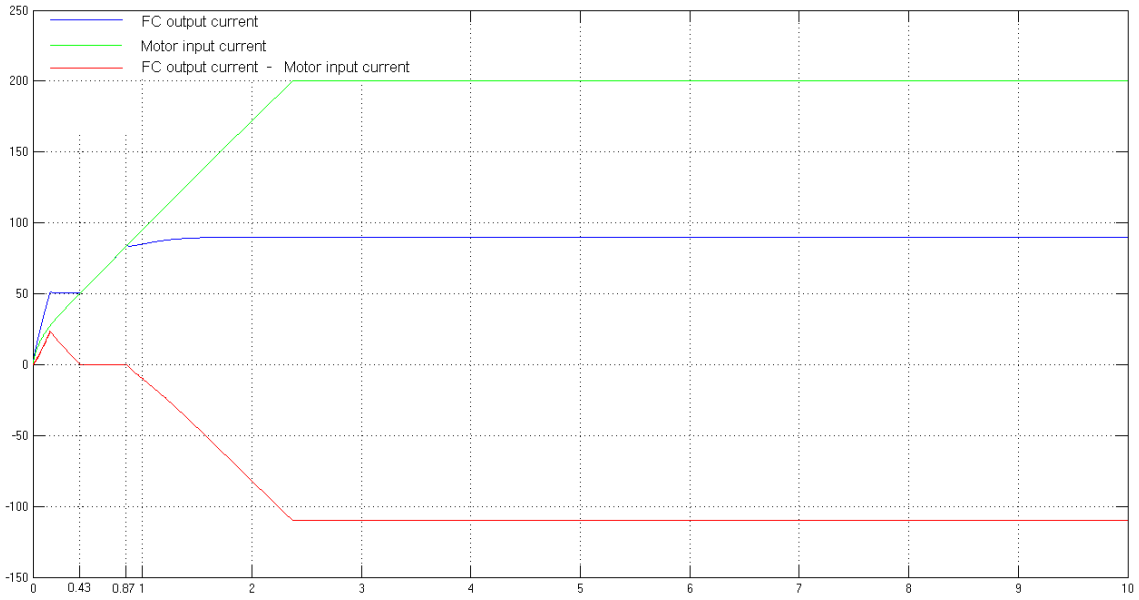

Figure 58 Output current of the fuel cell, input current of the motor and their difference with full load

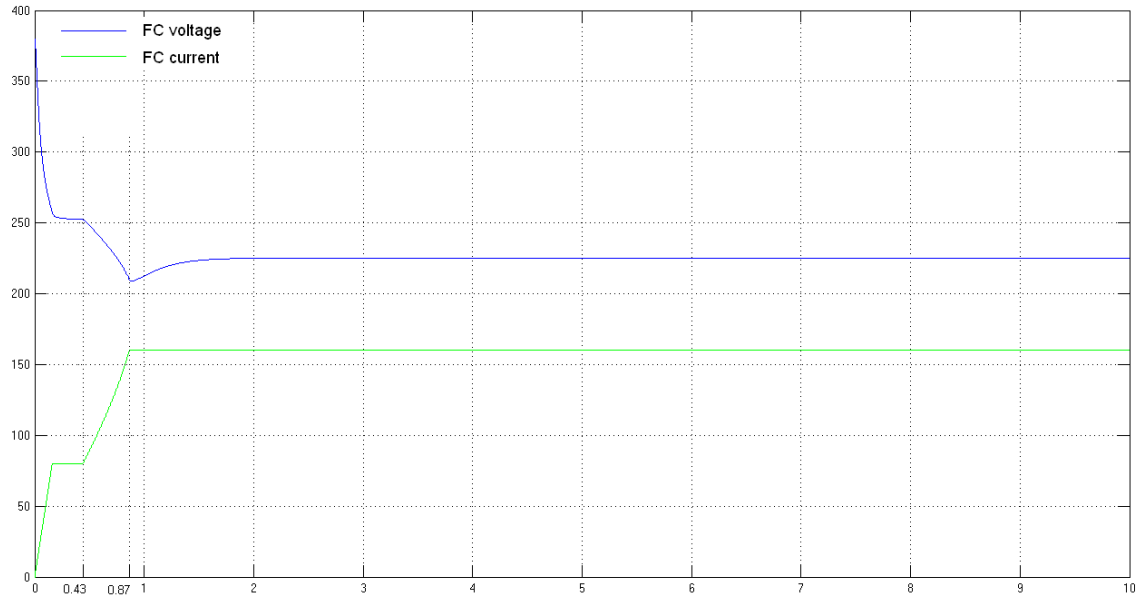

Figure 59 Fuel cell's voltage and current with full load

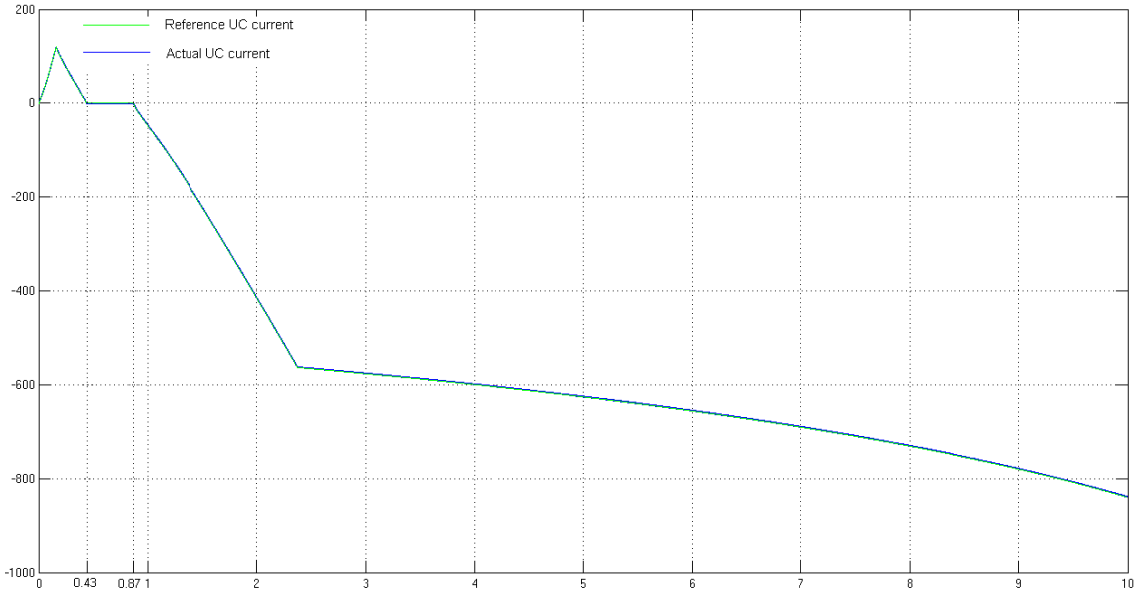

Figure 60 Ultracapacitor's current tracks the reference current with full load

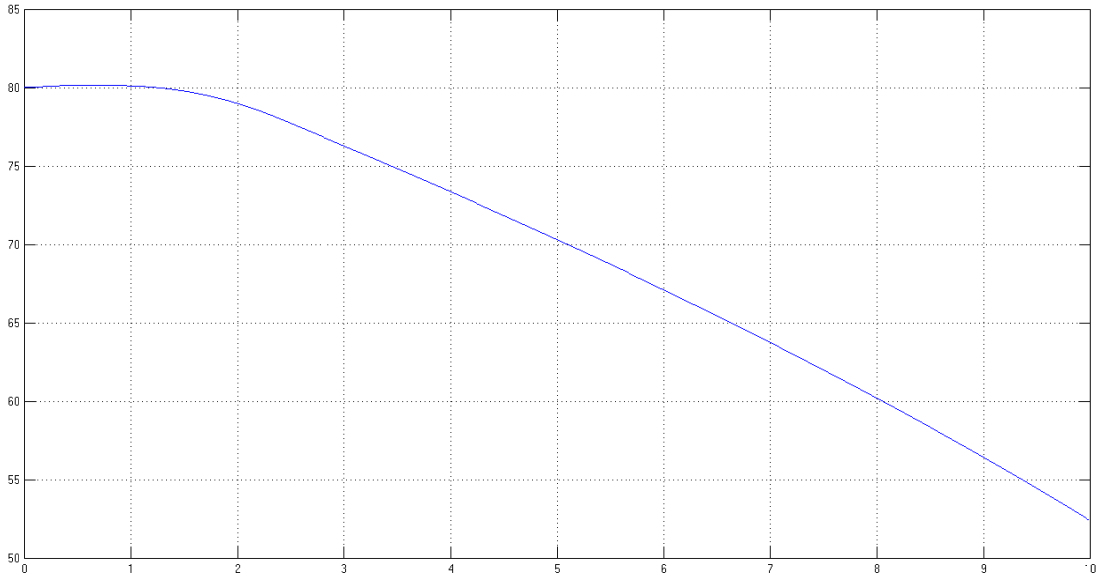

Figure 61 Ultracapacitor's voltage with full load

Figure 62 and Figure 63 show that the fuel cell reaches its rated power of 32.4 kW and motor with 72 kW during the full load operation. Figure 64 shows that the

ultracapacitor provides up to 44 kW peaking power to the load. The sum of the fuel cell power and the ultracapacitor power is larger than the motor's output power because there are power losses in the motor.

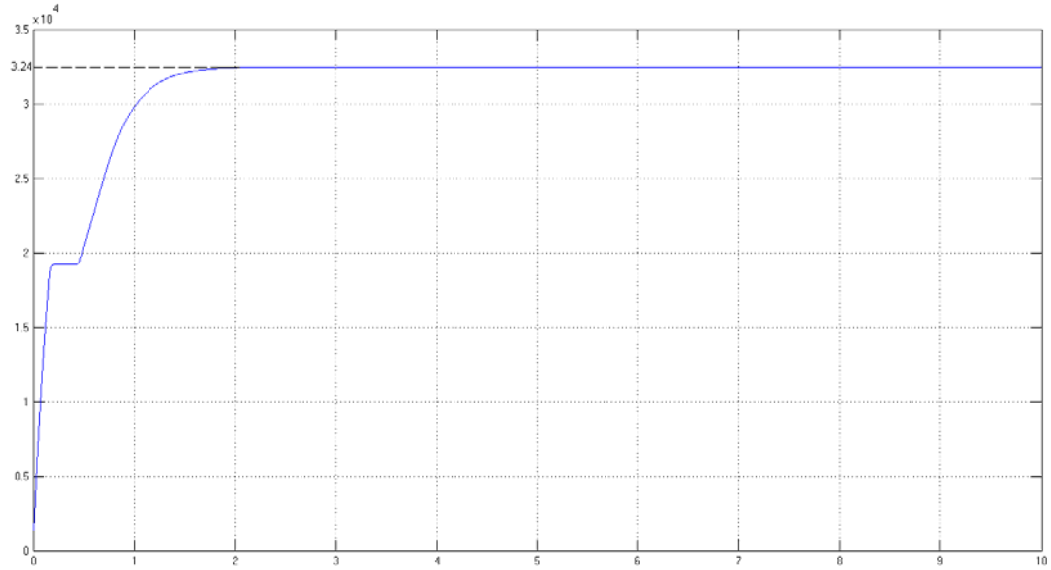

Figure 62 Fuel cell's output power with full load

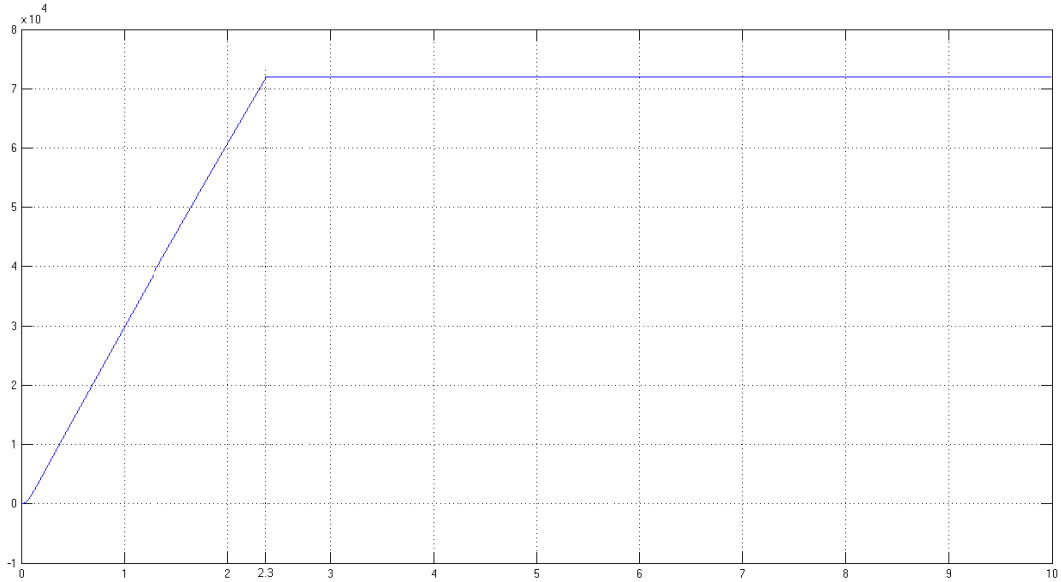

Figure 63 Motor's output power with full load

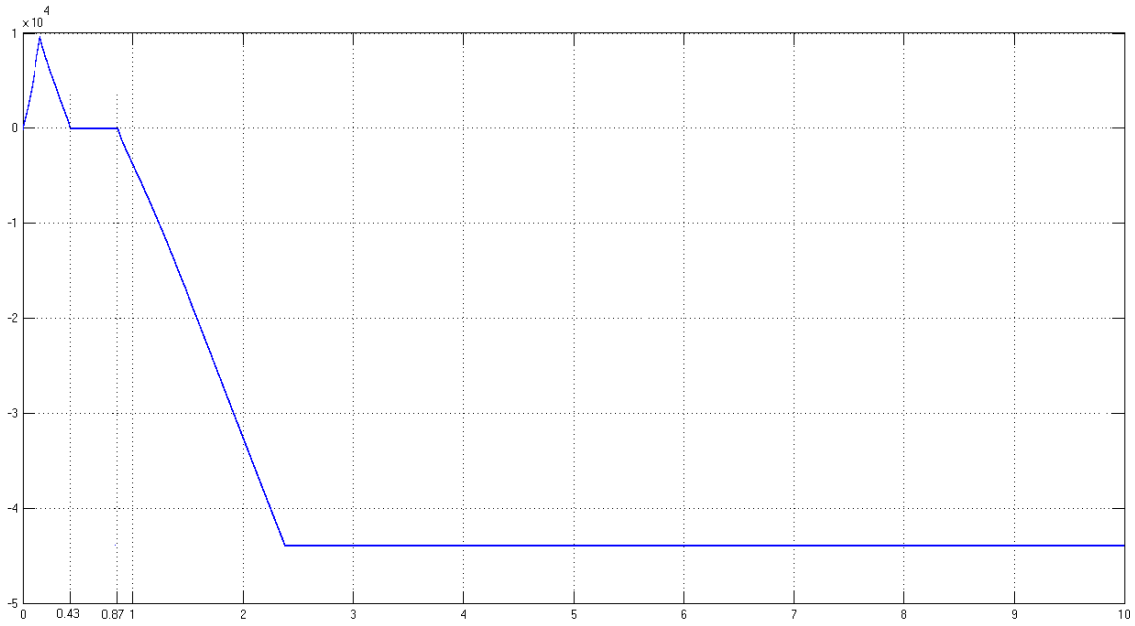

Figure 64 Ultracapacitor's output power with full load

6.2 Partial load operation

The following simulation results are based on changing the torque command from the driver. From t = 0 to t = 2 sec, full torque command is sent. From t = 2 sec to t = 5 sec, the torque command is reduced linearly from full torque to 70% of the rated torque. From t = 5 sec to t = 7 sec, the command keeps reducing from 70% of the rated torque to the zero torque command. From t = 7 sec to t = 9 sec, no torque command is sent and vehicle is in the idle condition. From t = 9 sec to t = 10 sec, the torque command goes from 0 to – 30% of the rated torque. The torque is reversed, indicating the braking pedal is pressed upon. From t = 10 sec to t = 12 sec, the foot on the braking pedal slightly looses and the torque command returns to 0 from – 30%. From t = 12 sec to 14 sec, the acceleration pedal is exerted again and the torque command goes from 0 to

70% of the rated torque. The torque produced by the motor is as shown in Figure 65 and the corresponding armature current is as Figure 66. The armature voltage of the motor is as Figure 67. And the resulting angular speed of the motor is as Figure 68.

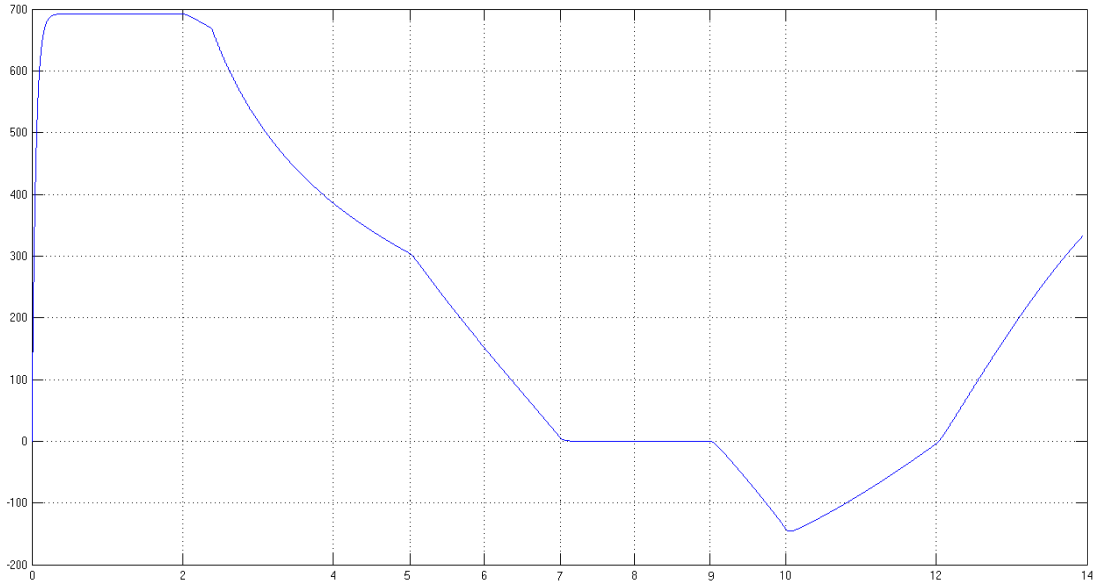

Figure 65 Torque generated by the motor with partial load

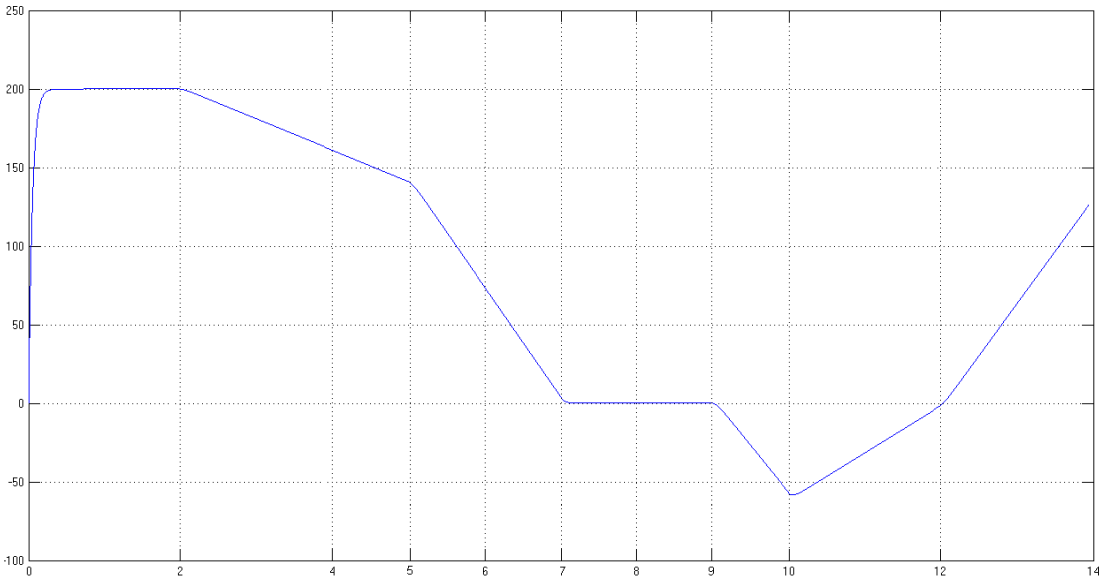

Figure 66 Motor's armature current with partial load

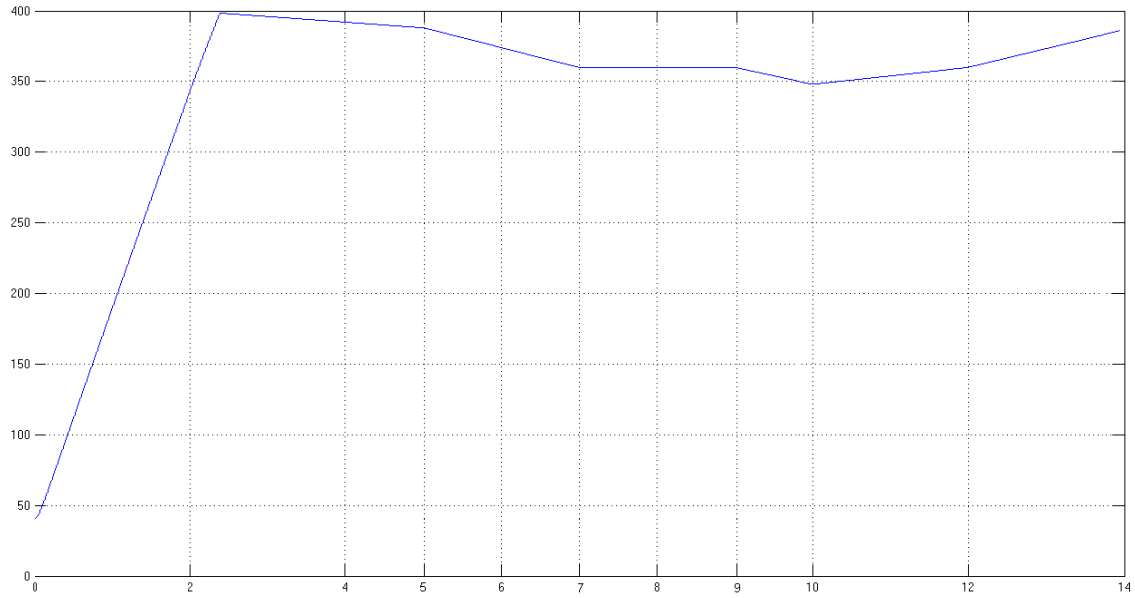

Figure 67 Motor's armature voltage with partial load

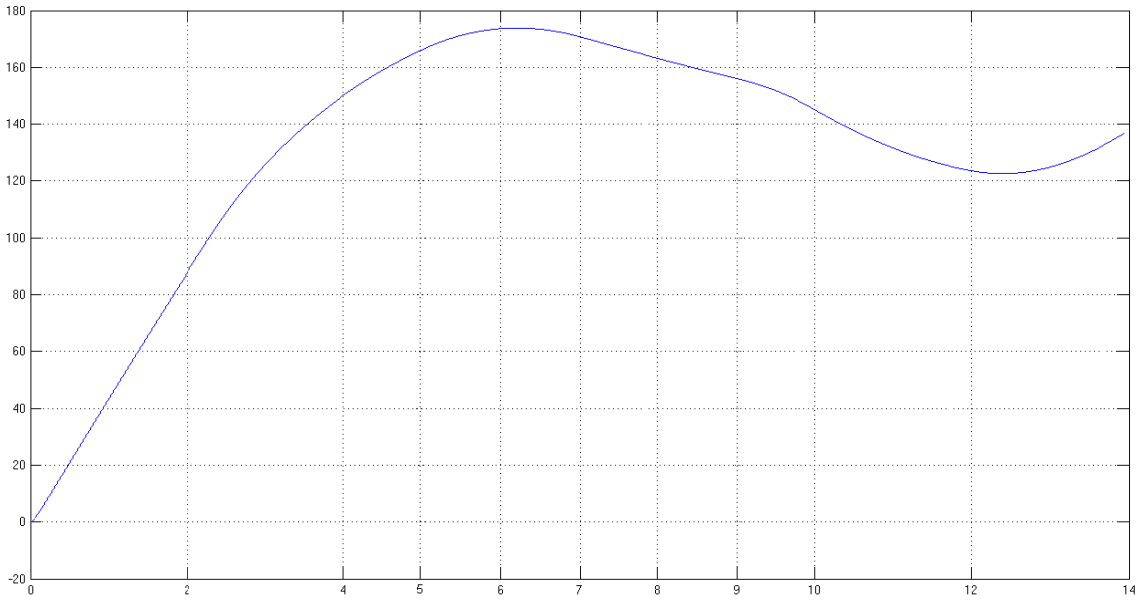

Figure 68 Motor's angular speed with partial load

Figure 69 shows the output current of the fuel cell, the blue line, the current flowing into the motor drives, the green line, and their difference, the red line. Figure 70

shows the changes of ultracapacitor's current i_{LUC}, the blue line. It follows the reference current i_{LUCref} mentioned in Chapter V, described in green in Figure 70. Figure 71 records the ultracapacitor's voltage. And Figure 72 represents the fuel cell's voltage in blue and current in green.

Mode 1: fuel cell powers the motor and ultracapacitor

As described in Figure 69, during t = 0 – 0.44 sec, t = 6.25 – 9 sec, and t = 12 – 12.87 sec, the fuel cell's minimum output current is larger than the motor drives' needing current. So the fuel cell maintains to produce the bottom limit of the current 80A as shown in Figure 72. The fuel cell voltage at this interval is 250V correspondingly. And the excessive current flows into the ultracapacitor to charge it. As in Figure 70, the current of the ultracapacitor is positive, indicating that the current is flow into the ultracapacitor to get charged. Also in Figure 71, the ultracapacitor's voltage is rising.

Mode 2: fuel cell powers the motor individually

During t = 0.44 – 0.86 sec, t = 5.69 – 6.25 sec, and t = 12.87 – 13.38 sec, the motor drives' current request falls into the fuel cell's operation range as represented in Figure 69. It can be observed in Figure 72 that the fuel cell provides its power to the motor and its current follows the motor drives' requisition. There is no power exchange in the ultracapacitor. The current of the ultracapacitor is zero during this period in Figure 70 and its voltage stays the same at 81.37V in Figure 71.

Mode 3: fuel cell and ultracapacitor charges the motor together

During t =0.86 – 5.69 sec, and t = 13.38 – 14 sec, the motor drives' required current is beyond the upper limit of the fuel cell current as in Figure 69, so the fuel cell

just provides the upper limit current 160 A and the voltage at this time is around 225V as in Figure 72. The gap is filled in by the ultracapacitor. It's discharged and sends out the power to the motor to meet the needs. As in Figure 70, the ultracapacitor's current goes negative, showing it's discharging. And the actual ultracapacitor's current tracks the i_{LUCref} closely. Also in Figure 71, the voltage of the ultracapacitor decreases.

Mode 4: ultracapacitor restores braking energy from the motor

During t = 9 - 12 sec, the current of the motor falls below zero, because the torque generated by motor changes directions. Therefore, the motor enters into the regenerative braking phase since t = 10 second. The fuel cell's accessory components continue to work, except that the fuel cell is disconnected from the system in this case. The ultracapacitor recaptures the braking energy from the motor and gets charged as the positive current in Figure 70 and increasing voltage in Figure 71.

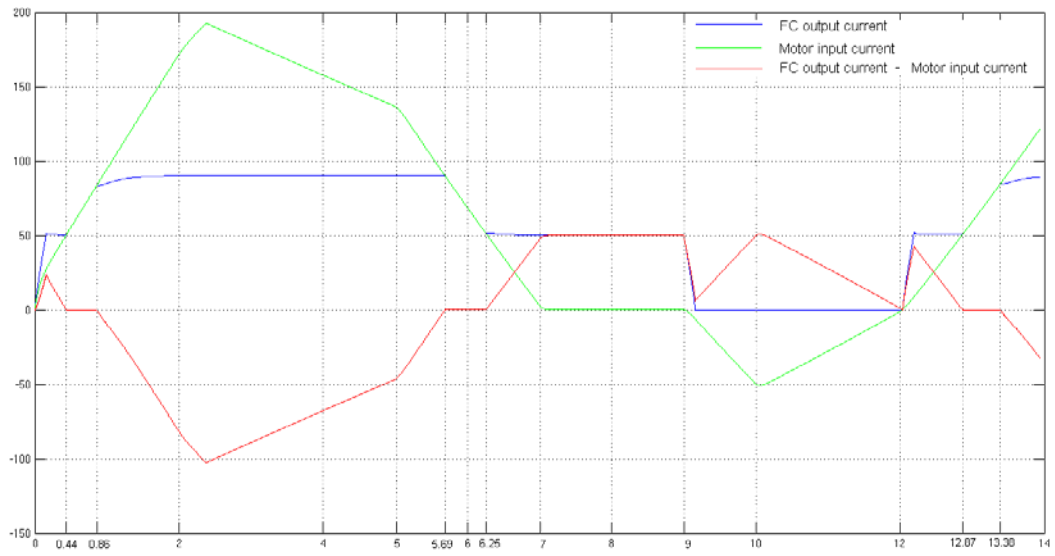

Figure 69 Output current of the fuel cell, input current of the motor and their difference with partial load

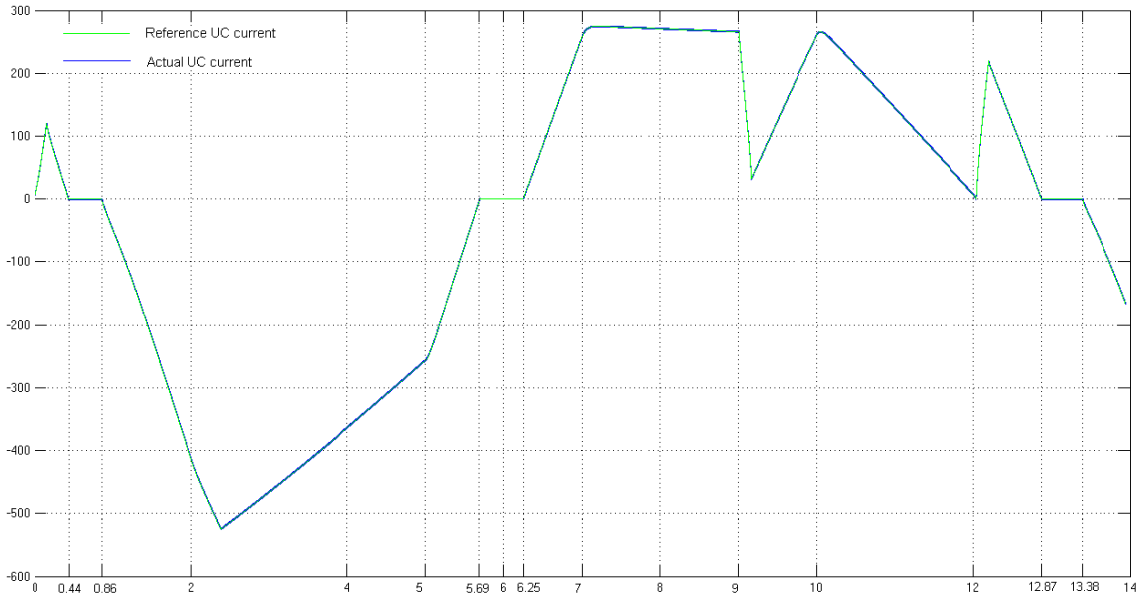

Figure 70 Ultracapcitor's current tracks the reference current with partial load

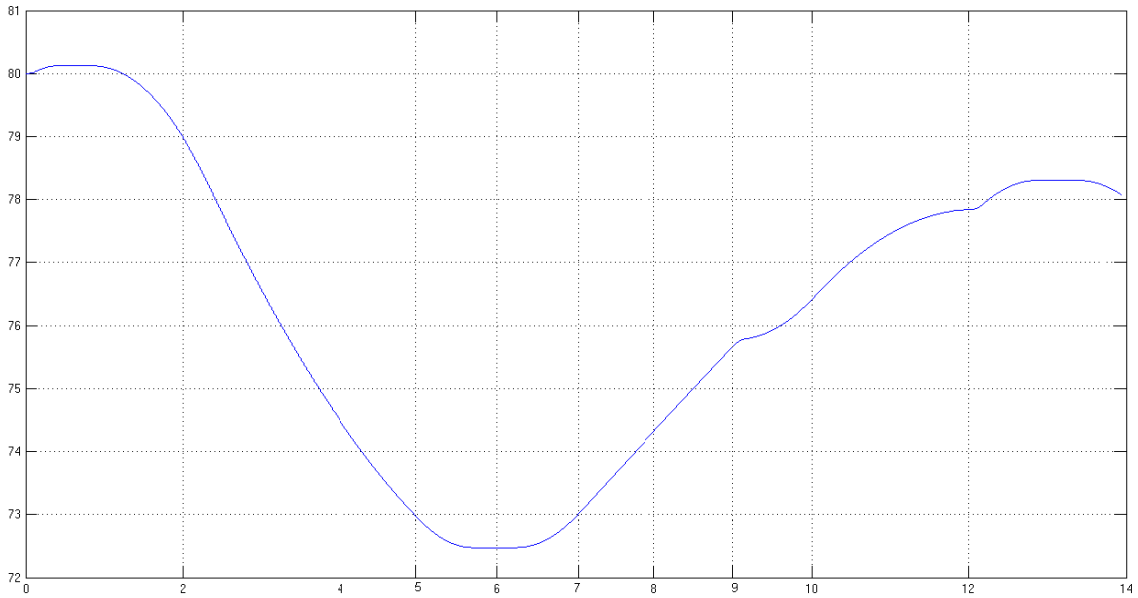

Figure 71 Ultracapacitor's voltage with partial load

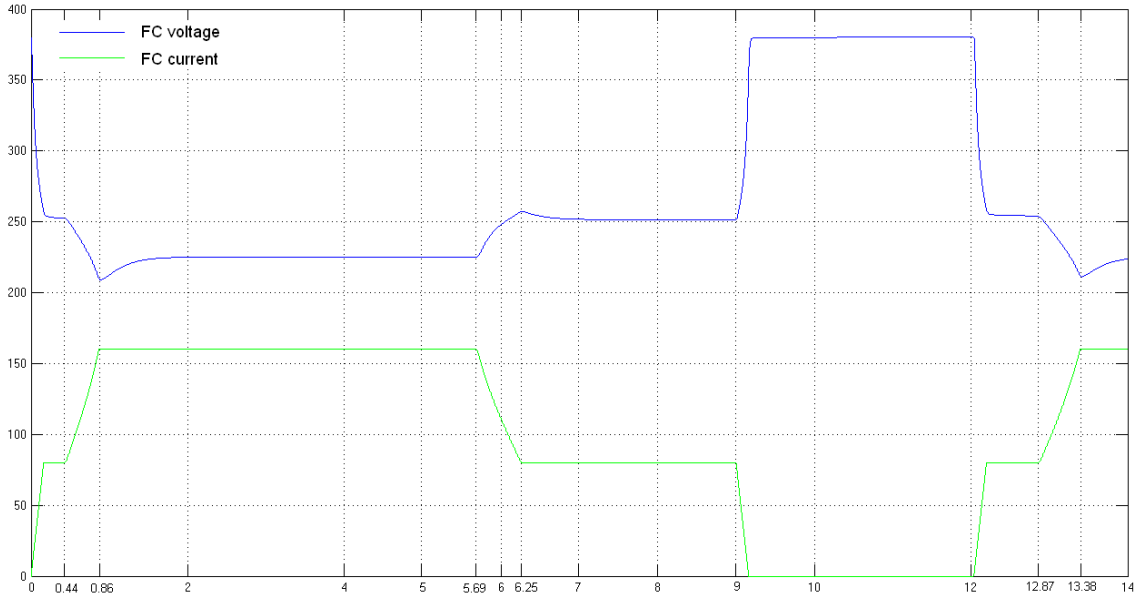

Figure 72 Fuel cell's voltage and current with partial load

CHAPTER VII

CONCLUSION

7.1 Summary

The fuel cell has attracted great attention due to its high energy density, low emissions, and quite performance. And it's been considered the most potential candidate to replace the internal combustion engine to drive the vehicle. Whereas, the fuel cell has several major weaknesses prohibiting the fuel cell vehicle's large-scale production, such as its high cost, slow transient response and so on. The thesis aims to solve these problems and make the fuel cell more viable in the cars. In the thesis, the drive train of the fuel cell vehicle is designed and a converter topology and the corresponding control scheme are proposed to apply in the fuel cell hybrid vehicles.

Chapter I reviewed the current situations of transportation, fuel consumption, and alternative energy technology. By comparing the different alternative sources, the fuel cell has been selected as the main energy source to drive the vehicle due to its high energy capacity, low emissions and advanced performance. And hydrogen is chosen to be the fuel on board. There are other novel fuels, such as methanol, natural gas and etc. Since their operation principles are basically the same, hydrogen is taken as an example here.

Chapter II described the fuel cell based hybrid vehicle structure and the criteria to evaluate the vehicle's performance. From the drive train structure point of view, the fuel cell hybrid vehicle is one type of series hybrid vehicle. By applying the criteria to

compare the vehicles' performance, it's concluded that the fuel cell hybrid vehicle can provide better performance than the conventional vehicle.

Chapter III explained the reason the fuel cell vehicle needs hybridization and the converter topology the thesis proposed. Although the fuel cell has many attractive features, it has some intrinsic weaknesses that it can't provide satisfactory driving experience alone. Since the electrochemical reactions happening in the fuel cell will always take some time, it can't effectively provide the transient power the dynamic load requires. Also, the fuel cell's efficiency is low during the light and heavy loads. Additionally, hybridization can reduce the fuel cell's size and cost. With the further comparison among other alternative sources, the ultracapacitor is selected as the auxiliary source to assist the fuel cell because of its high power density, quick response and long life time. As for the converter's design, the main goal is to achieve the high system efficiency, smooth driving performance, and low costs. In order to allow the fuel cell and the ultracapacitor work efficiently, both the fuel cell and the ultracapacitor are connected to the DC bus through a converter. With the aim to reduce the fuel cell's size, a boost converter is utilized at the end of the fuel cell so that the fuel cell's rating voltage can be lower than the DC bus. Similarly, when the power flows from the DC bus to the ultracapacitor, a buck converter is used. And a boost converter connects the ultracapacitor to the DC bus when the power is delivered from the ultracapacitor to the DC bus. Because fuel cell can't be recharged, and the ultracapacitor needs get charged and discharged, a unidirectional converter is enough for the fuel cell and a bi-directional converter is required for the ultracapacitor.

Chapter IV designs the fuel cell hybrid vehicle based on the vehicle performance set in Chapter II. In this chapter, the fuel cell's rating power, working range, ultracapacitor's rating power, maximum operating voltage and minimum operating voltage, and the traction motor's size are designed. These devices are designed to match the loads and sources and to minimize the devices' rating power.

Chapter V proposes the control methodology to make full use of the devices designed in Chapter IV. Thanks to the simple structure of the converter designed in Chapter III, the duty cycle of each converter can be mathematically analyzed. By changing the duty cycle of each converter with varying load requirements, the power flow can be controlled and optimized among the fuel cell, ultracapacitor and the loads.

Chapter VI carries out the simulation to verify the converters' normal operation and the effectiveness of control method described in Chapter V.

7.2 Future research

The thesis has designed the converter topology and the control method applied on it. Its feasibility is validated by the simulation. The future research involves implementing the design and control approach on the hardware. With the testing on the actual devices, further enhancement can be made based on the results taking the practical operation issues, such as the device integration, real-time response and etc., into consideration.

REFERENCES

[1] J. Larminie, and A. Dicks, *Fuel Cell Systems Explained.* West Sussex, England: Wiley, 2003.

[2] S. Thomas, and M. Zalbowitz, *Fuel Cells Green Power.* Los Alamos, NM: Los Alamos National Laboratory, 2000.

[3] M. Ehsani, Y. Gao, S.E Gays, and A. Emadi, *Modern Electric, Hybrid Electric and Fuel Cell Vehicle—Fundamentals, Theory and Design.* Boca Raton: CRC press, 2005.

[4] A. Emadi, M. Ehsani, and J. Miller, *Vehicular Electric Power Systems: Land, Sea, Air and Space Vehicles.* New York: Marcel Dekker, 2004.

[5] J. Pukrushpan, A. Stefanopoulou, and H. Peng, *Control of Fuel Cell Power Systems: Principles, Modeling, Analysis and Feedback Design.* New York: Springer, 2004.

[6] S. Srinivasan, *Fuel Cells: From Fundamentals to Applications*. New York: Springer, 2008.

[7] H. Chiu, and L. Lin, "A Bidirectional DC–DC Converter for Fuel Cell Electric Vehicle Driving System," *IEEE Trans. Power Electron.*, vol. 21, no. 4, pp. 950 – 958, Jul. 2006.

[8] M. I. Marei, S. Lambert, R. Pick, and M. M.A. Salama, "DC/DC Converters for Fuel Cell Powered Hybrid Electric Vehicle," in *Proc. IEEE Vehicle Power Propulsion Conf.*, 2005, vol. 1, pp.126 – 129.

[9] G. Calderon-Lopez, A. J. Forsyth, and D. R. Nuttall, "Design and Performance Evaluation of a 10-kW Interleaved Boost Converter for a Fuel Cell Electric Vehicle," in *Proc. CES/IEEE Int. Power Electron .Motion Control Conf.*, 2006, vol. 2, pp. 1 – 5.

[10] K.P. Yalamanchili, M. Ferdowsi, and K. Corzine, "New Double Input DC-DC Converters for Automotive Applications," in *Proc. IEEE Vehicle Power and Propulsion Confs*, 2006, vol. 2, pp. 1 – 6.

[11] G.-J. Su, and F.Z. Peng, "Triple-Voltage Bus DC-DC Converter for Automotive Applications," in *Proc. Applied Power Electron. Conf. and Exposition*, 2005, vol. 2, pp. 1015 - 1021.

[12] X. Kong, and A.M. Khambadkone, "Analysis and Implementation of a High Efficiency Interleaved Current-Fed Full Bridge Converter for Fuel Cell System," *IEEE Trans. Power Electron.*, vol. 22, no. 2, pp. 543 – 550, Mar. 2007.

[13] S. Lu, K. A. Corzine, and M. Ferdowsi, "An Unique Ultracapacitor Direct Integration Scheme in Multilevel Motor Drives for Large Vehicle Propulsion," in *Proc. IEEE Ind. Appl. Conf.*, 2006, vol. 5, pp. 2419 – 2426.

[14] J. L. Duarte, M. Hendrix, and M. G. Simões, "Three-Port Bidirectional Converter for Hybrid Fuel Cell Systems," *IEEE Trans. Power Electron.*, vol. 22, no. 2, pp. 480 – 487, Mar. 2007.

[15] S. Basu, *Recent Trends in Fuel Cell Science and Technology*. New York: Springer, 2007.

[16] M. Amirabadi, and S. Farhangi, "Fuzzy Control of a Hybrid Power Source for Fuel Cell Electric Vehicle using Regenerative Braking Ultracapacitor," in *Proc. Int. Power Electron. and Motion Control Conf.*, 2006, vol. 1, pp. 1389 – 1394.

[17] M.J. Gielniak, and Z.J. Shen, "Power Management Strategy Based on Game Theory for Fuel Cell Hybrid Electric Vehicles," in *Proc. IEEE Vehicular Tech. Conf.,* 2004, vol. 1, vol. 6, pp. 4422 - 4426.

[18] M.Y. Ayad, M.Becherif, A. Djerdir, and A. Miraoui, "Sliding Mode Control for Energy Management of DC Hybrid Power Sources Using Fuel Cell, Batteries and Supercapacitors," in *Proc. Int. Conf. Clean Elect. Power*, 2007, vol. 1, pp. 500 - 505.

[19] Z. Tao, S.R. Shaw, and S.B. Leeb, "Transient Recognition Control for Hybrid Fuel Cell Systems," *IEEE Trans. on Energy Conversion*, vol. 21, no. 1, pp. 195 – 201, Mar. 2006.

[20] Z. Jiang; L. Gao, and R.A. Dougal, "Adaptive Control Strategy for Active Power Sharing in Hybrid Fuel Cell/Battery Power Sources," *IEEE Trans. Energy Conversion*, vol. 22, no. 2, pp. 507 - 515, Jun. 2007.

[21] K. W. Harrison, *Renewable Hydrogen Integration, Validation, and Demonstration*. Golden, CO: National Renewable Energy Laboratory, 2008.

[22] M. Ehsani, Y. Gao, J. Miller, "Hybrid Electric Vehicles: Architecture and Motor Drives," in *Proc. IEEE*, 2007, vol. 1, pp. 719-728.

[23] W. Na, and B. Gou, "Feedback-Linearization-Based Nonlinear Control for PEM Fuel Cells," *IEEE Trans. Energy Conversion*, vol. 23, no. 1, pp. 179 - 190, Mar. 2008.

[24] D. Doerffel, and S. A. Sharkh, "System modeling and simulation as a tool for developing a vision for future hybrid electric vehicle drivetrain configurations," in *Proc. IEEE Vehicle Power and Propulsion Conf.*, 2006, vol. 1, pp. 1 - 6, 6-8.

[25] L. Eudy, K. Chandler, and C. Gikakis, *Fuel Cell Buses in U.S. Transit Fleets: Summary of Experiences and Current Status.* Golden, CO: National Renewable Energy Laboratory, 2007.

[26] K. Kawashima, Y. Hori, and T. Uchida, "Stabilizing Control of Vehicle Motion Using Small EV driven by Ultra Capacitor," in *Proc. Conf. of IEEE Ind. Electron. Soc.*, 2005, vol. 1, pp. 6-10.

[27] M. Mench, *Fuel Cell Engines*. Hoboken, NJ: John Wiley & Sons, 2008.

[28] M.Y. Ayad, M. Becherif, D. Paire, A. Djerdir, and A. Miraoui, "Passivity-Based Control of Hybrid Power Sources using Fuel Cell, Supercapacitors, and Batteries on the DC link for Energy Traction System," in *Proc. Int. Elect. Machines & Drives Conf.*, 2007, vol. 1, pp. 453 - 458.

[29] Maxwell Technologies, Ultracapacitor Sizing Selector, updated July 2008. [On-line]. Available: http://www.maxwell.com/ultracapacitor/technical-support/tools-models.asp

VITA

Bo Chen received her Bachelor of Science degree in electrical engineering from Wuhan University in 2007. She entered the Department of Electrical & Computer Engineering at Texas A&M University in August 2007 and received her Master of Science degree in August 2009. Her research interests include electrical power system & power electronics.

Ms. Chen may be reached at Department of Electrical Engineering, Texas A&M University, College Station, TX 77843-3128. Her email is chenboee@neo.tamu.com.